Technische Universität München

TUM School of Medicine and Health

Characterization of Inceptor in Spermatogenesis and its Role in Prostate Cancer

Sara Bilekova

Vollständiger Abdruck der von der TUM School of Medicine and Health der Technischen Universität München zur Erlangung einer

Doktorin der Naturwissenschaften (Dr. rer. nat.)

genehmigten Dissertation.

Vorsitz: Prof. Dr. Maximilian Reichert

Prüfende der Dissertation:

1. Prof. Dr. Heiko Lickert
2. Prof. Dr. Dr. h.c. mult. Martin Hrabé de Angelis

Die Dissertation wurde am 23.04.2024 bei der Technischen Universität München eingereicht und durch die TUM School of Medicine and Health am 07.08.2024 angenommen.

Abstract

This thesis investigates inceptor's diverse roles in male reproductive tissues, particularly its effects on prostate cancer and sperm formation in the testis. Prostate cancer, a malignant tumor that originates in the prostate gland, is one of the most common cancers affecting men, particularly those over the age of 50. Aggressive forms that can metastasize rapidly have generally poor outcomes. Further studies are necessary to understand the biological mechanisms, progression patterns, and response to treatments and develop targeted therapies against prostate cancers. Spermatogenesis is the process by which sperm are produced in the testes, crucial for male fertility. Studying this process will help us understand male infertility and its genetic factors and identify potential therapeutic targets.

Despite initial descriptive studies in cancers of female reproductive tissues, the stomach, and pancreas, the molecular aspect of inceptor’s role in cancer progression is mostly unknown. In the prostate, inceptor localized to luminal and intermediate cells of the glandular epithelium. In prostate cancer, the expression levels of inceptor exhibited a correlation with prostate cancer markers. Overexpression of inceptor in a prostate cancer cell line positively impacted growth hormone signaling, androgen receptor activation, and cell migration, suggesting inceptor’s functions as an oncogene in prostate cancer.

In the testis, inceptor proved indispensable for spermatid development. Its absence resulted in male infertility, caused by malformations of the acrosome, a highly specialized organelle in sperm essential for fertilization. In developing spermatids, we have uncovered a direct role of inceptor in acrosome formation by mediating cargo delivery to this growing organelle. These findings underscore inceptor's significance as an intracellular sorting receptor and act as a basis for studying its role in other secretory organs.

Building on our research in pancreatic beta cells, our studies shed light on Inceptor's dual role: modulating growth hormone pathways on the cell surface and facilitating intracellular vesicular trafficking across secretory, lysosomal, and acrosomal compartments.

Index

1 Introduction

This thesis focuses on characterizing the cell biological relevance of inceptor, which we named the insulin inhibitory receptor (gene *IIR*), in the testes and the role of inceptor in prostate cancer. Understanding the role of inceptor across different tissues and disease models contributes to the more thorough functional description of this new receptor and provides basic knowledge on the potential of inceptor as a therapeutic target.

1.1 The male reproductive system

The organs of the murine male reproductive system such as testes, epididymis, vas deferens, and prostate are essential for the formation, maturation, storage, and eventual ejaculation of mature sperm. The development and function of the male reproductive system are steered by the hormones of the hypothalamic-pituitary-gonadal axis. Of high importance is the gonadotropin-releasing hormone produced by the hypothalamus, which stimulates the anterior pituitary to release hormones such as luteinizing hormone and follicle-stimulating hormone, which act on the somatic cells of the testis (Clavijo & Hsiao, 2018).

1.1.1 Function and anatomy of the testes

The testes are a pair of organs comprised of long tubules that contain the germ cells, as well as the interstitial space (Figure 1). The two main somatic cell types of testes are Leydig cells and Sertoli cells. Leydig cells produce testosterone, which is vital for male development and function. Androgens such as testosterone bind to the androgen receptor (AR), which is broadly expressed across many cell types, with important roles in the somatic cells of testes and prostate (Ruizeveld De Winter et al., 1991). The AR is an intracellular steroid hormone receptor that translocates to the nucleus upon activation, thus stimulating the transcription of androgen-responsive genes. Sertoli cells are part of the germinal epithelium and support the spermatogonial stem cells and their meiotic and post-meiotic development, maintain the function of Leydig cells as well as provide structural support (O'Donnell et al., 2022).

The germ cells of the testes are composed of diploid spermatogonia, which differentiate towards mature spermatozoa in the process of spermatogenesis (Cheng & Mruk, 2010). In the process, spermatogonia generate primary spermatocytes, which undergo meiosis to

produce spermatids. In the first part of meiosis, the primary spermatocyte produces two secondary spermatocytes, which divide into four round spermatids in the second meiotic step. Spermatids develop into sperm in a multistep process called spermiogenesis (Oakberg, 1956). In this process, a characteristic organelle, the acrosome is shaped (Khawar et al., 2019). The acrosome is a large vesicle docked at the anterior of the sperm that is essential for oocyte recognition and oocyte-sperm fusion in a process called acrosome reaction (Aldana et al., 2021). Acrosomal material is synthesized through the endoplasmic reticulum and Golgi apparatus in spermatocytes and stored in vesicles until meiosis is completed (Anakwe, 1990; Escalier et al., 1991; Kashiwabara et al., 1990). The resulting cell is called a Golgi-stage spermatid, as the acrosomal cargo is near the Golgi apparatus. In the next step, the vesicles containing the acrosomal material, called proacrosomal vesicles, fuse to form the acrosomal vesicle harbored to the nuclear membrane at the anterior of the spermatid. The acrosomal vesicle continues to receive more cargo from the Golgi, resulting in the growth of the vesicle. As the acrosome grows, it expands over the nuclear surface, creating the cap-phase spermatid, since the acrosome resembles a cap on the nuclear surface. After this stage, the round spermatid starts to elongate, while the acrosome continues to expand on the nuclear surface until it covers most of the nucleus and the acrosomal phase spermatid emerges. During the maturation stage, the spermatid undergoes further maturation until it is released into the seminiferous tubule and advances to the epididymis, where sperm maturation continues (James et al., 2020). Released mature sperm passes through the *vas deferens* and the ampulla above the prostate and seminal vesicles and continues to the ejaculatory tract.

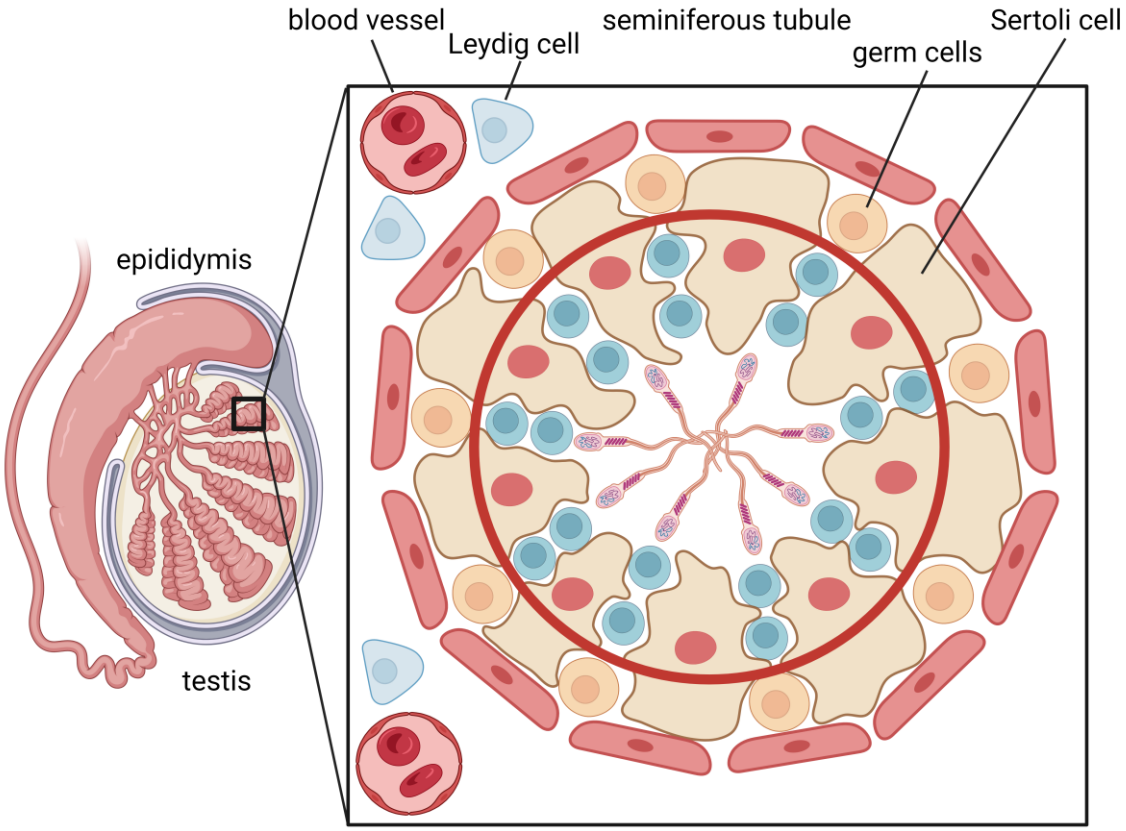

Figure 1 – Schematic representation of the testis and seminiferous tubule. The gross morphology of the testis and epididymis (left) and cross-section of the seminiferous tubule (right). The seminiferous tubule contains Sertoli cells that support the development of the germ cells towards sperm. Round spermatids (cyan) develop into maturing sperm, which then migrates through the seminiferous tubules towards the epididymis. Created with BioRender.com.

1.1.2 Function and anatomy of the prostate

The prostate is an accessory male reproductive organ located below the bladder, in conjunction with the seminal vesicles. The prostate produces seminal fluid, thus contributing essential components of ejaculate, which maintains sperm viability. The human prostate is separated into central, peripheral, and transition zones (Figure 2A). In general, the prostate consists of ducts and acini embedded in stroma. The peripheral zone contains the majority of the functional glandular tissue and also gives rise to most prostate tumors in humans. On the other hand, the transition zone is the smallest zone in healthy young individuals, it is however commonly prone to benign prostatic hyperplasia with advanced age and is less commonly an origin of prostate cancers. The central zone is not commonly the primary source of prostate cancers (McNeal, 1981; Zlotta et al., 2013).

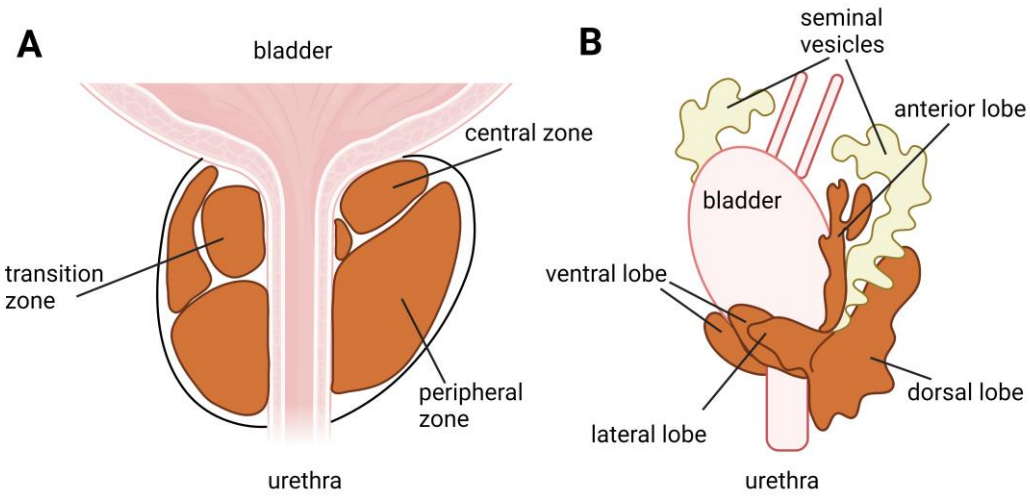

Figure 2 – Schematic representation of the lateral view of the human (A) and murine (B) prostate. The human prostate consists of the central, peripheral, and transition zones and is located below the bladder (A). The murine prostate consists of the anterior, ventral, dorsal, and lateral lobes (B). Created with BioRender.com.

The murine prostate consists of the anterior, ventral, dorsal, and lateral prostate lobes which warp around the urethra (Figure 2B). Even though the anatomy of the murine prostate is considerably different from human, the general structure also carries many similarities. As primary human tissue is only available for descriptive studies, murine models have been used extensively to study the healthy and diseased prostate. Among the different lobes of the murine prostate, the anterior lobe shows the most distinct morphology, as it mostly consists of papillary structures, therefore resembling the human central zone. The ventral prostate on the other hand has medium or large acini and sparse infoldings. The two murine dorsal lobes are analogous to the human peripheral zone and are composed of relatively small acini that are lined by columnar epithelium. The lateral prostate consists of large acini with cuboidal cells (Ittmann, 2018).

The ducts and acini of the prostate carry out the primary secretory function of the prostate and are lined by a simple epithelium. The prostate develops from the embryonic prostatic bud and is morphologically developed at birth in humans and at the time of sexual maturity in rodents (Aaron et al., 2016). The epithelium upon activation of the AR, develops into two layers: the basal and luminal layers. These layers contain four distinct epithelial cell types: the small and flat basal cells, the larger luminal epithelial secretory cells, intermediate cells, and

neuroendocrine cells (Figure 3). Additionally, stem cells have been also reported within both the epithelial and stromal layers (Gangavarapu et al., 2022).

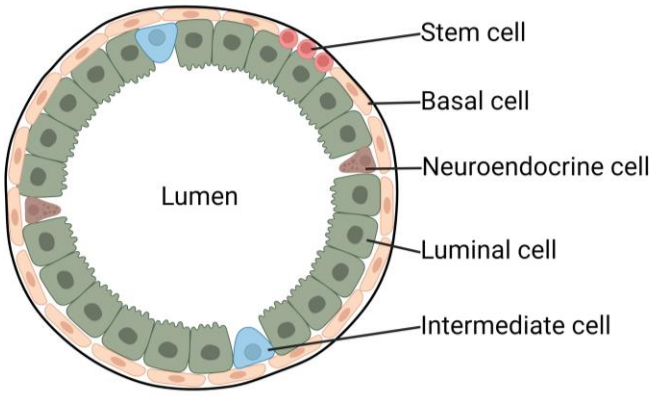

Figure 3 – Schematic representation of the cross-section of the prostate epithelium. The prostate epithelium consists of the basal and luminal layers, containing distinct cell types, such as basal cells, luminal cells, intermediate cells, stem cells, and neuroendocrine cells. Created with BioRender.com.

Prostate cancer is the most frequently diagnosed cancer in men (Bashir, 2015). Around 80% of prostate cancers originate from the peripheral zone which is analogous to the murine dorsal lobe (Zlotta et al., 2013). Prostate cancers are classified based on clinical stage, Gleason score, and prostate-specific antigen (PSA) levels of the patient (Litwin & Tan, 2017). Localized prostate cancer is managed either by monitoring, or treatment via surgery and/or radiation. Metastatic prostate cancer is most commonly treated by chemotherapy and androgen deprivation, which causes various side effects and resistance to these therapies in many cases (Litwin & Tan, 2017). Whereas the relative survival rate for patients with localized and regional prostate cancer is nearly 100%, this rate is only around 32% for patients with metastatic cancer (Cancer.Net, 2023).

1.2 Prostate Cancer

1.2.1 Modeling prostate cancer

In the past decades, much of our knowledge of prostate cancer came from correlative studies using human biopsy samples (Taylor et al., 2010). These data provide a strong basis for research, which is complemented with functional studies in mice. Mice typically do not develop spontaneous prostate cancers, therefore two fundamentally different approaches have been

used (Ittmann et al., 2013). Firstly, genetically engineered mouse models carry oncogenes or recombinases restricted to the prostate to induce tumorigenesis. Secondly, xenograft models utilize human cancer cell lines, and epithelial or stromal cells injected into immunocompromised mouse models. Murine models provide an opportunity to describe the physiology of tumors in an *in vivo* setting, allowing for studying metastases and tumor microenvironments. However, to study the cell biology of cancers, cultured human cells are commonly utilized. One of the most widely used *in vitro* models is the lymph node metastasis of prostate cancer (LNCaP) cell line, which is androgen-dependent and retains its malignant phenotype and testosterone responsiveness in xenografts in mice (Abate-Shen & de Almeida, 2022; Horoszewicz et al., 1983). A subline of LNCaP, the LNCaP C4-2 cell line, has been generated by co-inoculation with a bone stromal cell line in castrated male mice, and even though they retained their tumor-forming capability, they do not show a dose-dependent response to testosterone (Van Bokhoven et al., 2003; Wu et al., 1994). PC-3 cells have been isolated from bone metastasis of prostate adenocarcinoma and they do not respond to testosterone in culture (Kaighn et al., 1979).

1.2.2 Signaling pathways in prostate cancer

As in many other cancers, tyrosine kinase signaling is pivotal in prostate cancer development and progression. Tyrosine kinases are a large class of proteins that bind extracellular ligands which cause activation of their kinase activity. Generally, they are single-pass transmembrane proteins with a cell-cell communication function relaying cell growth, motility, differentiation, and metabolic signals. Extracellular ligands, such as growth factors, bind to the extracellular region of receptor tyrosine kinases. The receptors can exist as monomers or dimers, and ligand binding will either drive or stabilize active dimers/oligomers and in most cases induce *trans*-autophosphorylation, meaning the two proteins phosphorylate each other (Lemmon & Schlessinger, 2010; Schlessinger, 2000). Phosphorylation of receptor tyrosine kinases drives the recruitment of a variety of signaling proteins and the engagement of downstream signaling pathways. This is mediated through Src-homology-2 (SH2) or phosphotyrosine-binding (PTB) domains, which bind to specific phosphotyrosine residues, acting as protein-interaction modules (Margolis, 1999; Pawson et al., 2001; S. Zhou et al., 1993). Downstream signaling proteins can bind either directly or through docking proteins that create large multiprotein platforms serving as assembly stations for a wide variety of signaling molecules. These

regulate a variety of downstream signaling pathways, such as those mediated by rat sarcoma virus proteins (RAS) and mitogen-activated protein kinase (MAPK), phosphoinositide 3-kinases (PI3K), and AKT, or Janus kinase 2 (JAK2)/ signal transducers and activators of transcription (STAT). In summary, receptor tyrosine kinase signaling pathways transfer extracellular signals that can drive transcriptional responses in the nucleus, thus modifying cell growth, migration, and metabolism. Cancer cells often rely on aberrant receptor tyrosine kinase signaling and constitutive activation of the downstream pathways for growth and survival advantages. Cancers achieve constitutive receptor tyrosine kinase activation by either gain-of-function mutations, genomic amplification, chromosomal rearrangements, and/or autocrine activation (Du & Lovly, 2018).

1.2.2.1 Insulin and IGF receptor signaling

The insulin and insulin-like growth factor 1 receptors (IR and IGF1R) convey cell-cell communication and promote survival, proliferation, metabolism, and protein synthesis. IR has two splice variant isoforms, IR-A and IR-B, which form homo- and heterodimers (Ebina et al., 1985; Ullrich et al., 1985). IR-B predominantly mediates insulin action in metabolic tissues (Leibiger et al., 2001). This leads to significant challenges in preserving insulin function in therapies targeting receptor tyrosine kinases. IGF1R can also dimerize with either of the IR isoforms, forming a hybrid receptor. Both IR and IGF1R are heterotetramers, with two α chains and two β chains (LeRoith et al., 2021). Upon activation, insulin and IGF receptors convey signals through several signaling pathways. For instance, phosphorylation of insulin receptor substrate 1/2 (IRS1/2) activates PI3K, which regulates AKT signaling. AKT is an important regulator of cell survival, apoptosis, proliferation, cell cycle, and glucose metabolism. It is also regulated by the mammalian target of rapamycin complex 2 (mTORC2), which influences various cellular processes, including protein synthesis and autophagy (Hoxhaj & Manning, 2019). Additionally, the activation of insulin and IGF receptors can lead to the stimulation of not only the PI3K-AKT signaling axis but also the MAPK pathway. While MAPK signaling primarily regulates cell division, growth, and differentiation, there is notable cross-talk between the MAPK pathway and AKT signaling (Wei & Liu, 2002). Through such mechanisms, cells integrate mitogenic signals with survival and growth cues that maintain cellular and physiological homeostasis.

The relevance of the insulin and IGF signaling pathways in prostate cancer progression is also demonstrated by the connection between diabetes incidence and prostate cancer survival (Lutz et al., 2018). Based on a tissue microarray assay for immunohistochemistry on samples from 360 patients with benign prostatic hyperplasia or prostate cancer, IR-α was more expressed in patients with prostate cancer, and IGF1R was associated with proliferation, as well as with tumor aggressiveness, especially in patients with diabetes (Broggi et al., 2021).

1.2.2.2 Androgen receptor signaling

Prostate development, function, and homeostasis are dependent on androgen signaling. AR is a nuclear transcription factor that consists of four distinct domains, the N-terminal domain, a highly conserved deoxyribonucleic acid (DNA)-binding domain, a hinge region, and a ligand-binding domain (Claessens et al., 2008). It is activated by androgenic steroids, such as testosterone. Testosterone can activate AR directly or it can be converted into dihydrotestosterone (DHT) first, which has a higher affinity to AR (Wright et al., 1996; Z. X. Zhou et al., 1995). AR is found in its inactive state in the cytosol, stabilized by chaperones. Filamin-A tethers the hinge domain to the cytoskeleton and is responsible for the release of AR upon its activation (Loy et al., 2003; Ozanne et al., 2000). Ligand binding activates the AR and induces a conformational change and nuclear translocation (Figure 4A). In the nucleus, AR binds to androgen response elements and thereby modulates target gene expression, in conjunction with almost 200 coregulators. Additionally, the growth hormone pathway has been shown to modulate AR signaling via different mechanisms of crosstalk, such as through the PI3K-AKT or Raf-MEK-Erk pathways (Figure 4B) (Zhu & Kyprianou, 2008).

Prostate cancer formation and progression are dependent on AR activation. Therefore, androgen deprivation therapy is commonly chosen; however, after 18-24 months the symptoms usually return and the disease progresses (Feldman & Feldman, 2001; Pienta & Bradley, 2006). This is attributed to the restoration of AR signaling, which is possible through the following mechanisms: (i) AR amplification or overexpression, (ii) gain-of-function AR mutations, (iii) intracrine androgen production, (iv) overexpression of AR cofactors, (v) cross-talk with other signaling pathways, and (vi) expression of constitutively active AR splice variants (Buchanan et al., 2001; Lonergan & Tindall, 2011).

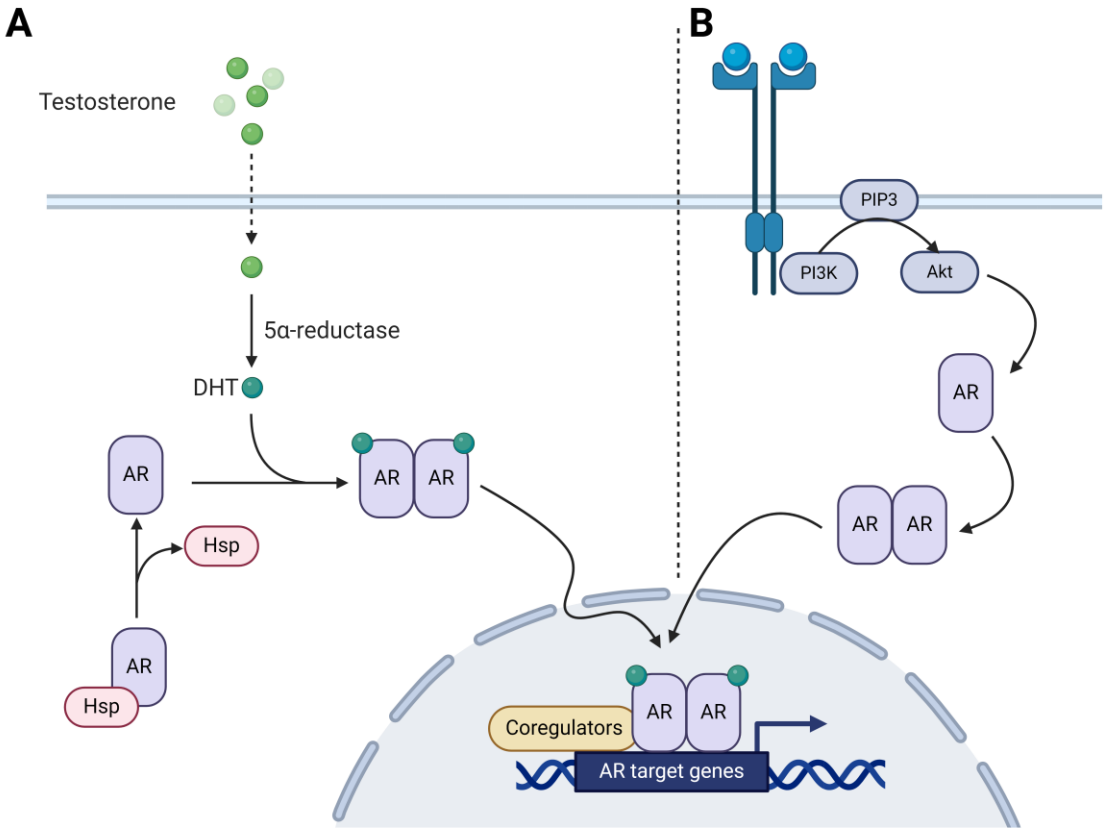

Figure 4 – Androgen-dependent (A) and androgen-independent (B) AR activation pathways. Under androgen-dependent conditions, testosterone or its converted form DHT binds to the AR, released from chaperones and translocates to the nucleus, activating downstream target genes modulating growth and metabolism (A). The AR can also be cross activated via growth hormone receptors (blue) via the AKT pathway (B). Created with BioRender.com.

1.2.2.3 Modulating the growth hormone pathway in prostate cancer

IGF1R expression, unlike IR, is linked to lethal prostate cancer development (Ahearn et al., 2018). IGF1R has been found to activate AR cofactors, thereby stimulating the AR pathway (Zhu & Kyprianou, 2008).

Several studies showed a correlation between IGF signaling and prostate cancer progression, highlighting the potential of this signaling pathway in prostate cancer therapies (Liu et al., 2023). Small molecule inhibitors of IGF1R have been developed and tested in animal models. However, inhibitory small molecules might not be specific enough to avoid cross-reactivity with the insulin receptor. In contrast, monoclonal antibodies (mAbs) offer a more targeted approach.

In preclinical models, several IGF1R-binding mAbs have been investigated. For instance, the two IGF1R-blocking mAbs cixutumumab and figitumumab have been tested in phase II clinical trials. Cixutumumab did not alter prostate cancer biomarkers (Yu et al., 2015), while figitumumab successfully lowered PSA levels (Chi et al., 2012). After the initial studies, further trials in combination with other therapeutics were performed, alas with mixed results, likely due to the patients being in different stages of the disease (Liu et al., 2023). A few antibodies blocking IGF directly have been developed, such as xentuzumab (Doi et al., 2022) and dusigitumab (Gao et al., 2011) but their effect on prostate cancer in humans has not yet been investigated.

Downstream effectors of the growth hormone pathways have also been proposed as therapy targets. For instance, inhibitors of PI3K-AKT, often combined with mTOR modulators, have also been investigated for their anti-cancer potential in clinical trials (Gasmi et al., 2022; Roudsari et al., 2021; Tortorella et al., 2023). Overall, the initial results were encouraging and several of the trials are still ongoing. Learning more about prostate cancer progression might help identify which patient groups could benefit from modulating these pathways and pave the way toward personalized medicine.

1.3 Secretory cells

1.3.1 Types of secretory cells

Secretion is a fundamental process of all cells, starting from prokaryotic cells, through plants, and mammalian cells, releasing intracellular products from the cell. The functions of secretion include vital processes such as cell-cell communication, neurotransmission, and digestion. Secretory cell types are found throughout the mammalian body, within various organs and tissues, either dispersed in the epithelium or grouped in glands. Glands are an organized collection of secretory epithelial cells, and they can have an endocrine or exocrine function. Endocrine glands secrete substances, such as hormones, directly into the bloodstream. On the other hand, exocrine glands secrete into ducts, which collect their products within tubular, acinar, or alveolar cavities. Tubular glands have a simple tube-like structure, acinar glands are pear-shaped with a relatively small cavity or lumen, whereas alveolar cells have large round inner spaces. Glands might form branched or compound structures, consisting of several branches and lobules, for example in the prostate (Rehfeld et al., 2017).

1.3.2 The mechanism of cargo sorting and secretion

In classical secretory pathways, the secretory protein is translated directly into the lumen of the endoplasmic reticulum (ER) via its signal peptide. The protein is then directly processed and folded in the ER and passed on to the Golgi apparatus for further processing. The Golgi apparatus consists of stacks of *cis*, medial, and *trans* cisternae, as well as the *trans*-Golgi network (TGN) (Day et al., 2013). The TGN is a major sorting hub in the cell, where newly synthesized cargo is packaged into vesicles. Additionally, recycled endosomal or endocytosed cargo can also be returned to the TGN (Gu et al., 2001).

1.3.2.1 Endo-lysosomal protein sorting

Vesicles originating from the cell surface or TGN are referred to as endosomes. Endosomes form a dynamic system of membranous compartments that act as a trafficking center of the cell. The primary roles of the endo-lysosomal compartment are degradation, recycling, and modulation of proteins, thus contributing to cellular homeostasis. Its constituents are early endosomes, recycling endosomes, late endosomes, and lysosomes. The maturation of early endosomes to lysosomes is characterized by a decrease in pH as well as changes in the composition, achieved by tightly regulated sorting systems (Hu et al., 2015). A closely related degradation machinery, mostly responsible for the degradation of damaged or unused whole organelles, is defined as macroautophagy. Phagophores encapsulate large subcellular structures and eventually fuse with a lysosome to form the autolysosome and initiate degradation (Feng et al., 2013). In secretory cells, which are rich in secretory granules, a special type of degradation was observed, coined crinophagy by Christian de Duve. In these instances, secretory granules fuse with lysosomes directly to degrade cargo to prevent unwanted secretion or gain catabolites.

The TGN is an important hub of pathway branching (Figure 5) (Kienzle & von Blume, 2014). Cargo from the TGN is “shipped off” to various destinations, such as the endosomes, lysosomes, plasma membrane, or secretory granules. However, the regulation of these sorting decisions is not well understood. There are a few known receptors that transport lysosomal hydrolases to lysosomes by recognizing the mannose-6-phosphate (M6P) tag on the cargo protein. These are collectively called M6P receptors (M6PRs) and comprise the cation-independent M6PR (also known as insulin-like growth factor 2 receptor (IGF2R)), the cation-dependent M6PR, lysosomal integral membrane protein 2 (LIMP-2), and sortilin (Braulke &

Bonifacino, 2009). The heterotetrameric adaptor protein complexes (AP-1 through AP-5) and the Golgi-localizing, g-adaptin ear domain homology, ARF-binding protein (GGA) complexes play an important role in lysosomal targeting of receptors (Gadila & Kim, 2016). The adaptor proteins are recruited to the membrane via binding to the cytoplasmic portions of receptors carrying specific signal sequences, such as the YXXΘ or DXXLL motifs (Bonifacino & Traub, 2003). Clathrin or other coat proteins bind to adaptor proteins and induce vesicle formation. AP-1 mediates clathrin-coated vesicle trafficking between the TGN and late endosomes, whereas AP-2 mediates endocytosis from the plasma membrane. AP-3 mediates the transport of selected cargo towards lysosomes (Braulke & Bonifacino, 2009).

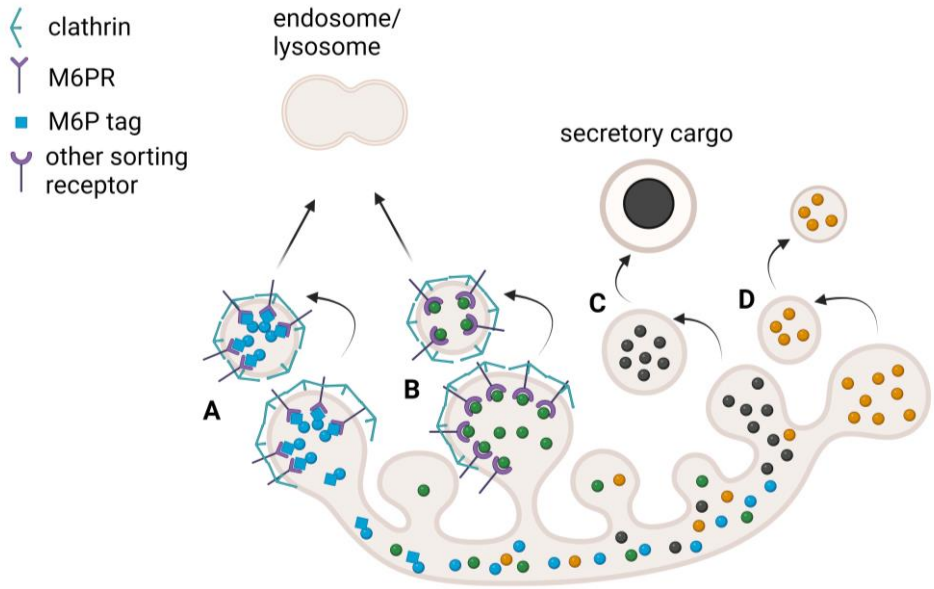

Figure 5 – Schematic representation of cargo sorting at the TGN. Sorting receptors recognize cargo at the TGN, such as M6PRs recognizing M6P-tagged cargo (A) or sortilin mediating lysosomal trafficking of other soluble factors (B). Some secretory cargo is sorted for regulated secretion (C), while other factors, such as basolateral cargo might be sorted for constitutive secretion, which is poorly characterized (D). Created with BioRender.com.

1.3.2.2 Dense-core secretory granule sorting

Peptide prohormones are sorted from the TGN to immature granules, which undergo cargo processing, such as prohormone cleavage, cargo aggregation, lumen acidification, missorted cargo retrieval, and ion exchange (Baker et al., 1988; Kuliawat et al., 1997; Orci et al., 1987). Therefore, immature granules undergo numerous changes and molecular events. Mature granules, on the other hand, are more static and are stored until a specific stimulus triggers regulated exocytosis (Kögel & Gerdes, 2010). The process of exocytosis is regulated by

calcium ions (Xue et al., 2021). During this tightly controlled reaction, the secretory granule's membrane fuses with the plasma membrane, and cargo is released from the cell (Gerber & Südhof, 2002).

Even though mature dense-core secretory granule formation is well-described, the sorting and packaging of cargo from the TGN into clathrin-coated vesicles is poorly understood (Dikeakos & Reudelhuber, 2007; Germanos et al., 2021; Orci et al., 1984). Several mechanisms have been proposed for Golgi exit. Initially, two basic mechanisms were proposed. Firstly, the existence of a specific sorting receptor ("sorting by entry") has been suggested in several studies, but the existence of one general sorting receptor has not been confirmed (Cool et al., 1997; Irminger et al., 1997). Secondly, a non-selective "bulk-flow" entry from TGN to the immature granule was proposed, and it was suggested that the content of the maturing granule is shaped by the selective exit of unwanted proteins, by the mechanism termed "sorting by exit". An example of a receptor sorting by exit is the M6PR, mediating the budding of small vesicles from maturing granules via AP1 (Klumperman et al., 1998). Currently, the general understanding is that various proteins likely end up in mature secretory granules through a combination of these mechanisms (Germanos et al., 2021). Very recently, a mechanism suggesting liquid-liquid phase separation of chromogranin B in beta cells has been proposed to aid proinsulin sorting at the TGN (Parchure et al., 2022).

1.3.3 Acrosome formation as a special type of secretion

In simple terms, a spermatozoon is a tightly compacted motile DNA package. Spermatids are the product of the meiotic division of spermatogonia in the testes and are an important developmental step toward mature sperm. Therefore, round spermatids undergo dramatic differentiation that changes the cell morphology, cell biology, and metabolism of the cell. During the process, several organelles are remodeled or discarded (Breucker et al., 1985). One essential organelle, the acrosome, however, is a characteristic feature of sperm cells. The acrosome is an acidic organelle that contains many receptors and enzymes that play a role in sperm-egg recognition and fusion and is irreversibly exocytosed upon sperm-egg contact (Tulsiani et al., 1998). The synthesis of heavily glycosylated acrosomal material begins during meiosis in spermatocytes. The cargo is trafficked out of the TGN and remains docked in proacrosomal vesicles near the Golgi apparatus until meiosis is fully completed and the round spermatid is formed (Anakwe, 1990; Escalier et al., 1991; Kashiwabara et al., 1990). In

the next step, the proacrosomal vesicles move towards the nucleus and attach to the nuclear membrane, forming a small single acrosome. The acrosome continues to receive cargo from the Golgi via vesicles, which allows it to grow and expand (Moreno et al., 2000). At the same time, the nucleus condenses and elongates. By the end of the maturation process, the acrosome covers most of the nuclear surface, except for the very posterior, where the tail is located. The process of acrosome formation mirrors the features of secretory granule formation, as well as lysosome formation (Khawar et al., 2019). Similarly to secretory granules, the acrosome contains certain secretory components and can be exocytosed. The resemblance of the acrosome with the lysosome is demonstrated by its acidic pH, the presence of lysosomal enzymes, and the presence of cargo derived from the Golgi as well as endosomal compartments. This led to the characterization of the acrosome as a secretory lysosome, which is a specialized dual-function organelle carrying out both lysosomal and secretory storage functions present in immune cells and melanocytes (Blott & Griffiths, 2002; Moreno & Alvarado, 2006). However, a truly unique feature of the acrosome is that it can form and secrete only a single time in the cell's lifetime.

1.4 Inceptor

1.4.1 Inceptor expression pattern in healthy tissue

Inceptor has been previously described as KIAA1324, EIG121, and ELAPOR1 in a handful of studies. Based on the human protein atlas, high expression has been found in the gastrointestinal tract, pancreas, prostate, and female reproductive tissues. Comparatively lower expression was seen in the brain, bronchus, and testis. Tissue-specific cell type analysis showed a specific enrichment in secretory cells and glands (Bilekova et al., 2023; The Human Protein Atlas). Among the secretory cell types, inceptor is expressed in both endocrine (pancreatic islets, pituitary, thyroid) and exocrine tissues (prostate, breast, gastric mucous cells), as well as special cell types (spermatids).

1.4.2 Inceptor expression in various cancers

It was shown that inceptor expression levels were increased in estrogen-replacement therapy and endometrial neoplastic proliferations associated with estrogen excess but not in other uterine tumors that do not rely on estrogen exposure (Deng et al., 2005). The expression of

inceptor was associated with shorter survival in advanced-stage ovarian/primary peritoneal high-grade serous carcinoma, and high co-expression with estrogen receptor alpha was predictive of shorter survival (Schlumbrecht et al., 2011). On the other hand, in gastric cancer, inceptor was associated with tumor suppression by interacting with 78 kDa glucose-regulated protein (GRP78) thereby blocking AKT activation (Kang et al., 2015).

1.4.3 Functional studies of inceptor

Further functional studies of inceptor have been done in the cell lines MCF-7 and T-Rex-293, which proposed the presence of inceptor in the endo-lysosomal system and linked inceptor to upregulation of autophagy and protection against cell death (Deng et al., 2010). Another study was done in the stomach, where inceptor was expressed specifically in zymogenic cells, gland cells that secrete pepsinogen and gastric lipase (Cho et al., 2022). The study builds upon the transcription factor Muscle, intestine and stomach expression 1 (MIST1), which supports secretion in several exocrine secretory tissues, such as pancreatic acinar cells and gastric zymogenic cells. It was demonstrated that inceptor is a target of MIST1, and in the stomach, it is associated with the Golgi and endosomal compartments. Inceptor knockout zymogenic cells showed defective secretory granule formation, suggesting the role of inceptor in cargo sorting at the TGN. Interestingly, no autophagy defect has been observed in knockout stomach tissue.

We have previously studied the role of inceptor on the cell surface of pancreatic beta cells (Ansarullah et al., 2021). Beta cells are the insulin-producing cells in the endocrine islets of Langerhans within the pancreatic tissue. Interestingly, as they release insulin upon a glucose stimulus, the local concentration of insulin rapidly increases. This potentially triggers the abundantly present cell-surface pool of IR. This would overactivate the IR signaling pathway and trigger downstream AKT signaling, potentially causing unwanted proliferation and altered metabolism. The mechanism by which beta cells avoid this overactivation is still unknown. We showed that on the cell surface, inceptor interacted with IR and IGF1R through AP-2 and facilitated their clathrin-mediated endocytosis, preventing active signaling. In inceptor knockout mice and cells, we found higher activity of the insulin/IGF signaling pathways. Therefore, inceptor could be a target to modulate the insulin-IGF signaling pathway and eventually diabetes progression.

Our most recent results were obtained from human-induced pluripotent stem cell-derived beta-like cells (SC-β-cells). We found greatly increased proinsulin and insulin stores, glucose-stimulated insulin secretion, and beta-cell survival in inceptor knockout cells (Siehler et al., in revision). We showed that inceptor interacted with proinsulin and insulin and targeted them toward lysosomes for degradation.

2 Aims of the thesis

This thesis offers a follow-up on our two most recent findings on inceptor in pancreatic beta cells, the first one describing how inceptor regulates receptor tyrosine kinases (Ansarullah et al., 2021) and the second one describing the intracellular trafficking and function of inceptor in the endo-lysosomal compartment (Siehler et al., in revision). These results help us understand the function of inceptor across different tissues and profile the role of this potentially druggable target in different diseases.

Aim 1: Describing inceptor in the context of spermatid development.

Male inceptor knockout mice were found to be infertile. This project aims to characterize male infertility caused by the lack of inceptor and link the function of inceptor in the testis tissue to its functions in pancreatic beta cells. By studying the acrosome formation defect in spermatid development, we can learn about the relationship between inceptor, lysosomes, and secretory granules and potentially apply the findings to the treatment of male infertility as well as other secretory diseases.

Aim 2: Understanding the role of inceptor in prostate cancer progression.

The insulin/IGF signaling pathways have been proposed as a molecular target in several cancers, yet specific targeting of this pathway has not been successful so far. Therefore, novel molecular targets that modulate this pathway could be used to develop therapies against various cancers. The scope of the project is to understand the role of inceptor in benign prostate tissue as well as prostate cancer and how inceptor modulates insulin/IGF signaling and metastatic processes, such as cell migration.

3 Methods

3.1 Mouse models

Animal experiments were carried out in compliance with the German Animal Protection Act and with the approved guidelines of the Society of Laboratory Animals (GV-SOLAS) and of the Federation of Laboratory Animal Science Associations (FELASA). The GeneTrap allele has been generated as previously described (Ansarullah et al., 2021). This mouse line was crossed with FLPe mice (Dymecki, 1996) and the floxed allele was generated (*Iir*^{fl}). Homozygous *Iir*$^{fl/fl}$ mice were crossed with the Rosa26R-Cre mouse line (Soriano, 1999) to delete the floxed region, resulting in heterozygous inceptor knockout mice (*Iir*$^{+/-}$). These mice were backcrossed onto a C57BL/6 J (Charles River) background and were further used for colony maintenance. Wildtype, heterozygous, and knockout mice were bred for organ withdrawal. For downstream analysis, tissues of males between the age of 9-12 weeks were used. The following primers were used to determine the genotype: 5′-CCAAGGCCAGCGATA CAACC-3′, 5′-GGAACTTCGTCGAGATAACTTCGTATAG-3′, 5′-GTGCACTCTGGGTAGTGT TC-3’.

3.2 Human samples

Informed written consent was obtained from all participants and the Ethics Committee of the University of Tübingen approved the protocol according to the Declaration of Helsinki. Benign and cancerous prostate tissue samples were acquired from newly diagnosed prostate cancer patients who did not receive hormone-altering therapy. The mean age of the patients was 64 years. The tissue samples were snap-frozen for ribonucleic acid (RNA) extraction or paraffinized for Gleason score determination. For immunohistochemistry, paraffin sections from prostate cancer patients aged 55-76 with a Gleason score of 3-4 were analyzed.

3.3 Cell culture

LNCaP cells (ATCC, CRL-1740) were cultured in RPMI 1640 supplemented with L-glutamine (Gibco) with 10% fetal bovine serum (FBS; PAN-Biotech) and passaged twice a week. For androgen deprivation experiments, the cells were seeded in a 6-well plate and cultured in RPMI 1640 without phenol red, supplemented with 10% charcoal-stripped FBS for five or

fourteen days. The medium was changed every two to three days. Cell line generation, as well as the proliferation, migration, and endocytosis assays, were performed by Katharina Wissmiller.

3.4 Immunofluorescence

Murine tissue was fixed in 4% paraformaldehyde (PFA) overnight at 4°C, washed with phosphate-buffered saline (PBS), and dehydrated in 10-30% sucrose. The tissue was embedded in a tissue-freezing medium (Leica) and frozen on dry ice. The samples were stored at -80°C. From the cryoblock, sections of 10 µm thickness were cut and dried on glass slides. The sections were kept frozen at -20°C.

For immunostaining, the cryo-sections were washed in PBS and permeabilized in 0.2% Triton-X100. Paraffin sections were deparaffinized by washing twice in xylol, rehydrated by a series of ethanol washes, from 100% to 40%, and finally rinsed in water. For antigen retrieval, the slides were boiled in 100 mmol/L sodium citrate, pH 6.0.

Both cryo-sections and paraffin sections were stained as follows. First, the tissue was blocked with 10% FBS, 0.1% bovine serum albumin (BSA), and 3% donkey serum in PBS with 0.1% Tween-20 (PBS-T) for one hour at room temperature, then incubated with primary antibodies (Table 1) diluted in blocking solution at 4°C overnight. Then, the slides were washed in PBS and PBS-T and incubated with secondary fluorophore-conjugated antibodies 1:800 (Table 2) and 4′,6-diamidino-2-phenylindole (DAPI) for 2-4 hours at room temperature. The slides were then washed in PBS and PBS-T and a coverslip was mounted on the slide with mounting medium (25% Glycerol, 10% Polyvinyl alcohol, 2% 1,4-Diazabicyclo [2.2.2] octan, 100 mM Tris). The slides were dried at room temperature overnight and imaged on a Zeiss LSM 880 Airyscan microscope. The images were acquired with Zen Black 2.3 (Zeiss) and the maximum intensity projection, brightness, and contrast adjustments, as well as noise reduction, were done in Fiji (Schindelin et al., 2012).

3.5 Co-immunoprecipitation (co-IP), western blotting, and mass spectrometry

LNCaP cells were seeded in 10-cm cell culture dishes and harvested after three days with lysis buffer (1% Triton-X-100, 20 mM Tris-HCl pH 7.5, 150 mM NaCl, 1 mM Ethylenediaminetetraacetic acid (EDTA)). After the cells were lysed, the lysate was centrifuged at 14,000 rpm, 4°C for 10 min. Murine testes were homogenized in a Potter-Elvehjem homogenizer in 125 mM KCl, 10 mM EDTA, 20 mM 4-(2-hydroxyethyl)-1-piperazineethanesulfonic acid (HEPES) (pH 7.2), and 1% protease inhibitor cocktail (Sigma). The homogenized tissue was transferred into a tube and centrifuged at 2000 *g*, 4°C for 10 min. the supernatant was retrieved, and Nonidet P-40 (NP-40) was added to a final concentration of 1% to solubilize the sample. A separate sample of the homogenate before centrifugation was taken and 1% NP-40 was added and this sample was sent to the core facility for mass spectrometry by Stefanie Hauck.

For co-immunoprecipitation, Protein G SureBeads (BioRad) were washed in PBS-T or Tris-buffered saline with 0.1% Tween-20 (TBS-T), incubated with corresponding antibodies (Table 1) for 30 minutes at room temperature, washed with PBS-T or TBS-T, and in case of testis samples, the beads were blocked with 1% BSA for 30 minutes, and washed with TBS-T. The lysate was added to the beads and incubated with agitation at 4°C overnight. The next day, the beads were washed with PBS-T or TBS-T and eluted into Laemmli buffer by boiling for 10 minutes for western blotting or heated to 60°C for 10 minutes for mass spectrometry. In parallel, the input sample was prepared and boiled with Laemmli buffer.

Western blot samples from cell lysates were prepared by lysis in radioimmunoprecipitation assay (RIPA) buffer, whereas tissue lysates were prepared by adding detergent to homogenized tissue, as described above. After measuring the protein content by Bicinchoninic acid (BCA) assay, protein concentration was adjusted and 10 µg of the sample was boiled in Laemmli buffer. The sample was loaded on an SDS-polyacrylamide gel (BioRad or made in-house) and the electrophoresis was run at 60-120 V. The separated sample was transferred to a polyvinylidene fluoride (PVDF) membrane by semi-dry blotting (BioRad). The membrane was blocked in 5% milk in TBS-T and incubated with primary antibodies diluted in milk or TBS-T at 4°C overnight (Table 1). The next day, the membrane was washed with TBS-T and

incubated with secondary horse-radish peroxidase (HRP)-coupled antibodies for one hour at room temperature (Table 2). The membrane was again washed in TBS-T and developed with Clarity Western enhanced chemiluminescence (ECL) Substrate (BioRad) with a ChemStudio western blot imager (Analytik Jena). Signal intensities were quantified by Fiji.

3.6 Transmission electron microscopy (TEM) sample preparation

The 16% PFA stock was prepared by heating powdered PFA in water, and the cooled stock was kept at -20°C. 4% PFA was prepared freshly by diluting the stock solution in 100 mM phosphate buffer pH 7.4 by mixing 100 mM dibasic sodium phosphate and 100 mM monobasic sodium phosphate 81:19. Isolated murine testes were pre-fixed in 4% PFA for 30 minutes at room temperature and cut in half, then fixed for another 1.5 hours at room temperature. For embedding in epoxy resin, the tissue was stored in 4% PFA at 4°C and for Tokuyasu cryo-sectioning for immunogold labeling, the tissue was transferred to 1% PFA. The samples were then sent to Thomas Kurth (TU Dresden) for further processing and imaging.

3.7 Statistical analysis

Statistical analysis was performed in GraphPad PRISM 9.0, and the statistical test is indicated in the respective figure legend.

3.8 List of antibodies

Table 1 – List of primary antibodies. * inceptor antibodies were provided by Regina Feederle, Monoclonal Antibody Core Facility, Helmholtz Munich

Antibody	**Species**	**Manufacturer**	**Catalog number**	**Application**
Anti-5HT	Rabbit	Neuromics	RA20080	Immunofluorescence
Anti-AP1M1	Rabbit	Thermo Fisher Scientific	PA5104319	Co-IP
Anti-AP2B2	Rabbit	Abcam	ab205014	Co-IP
Anti-AP3D1	Mouse	DSHB	anti-delta SA4	Co-IP
Anti-AR	Mouse	Santa Cruz	sc-7305	Western blot
Anti-AR	Rabbit	Abcam	Ab133273	Immunofluorescence

Anti-Cathepsin Z	Rabbit	Abcam	ab182575	Co-IP
Anti-CI-M6PR	Rabbit	Thermo Fisher Scientific	PA3-850	Immunofluorescence
Anti-Cytokeratin 5	Rabbit	Abcam	Ab53121	Immunofluorescence
Anti-Cytokeratin 8/18	Guinea pig	OriGene	BP5007	Immunofluorescence
Anti-DDX-4	Rabbit	Cell Signaling Technology	8761	Immunofluorescence
Anti-E-cadherin	Rabbit	Cell Signaling Technology	3195	Immunofluorescence
Anti-EGFR	Rabbit	Cell Signaling Technology	4267	Western blot
Anti-GAPDH	Rabbit	Cell Signaling Technology	2118	Western blot
Anti-GATA-4	Rat	Thermo Fisher Scientific	14–9980–80	Immunofluorescence
Anti-Giantin	Rabbit	BioLegend	924302	Immunofluorescence
Anti-GM130	Mouse	BD Biosciences	610822	Immunofluorescence
Anti-HSP90	Rabbit	Cell Signaling Technology	4874	Western blot
Anti-IGF1R	Rabbit	Cell Signaling Technology	3024	Immunofluorescence
Anti-IGF1R	Rabbit	Cell Signaling Technology	9750	Western blot Co-IP
*Anti-inceptor**	Mouse	*	31A11	Immunofluorescence
*Anti-inceptor**	Rat	*	2G6	Immunofluorescence
*Anti-inceptor**	Rat	*	16F6	Immunofluorescence Western blot TEM
Anti-IR	Mouse	Cell Signaling Technology	3020	Western blot Co-IP

Anti-LAMP1	Rat	BD Biosciences	533792	Immunofluorescence
Anti-LAMP2	Rat	Abcam	ab13524	Immunofluorescence
Anti-LYZL4	Rabbit	Proteintech	17443-1-AP	Western blot Co-IP
anti-MAP1B	Rabbit	Abcam	ab224115	Co-IP
Anti-phospho EGFR	Rabbit	Cell Signaling Technology	3777	Western blot
Anti-phospho IR/IGF1R	Rabbit	Cell Signaling Technology	3024	Western blot
Anti-PSA	Rabbit	Abcam	ab53774	Western blot
Anti-PSMA	Mouse	Abcam	ab19071	Western blot
Anti-SPACA1	Rabbit	Abcam	ab191843	Western blot
Anti-STX7	Rabbit	Proteintech	12322-1-AP	Co-IP
Anti-TGN38	Rabbit	Novus Biologicals	NBP1-03495SS	Immunofluorescence
Anti-β-adaptin	Mouse	BD Biosciences	610382	Western blot
Anti-γ-tubulin	Mouse	Sigma Aldrich	T5326	Western blot
control IgG	Mouse	Cell Signaling Technology	5415	Co-IP
control IgG	Rabbit	Cell Signaling Technology	3900	Co-IP

Table 2 – List of secondary antibodies

Antibody	**Species**	**Manufacturer**	**Catalog number**	**Conjugation**
Anti-guinea pig IgG	Donkey	Dianova	706-545-148	Alexa Flour 488
Anti-mouse IgG	Donkey	Invitrogen	A21202	Alexa Fluor 488
Anti-mouse IgG	Goat	Jackson ImmunoResearch	115-035-146	HRP

Anti-rabbit IgG	Donkey	Invitrogen	A21206	Alexa Flour 488
Anti-rabbit IgG	Donkey	Invitrogen	A31572	Alexa Flour 555
Anti-rabbit-IgG	Goat	Jackson ImmunoResearch	111-035-144	HRP
Anti-rat IgG	Donkey	Invitrogen	A21208	Alexa Flour 488
Anti-rat IgG	Donkey	Dianova	712-605-150	Alexa Flour 647
Anti-rat IgG	Donkey	Jackson ImmunoResearch	712–165–153	Cy3
Anti-rat IgG	Goat	Jackson ImmunoResearch	112-035-175	HRP

4 Publications for dissertation

Bilekova, S., Garcia-Colomer, B., Cebrian-Serrano, A., Schirge, S., Krey, K., Sterr, M., Kurth, T., Hauck, S., Lickert, H. (2023). Inceptor facilitates acrosomal vesicle formation in spermatids and is required for male fertility. *Front. Cell Dev. Biol. - Molecular and Cellular Reproduction*. doi: 10.3389/fcell.2023.1240039.

Summary.

Spermatogenesis is an essential process in mammalian reproduction that allows for the production of mature sperm. During spermatogenesis, a unique organelle, the acrosome, develops from material originating from the Golgi apparatus. The acrosome is a lysosome-related organelle that shows similarities with lysosomes and secretory granules. In this publication, we described inceptor to localize to the proacrosomal vesicles which deliver cargo between the Golgi and acrosomal vesicle, as well as temporarily to the acrosome. Inceptor knockout mice showed malformation of the acrosome and thus deformations of the nuclear shape, as well as a disrupted mitochondrial distribution. We performed mass spectrometry and co-immunoprecipitation experiments and pinpointed the knockout phenotype to vesicle-fusion defects. Our findings, alongside other studies across various cell types, confirm that inceptor acts as a sorting receptor for secretory granules and lysosomes.

Declaration of contribution.

I planned the experiments and communicated the objectives to the collaborators. I bred the mice for organ withdrawal, as well as maintained the mouse colony. I performed the organ withdrawal, as well as tissue processing for downstream analyses. I performed the immunostaining, microscopy, and image processing. I performed the co-immunoprecipitation and western blotting experiments. I analyzed and interpreted data. I structured and wrote the manuscript, as well as prepared the figures.

Wissmiller, K.*, Bilekova, S.*, Franko, A., Lutz, S. Z., Katsburg, M., Gulde, S., Pellegeta, N. S., Stenzl, A., Heni, M., Berti, L., Haering, H-U., Lickert, H. (2023). Inceptor correlates with markers of prostate cancer progression and modulates insulin/IGF1 signaling and cancer cell migration. *Mol. Metab.* 71, 101706. doi: 10.1016/J.MOLMET.2023.101706 (* Co-first author).

Summary.

Metastatic prostate cancers frequently become hormone-independent, while still relying on active proliferation and cell survival pathways. Therefore, different pathways of androgen-receptor activation are used by later-stage prostate cancers. Oftentimes, the insulin/IGF pathway is active and provides signaling for the maintenance of the proliferative and migratory phenotype. We studied inceptor as a modulator of the insulin/IGF signaling pathway and described its expression in the prostate tissue and prostate cancer cell lines. Inceptor expression levels positively correlated with prostate cancer markers in human prostate cancer samples and with AR activity in prostate cancer cell lines. Inceptor interacted with IR and IGF1R and modulated their activity and trafficking in cultured cells. Overexpression of inceptor induced a higher migratory phenotype and increased IGF1R signaling. In summary, these findings provide a basic understanding of the role of inceptor in prostate cancer progression.

Declaration of contribution.

I established the staining for inceptor in human prostate samples, stained the samples, acquired the images, and prepared the figure. Additionally, I cultured the LNCaP cell line for experiments. I performed the co-immunoprecipitation and some of the western blotting experiments, as well as analyzed data. I wrote parts of the manuscript. I critically reviewed the entire manuscript.

5 Discussion

Previously, we have described inceptor in the regulation of glucose homeostasis and insulin signaling in murine pancreatic beta cells (Ansarullah et al., 2021). Additionally, we have recently described the importance of not only beta cells but also neurons in improved glucose homeostasis in inceptor knockout mice (Grandl et al., 2024). The aim of this thesis is the further characterization of inceptor, a protein highly expressed across various tissues and potentially regulated in human disease. By further investigating the phenotype of the inceptor knockout murine line, I followed up on the infertility of homozygous inceptor knockout male mice. There is also an emerging body of literature on inceptor's role in various cancers, such as ovarian, endometrial, and breast cancer (Deng et al., 2005; Meseure et al., 2020; Schlumbrecht et al., 2011), which inspired our research on inceptor's role in prostate cancer as a prognostic marker and a potential therapeutic target.

5.1 Inceptor's role across various tissues

Inceptor is expressed across many organs and cell types, with enrichment in secretory cells. In most organs, inceptor localizes to the perinuclear area, specifically to or close to the Golgi or TGN compartments. In glandular tissue, such as the prostate, the salivary gland, or the stomach, inceptor is similarly localized in luminal cells, resulting in a polarized localization of inceptor towards the lumen. In the cell types investigated, we have observed inceptor trafficking between the TGN and endosomal compartments. In LNCaP cells, we demonstrated that a small portion of inceptor reached the plasma membrane from where it was again endocytosed. Whether inceptor also reaches the plasma membrane in spermatids is unknown, however, it might be of interest for pharmacological targeting of inceptor in developing spermatids.

5.1.1 Inceptor's role in the secretory cells of the stomach

Inceptor is a single-pass transmembrane receptor with a domain with similarities to M6P-binding domains, as well as to the growth-hormone binding domains of the insulin and IGF receptors. Yet, future studies will be needed to investigate its ability to bind M6P-tagged proteins and growth hormones. Nevertheless, due to structural similarities, inceptor has been previously compared to CI-M6PR (Cho et al., 2022). In this study, the interactome of both

inceptor and CI-M6PR suggested they might have related roles. While inceptor's binding partners hinted towards a role related to secretory granule formation, CI-M6PR had a more important role in lysosomal trafficking. Our findings in spermatids also suggest that while CI-M6PR likely carries out a well-described lysosomal delivery function, inceptor has a role in acrosome formation and proacrosomal vesicle fusion.

5.1.2 Inceptor as a proinsulin degradation receptor

We have also conducted a follow-up study on inceptor's role in pancreatic beta cells (Siehler et al., in revision). After our results in murine beta cells (Ansarullah et al., 2021), which indicate the increase in insulin signaling and improved insulin secretion in inceptor knockout beta cells, we have investigated the role of inceptor in SC-β-cells. SC-β-cells are derived from human induced pluripotent stem cells in a six-stage 40-day protocol *in vitro* by mimicking murine *in vivo* development (Velazco-Cruz et al., 2019). Inceptor knockout SC-β-cells presented an astounding accumulation in proinsulin and insulin and presented a superior glucose-stimulated insulin secretion capacity, as well as greater survival *in vitro* and after transplantation *in vivo*. We have uncovered that the increase in proinsulin levels can be explained by a reduction in proinsulin degradation, rather than increased transcription or defective secretion (Siehler et al., in revision).

Proinsulin is translated directly into the ER and continues through folding and disulfide bridge formation through the Golgi. From the TGN, it is sorted into immature granules by a heavily studied, yet incompletely understood mechanism. In immature granules, the C-chain of proinsulin is cleaved out, whereas the A and B chains form the mature insulin (Germanos et al., 2021; Omar-Hmeadi & Idevall-Hagren, 2021).

Even though proinsulin is the direct precursor of insulin, it has been shown to be degraded by several mechanisms (Goginashvili et al., 2015; Orci et al., 1984; Pasquier et al., 2019; Riahi et al., 2016; Yamamoto et al., 2018). Mechanistically, we propose different pathways by which inceptor reduces the proinsulin content of the cell. Building upon the foundation of inceptor bearing resemblance to the M6PRs, we propose that inceptor removes proinsulin from maturing granules, evidenced by the increase of proinsulin in mature granules of inceptor knockout mice (Siehler et al., in revision). Additionally, we propose inceptor to mediate the fusion of proinsulin-containing granules with lysosomes, analogously to the evidence that

inceptor aids the fusion of proacrosomal granules in spermatids. This direct fusion is called crinophagy and has been the first observed insulin degradation mechanism (Orci et al., 1984), with novel insights gained just recently (Vivot et al., 2020).

5.2 Inceptor in male infertility

The male infertility of inceptor knockout has been observed in mice in previous publications (Cho et al., 2022; T. Tang et al., 2010). However, a mechanistic explanation has not been provided in these studies. One study suggested the origin of infertility in the prostate, as inceptor is highly expressed in the secretory cells of prostate epithelium (Cho et al., 2022). We have established whole-body knockout mice and confirmed that the line cannot be maintained on a homozygous background, due to male infertility. To investigate the reason for male infertility of the inceptor knockout line, we found that spermatocytes isolated from inceptor knockout mice are characterized by a round head (globozoospermia) and reduced motility, as well as disorganized mitochondria. Therefore, we aimed to perform a detailed analysis of spermatogenesis in inceptor knockout mice and uncovered that inceptor-knockout spermatids develop a failure in proacrosomal vesicle fusion at the time of attachment to the nuclear surface.

5.2.1 Inceptor localization in murine testes

We analyzed the murine testis for inceptor expression and found the highest expression in early meiotic (pachytene) spermatocytes and early spermatids and no expression in late spermatids. By confocal microscopy, we could localize inceptor expression close to the acrosome and TGN but without significant overlap. By immunogold staining and TEM, we could localize inceptor to proacrosomal vesicles and small vesicles trafficking between the Golgi and acrosome. These results hinted towards a vesicle-related trafficking role of the inceptor. Thus, we analyzed the morphology of proacrosomal vesicles and acrosome development in inceptor knockout testes. Therefore, we employed TEM and concluded that acrosome development starts normally with proacrosomal vesicle formation and delivery to the site of acrosome formation. However, the proacrosomal vesicles fail to fuse into a single acrosomal vesicle. From this point on, we observed fragmentation of the acrosome, and even though the acrosome attachment site (acroplaxome) develops fully, the acrosome is mostly lacking. As we also found acrosomal material to partially colocalize with a lysosomal marker

in inceptor knockout spermatids, we concluded that the fragmented acrosome is eventually degraded.

5.2.2 Proteins essential for acrosome formation

Other murine knockouts of Golgi and vesicular proteins with defects in spermatogenesis have been described previously (Fujihara et al., 2012; Han et al., 2017; Pierre et al., 2012; Xiao et al., 2009; Yao et al., 2002). Interestingly, the knockout of protein interacting with C kinase 1 (PICK1) was also characterized by defects in acrosome formation. PICK1 is a membrane-curvature-modulating protein, which has been proposed to be important for cargo retrieval from immature insulin granules (Andersen et al., 2022; Xiao et al., 2009). Similarly, the knockout of Golgi-associated PDZ and coiled-coil motif-containing protein (GOPC), which has been shown to regulate insulin secretion, also shows fragmented acrosomes and round spermatids (Wilhelmi et al., 2021; Yao et al., 2002). Further mouse models with similar phenotypes are the Golgi matrix protein 130 (*Gm130)*$^{-/-}$, Sperm acrosome associated 1 (*Spaca1)*$^{-/-}$, and Zona-pellucida binding protein 1 (*Zpbp1)*$^{-/-}$ mice. All these show nuclear shape defects, as well as an acrosomal defect (Fujihara et al., 2012; Han et al., 2017; Lin et al., 2007).

5.2.3 M6PR in acrosome formation

As inceptor shows similarities with the M6PRs which also facilitate lysosomal delivery, we investigated whether the two receptors show overlap in testes. Interestingly, CI-M6PR showed a vesicular diffused staining and occasionally overlapped with lysosomes but did not seem to localize close to the acrosome. In inceptor knockout spermatids, CI-M6PR and lysosomes still occasionally overlap, and their patterns seem to be largely unaltered.

Interestingly, previous literature had conflicting results on the involvement of the M6PRs in acrosome formation. In the earliest studies, M6PRs were found to associate rather with LAMP1-positive vesicles and not to colocalize with the acrosome (Martínez-Menárguez et al., 1996). Follow-up studies suggested that in later stages of spermatid development, CI-M6PR transiently colocalized with acrosomes and it was proposed to potentially play a role in shaping the acrosomal content (Moreno, 2003). Opposing this publication, it has been shown that knocking out the M6PRs did not alter the acrosomal content of selected hydrolases,

suggesting that there is a different mechanism for their delivery in spermatids (Chayko & Orgebin-Crist, 2000).

5.2.4 Implications of inceptor's role in acrosome formation for other tissues

The acrosome has been characterized as a secretory lysosome or lysosome-related organelle, a specialized organelle with lysosomal and secretory functions (Blott & Griffiths, 2002; Moreno & Alvarado, 2006). Secretory lysosomes are unique organelles present in only a few cell types. The biogenesis of the acrosome is mainly facilitated by the delivery of Golgi-derived cargo in small vesicles, whereas lysosomes contain endocytosed material in addition to Golgi-derived constituents (Khawar et al., 2019). In addition to the involvement of the secretory and endosomal machinery, the autolysosome has been proposed to play an important role in acrosome development (Wang et al., 2014). Specifically, Atg7 has been shown to be indispensable for acrosome formation. In addition, Atg7 has also been shown to play a role in the degradation of proinsulin in beta cells (Riahi et al., 2016).

Given the similarities between the acrosome and secretory granules, as well as lysosomes and autophagosomes, results obtained in inceptor's role in acrosome development can potentially be translated to other secretory cells. This is underlined by findings in the secretory cell of the stomach, which suggest inceptor's role in secretory granule maturation (Cho et al., 2022) and beta cells, where inceptor is involved in immature granule degradation (Siehler, 2023).

5.2.5 Evidence of inceptor's role in autophagy

Early studies on inceptor suggested its involvement in autophagy regulation (Deng et al., 2010; Ran et al., 2017). Inceptor overexpression was shown to induce vacuole formation, a hallmark of autophagy in cancer cell lines, such as T-Rex-293, MDA-231-t, and JEC cells (Deng et al., 2010; Ran et al., 2017). However, how direct is the effect of inceptor on the vacuolation remains to be further characterized. On the other hand, knockdown of inceptor in JEC cells resulted in a mild reduction of the autophagy factor microtubule-associated protein 1B light chain 3B (LC3B)-positive puncta (Ran et al., 2017), similarly to inceptor knockout SC-β-cells (Siehler et al., in revision).

Interestingly, autophagy factors have also been suggested to play a role in acrosome formation (Wang et al., 2014). However, inceptor was not required for the autophagic activity of stomach cells (Cho et al., 2022). Nevertheless, future studies in inceptor knockout or overexpressing cells are necessary to determine whether inceptor directly affects autophagy.

5.2.6 Inceptor as a vesicle-fusion factor

We have proposed inceptor to be directly involved in vesicle-fusion processes in both pancreatic beta cells and spermatids. In beta cells, we found inceptor localized to the site of proinsulin-positive secretory granules and lysosomes (Siehler et al., in revision). This closely resembles the process of crinophagy, which has been demonstrated in both stress and starvation, as well as steady-state conditions. In stress and starvation, the process has been termed stress/starvation-induced nascent granule degradation (SINGD) and has been proposed to be mediated by the tetraspanin CD63, which mediates the routing of proinsulin granules to degradation (Pasquier et al., 2019). Under growth conditions, RAS-related protein Rab-7-interacting lysosomal protein (RILP) was shown to prevent insulin granule secretion and mediate the lysosomal degradation of proinsulin granules (Y. Zhou et al., 2020). Another study suggested the involvement of vesicle-associated membrane protein 4 (VAMP4) in mediating the fusion of immature proinsulin-containing granules or small vesicles that bud off of maturing granules with lysosomes (Li et al., 2022). The latter process has been proposed to be mediated by M6PRs, clathrin, and AP-1 (Klumperman et al., 1998; Kuliawat et al., 1997). VAMP4 potentially also mediates the delivery to lysosomes through its interaction with AP-1 (Hinners et al., 2003). We propose that inceptor is also involved in this process with a similar role to the M6PRs, albeit by directly binding proinsulin and thus being the only direct proinsulin trafficking receptor yet.

In spermatids, at the time of acrosome formation, inceptor is mostly localized to the proacrosomal vesicles and less frequently to the acrosome. Our analysis of inceptor's interactome in the testis revealed that several vesicle-fusion proteins interact with inceptor. For instance, the Ras-related protein Rab-3A, has been shown to mediate vesicle transport towards regulated exocytosis in beta cells and neurons (Leenders et al., 2001; Yaekura et al., 2003) and insulin granule degradation via macroautophagy (Marsh et al., 2007). Additionally, we identified syntaxins 7 and 12, both endosomal vesicle fusion factors as interactors of inceptor (Mullock et al., 2000; B. L. Tang et al., 1998). Another study also investigated the

interactome of inceptor and found several vesicular trafficking and Rab-associated proteins (Cho et al., 2022).

In summary, inceptor acts in different tissues by mediating vesicle or granule trafficking, delivery, and fusion. In the secretory cells of the stomach, inceptor is necessary for granule maturation (Cho et al., 2022). In pancreatic beta cells, inceptor acts as a proinsulin and insulin delivery receptor towards lysosomal degradation, either via direct routing or mediating granule-lysosome fusion events (Figure 6A) (Siehler et al., in revision). In spermatids, inceptor mediates acrosomal vesicle formation by mediating vesicle-fusion events at the site of acrosome formation and acting as an acrosomal trafficking protein (Figure 6B).

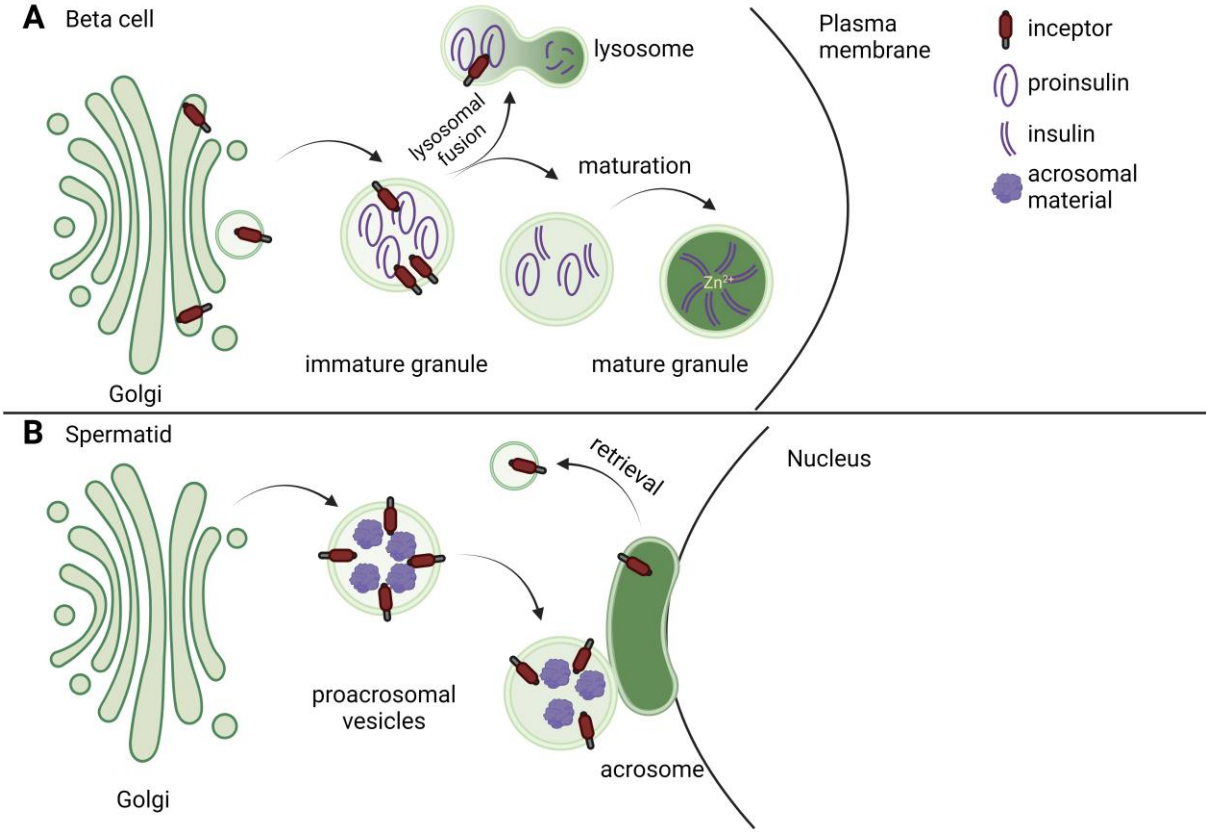

Figure 6 – Similarities between inceptor action in pancreatic beta cells (A) and developing spermatids (B). In beta cells, inceptor mostly localizes to the TGN and to a lesser extent immature insulin granules and lysosomes. Inceptor binds proinsulin and directs it for lysosomal degradation (A), adapted from (Siehler, 2023). In developing spermatids, inceptor is mostly localized to the proacrosomal vesicles and to a lesser extent to the acrosome, from which it is retrieved during maturation. Inceptor mediates the fusion between proacrosomal vesicles and the acrosome (B). Created with BioRender.com.

5.3 Inceptor in prostate cancer

Manipulating the insulin/IGF signaling pathway has been a proposed therapeutic approach for regulating the proliferation and survival of cancers (Pollak, 2008). The insulin/IGF signaling pathway is especially relevant in advanced prostate cancers, where it has a role in sustaining androgen signaling (Liu et al., 2023). Therefore, the development of therapeutics modulating insulin/IGF signaling is sought after. Considering our recent discovery of inceptor as a modulator of the insulin/IGF signaling pathway in pancreatic beta cells (Ansarullah et al., 2021), we have investigated the role of inceptor in healthy prostate and prostate cancer. We uncovered that inceptor overexpression in LNCaP cells increased IGF1R signaling and cell migration.

5.3.1 Inceptor expression in cancer

Previous studies have investigated the expression patterns of inceptor in various cancers. In pancreatic cancer, inceptor was downregulated (Wissmiller, 2021). Additionally, the expression of estrogen receptor β correlated with inceptor expression, and higher co-expression was also indicative of a better prognosis (Estrella et al., 2014). On the contrary, some subtypes of ovarian, endometrial, and breast cancer showed increased inceptor expression compared to healthy tissue. In ovarian cancer, it has been suggested that inceptor expression was induced by estrogen replacement therapy, and it promoted tumor growth *in vitro* (Deng et al., 2010; Ran et al., 2017). In high-grade serous ovarian carcinoma, high inceptor expression was predictive of shorter survival (Schlumbrecht et al., 2011). In breast cancer, inceptor expression varied based on the cancer subtype, however, high expression was observed with high hormone-receptor expression. At the same time, high inceptor expression was predictive of metastasis-free survival in invasive breast carcinomas (Meseure et al., 2020). Together, these studies linked inceptor to active hormone signaling in hormone-dependent cancers.

Based on our findings, inceptor expression positively correlated with the expression of PSA and prostate-specific membrane antigen (PSMA), two AR-regulated genes that are important biomarkers of prostate cancer. Therefore, higher inceptor expression is observed in more progressed cancers, similar to endometrial and ovarian carcinomas. Moreover, inceptor expression also correlated with the expression of the growth hormone receptors IR, IGF1R,

and epidermal growth factor receptor (EGFR). Another metric we investigated was the IR-A/IR-B ratio, which was found to be higher in prostate cancer tissue compared to benign tissue (Heni et al., 2012). IR-A binds insulin, IGF1, and IGF2 and preferentially activates the proliferative signaling pathways, whereas IR-B regulates metabolism (Belfiore et al., 2009; Leibiger et al., 2001). We found that inceptor positively correlated with this ratio, further suggesting the involvement of inceptor in the regulation of prostate cancer survival through the growth hormone pathway. Interestingly, another study profiling the expression of novel cancer markers found lower expression of inceptor to correlate with more aggressive prostate cancer (Stinnesbeck et al., 2021). It should be noted that this study analyzed samples across all prostate cancer stages, while our samples were only taken from patients who had not previously received hormone-altering therapy. These results illustrate the complexity and variability of marker expression across patient cohorts.

5.3.2 The role of inceptor in AR activation

Furthermore, we aimed to investigate the regulation of inceptor expression. Interestingly, during androgen deprivation, LNCaP cells upregulated their inceptor levels with the same pattern as PSMA. At the same time, active nuclear AR localization correlated with inceptor expression under androgen deprivation conditions. These results are in line with our hypothesis of the involvement of inceptor in sustaining AR activity, possibly through its cross-activation via the IGF1R.

5.3.3 The role of inceptor in growth hormone signaling

Tamoxifen-inducible β-cell-specific knockout of inceptor increased IR/IGF1R signaling in murine islets as evidenced by increased phosphorylation of the IR/IGF1R and AKT (Ansarullah et al., 2021). Inceptor overexpression in the MIN6 cell line, on the other hand, increased the phosphorylation of IR/IGF1R.

To further investigate whether inceptor modulates the growth hormone pathway in prostate cancer, we studied inceptor in the LNCaP cell line. Similarly to beta cell lines, inceptor bound both the IR and IGF1R. We also found that inceptor overexpressing cells increased their IGF1R pool on the membrane, as well as upregulated the phosphorylation levels of IR or IGF1R when stimulated with IGF1. Further, inceptor overexpression increased cell migration

but not proliferation in LNCaP cells. These results suggest that inceptor positively regulates IGF1R signaling and allows for cross-activation of AR under androgen-deprivation conditions in LNCaP cells. These findings also highlight the different regulation of the IR/IGF1R pathways by inceptor in different cell lines, as inceptor overexpression in the murine insulinoma cell line MIN6 had a negative effect on the IR/IGF1R signaling (Ansarullah et al., 2021).

The limitation of the study of inceptor in LNCaP cells was the technical difficulty achieving a knockout or knockdown in LNCaP cells. Despite Katharina Wissmiller's efforts to achieve a Clustered Regularly Interspaced Short Palindromic Repeats (CRISPR)/Cas9-mediated knockout, these attempts did not yield successful results (Wissmiller, 2021). Loss-of-function studies are important for understanding the molecular functions of proteins and are particularly useful in comparing different loss-of-function phenotypes with cancer progression. Given that lower expression levels in pancreatic neuroendocrine tumors have been linked to a more favorable prognosis (Estrella et al., 2014), and since inceptor has been shown to induce tumor growth *in vitro* (Ran et al., 2017), exploring loss-of-function studies can provide deeper insights into tumor suppression in the absence of inceptor. In particular, loss-of-function studies could provide more mechanistic insight into inceptor’s role in the IGF signaling pathway.

In summary, this thesis has explored the role of inceptor, a protein that plays significant roles in various biological processes, including glucose homeostasis, insulin signaling, cancer, and male infertility. Initially, our studies highlighted how inceptor affects insulin signaling and secretion in pancreatic beta cells, showing that mice lacking inceptor exhibit improved glucose homeostasis. Further research expanded our understanding to include inceptor's importance in proinsulin and insulin homeostasis, with a focus on proinsulin degradation. We also investigated inceptor's role in male fertility, identifying its essential function in the formation of the acrosome, a key structure in sperm cells. Moreover, we also described the function of inceptor in prostate cancer, suggesting inceptor's potential as a marker of disease progression. Mechanistically, our key observations include inceptor's presence in secretory and glandular tissues, its involvement in the transport of cellular vesicles in different cell types, and its potential involvement in vesicle fusion events. Further investigation of the mechanism of inceptor’s action across various tissues could serve as a base for the development of targeted therapies.

5.4 Future research directions

Considering the limited number of publications exploring the molecular mechanisms of inceptor, there is a clear need for additional research to comprehensively understand its role in health and disease. This could serve as a basis for the development of targeted therapies.

Firstly, we have good evidence of inceptor acting as an insulin/proinsulin degradation receptor in beta cells. Additionally, future studies could explore whether other peptide hormones or growth factors also interact with inceptor and what is the physiological effect of this interaction. Additionally, therapies targeting inceptor for the improvement of glucose homeostasis in diabetes could offer novel antidiabetic treatment.

In cancer research, it might be worthwhile to further investigate inceptor in the progression of different types of cancer, particularly hormone-dependent cancers. This could open new possibilities for cancer diagnostics and therapy.

Finding out that inceptor's roles are linked across different tissues and processes shows us that learning about its function in one area could help us understand its roles in others. This approach could lead to new ways to treat diseases, including metabolic disorders, infertility, and cancer.

6 List of publications

Siehler, J.*, Bilekova, S.*, Chapouton, P. Dema, A., Albanese, P., Tamara, S., Jain, C., Sterr, M., Enos, S.J., Chen, C., Malhotra, C., Villalba, A,., Schomann, L., Bhattacharya, S., Feng, J., Akgün, M., Ribaudo, F., Ansarullah, Burtscher, I., … Lickert, H. **Inceptor binds and directs insulin to lysosomal degradation in β-cells.** *In revision*, *Co-first author

Grandl, G., Collden, G., Feng, J., Bhattacharya, S., Klingelhuber, F., Schomann, L., **Bilekova, S.**, Ansarullah, Xu, W., Far, F. F., Tost, M., Gruber, T., Bastidas-Ponce, A., Zhang, Q., Novikoff, A., Liskiewicz, A., Liskiewicz, D., Garcia-Caceres, C., Feuchtinger, A., … Müller, T. D. (2024). **Global, neuronal or β cell-specific deletion of inceptor improves glucose homeostasis in male mice with diet-induced obesity**. *Nature Metabolism* 2024, 1–10. https://doi.org/10.1038/s42255-024-00991-3

Bilekova, S., Garcia-Colomer, B., Cebrian-Serrano, A., Schirge, S., Krey, K., Sterr, M., Kurth, T., Hauck, S. M., & Lickert, H. (2023). **Inceptor facilitates acrosomal vesicle formation in spermatids and is required for male fertility.** *Frontiers in Cell and Developmental Biology*, *11*, 1240039. https://doi.org/10.3389/FCELL.2023.1240039

Wissmiller, K.*, **Bilekova, S.***, Franko, A., Lutz, S. Z., Katsburg, M., Gulde, S., Pellegata, N. S., Stenzl, A., Heni, M., Berti, L., Häring, H.-U., & Lickert, H. (2023**). Inceptor correlates with markers of prostate cancer progression and modulates insulin/IGF1 signaling and cancer cell migration.** *Molecular Metabolism*, *71*, 101706. https://doi.org/10.1016/J.MOLMET.2023.101706, *Co-first author

Jain, C., Ansarullah, **Bilekova, S.**, & Lickert, H. (2022). **Targeting pancreatic β cells for diabetes treatment.** In *Nature Metabolism* (Vol. 4, Issue 9, pp. 1097–1108). Nat Metab. https://doi.org/10.1038/s42255-022-00618-5

Bilekova, S., Sachs, S., & Lickert, H. (2021). **Pharmacological Targeting of Endoplasmic Reticulum Stress in Pancreatic Beta Cells.** *Trends in Pharmacological Sciences*, *42*(2), 85–95. https://doi.org/10.1016/J.TIPS.2020.11.011

Ansarullah, Jain, C., Far, F. F., Homberg, S., Wißmiller, K., von Hahn, F. G., Raducanu, A., Schirge, S., Sterr, M., **Bilekova, S.**, Siehler, J., Wiener, J., Oppenländer, L., Morshedi, A., Bastidas-Ponce, A., Collden, G., Irmler, M., Beckers, J., Feuchtinger, A., … Lickert, H. (2021**). Inceptor counteracts insulin signalling in β-cells to control glycaemia.** *Nature*, *590*(7845), 326–331. https://doi.org/10.1038/s41586-021-03225-8

Truong, M. E., **Bilekova, S.**, Choksi, S. P., Li, W., Bugaj, L. J., Xu, K., & Reiter, J. F. (2021). **Vertebrate cells differentially interpret ciliary and extraciliary cAMP.** *Cell*, *184*(11), 2911-2926.e18. https://doi.org/10.1016/j.cell.2021.04.002

7 Abbreviations

AP-1, 2, 3	Adaptor protein complex 1, 2, 3
AR	Androgen receptor
BCA	Bicinchoninic acid
BSA	Bovine serum albumin
co-IP	Co-immunoprecipitation
CRISPR	Clustered Regularly Interspaced Short Palindromic Repeats
DAPI	4′,6-diamidino-2-phenylindole
DHT	Dihydrotestosterone
DNA	Deoxyribonucleic acid
ECL	Enhanced chemiluminescence
EDTA	Ethylenediaminetetraacetic acid
EGFR	Epidermal growth factor receptor
ER	Endoplasmic reticulum
FBS	Fetal bovine serum
FELASA	Federation of European Laboratory Animal Science Associations
GGA	γ ear-containing, ADP-ribosylation factor-binding protein
Gm130	Golgi matrix protein 130
GOPC	Golgi associated PDZ and coiled-coil motif containing
GRP78	78 kDa glucose-regulated protein
GV-SOLAS	Gesellschaft für Versuchstierkunde / Society of Laboratory Animal Science
HEPES	4-(2-hydroxyethyl)-1-piperazineethanesulfonic acid
HRP	Horse-radish peroxidase
IGF	Insulin-like growth factor
IGF1/2R	Insulin-like growth factor 1/2 receptor
IIR	Insulin inhibitory receptor
IR	Insulin receptor
IRS1/2	Insulin receptor substrate 1/2
JAK2	Janus kinase 2
LC3B	Microtubule-associated protein 1B light chain 3B
LIMP-2	Lysosomal integral membrane protein-2
LNCaP	Lymph node metastasis of prostate cancer (cell line)
M6P	Mannose-6-phosphate
M6PR	Mannose-6-phosphate receptor
mAb	Monoclonal antibody
MAPK	Mitogen-activated protein kinase
MIST1	Muscle, intestine and stomach expression 1 (transcription factor)
mTORC2	Mammalian target of rapamycin complex 2
NP-40	Nonidet P-40
PBS	Phosphate-buffered saline
PBS-T	Phosphate-buffered saline with 0.1 %Tween 20
PFA	Paraformaldehyde
PI3K	Phosphoinositide 3-kinases
PICK1	Protein Interacting with C Kinase 1
PSA	Prostate-specific antigen
PSMA	Prostate-specific membrane antigen
PTB	Phosphotyrosine-binding (domain)
PVDF	Polyvinylidene fluoride
RAS	Rat sarcoma virus (protein)
RILP	Rab-interacting lysosomal protein
RIPA	Radioimmunoprecipitation assay
RNA	Ribonucleic acid

SC-β-cells	Human-induced pluripotent stem cell-derived beta-like cells
SH2	Src-homology-2
SINGD	Stress/starvation-induced nascent granule degradation
Spaca1	Sperm Acrosome Associated 1
STAT	Signal transducers and activators of transcription
TBS-T	Tris-buffered saline with 0.1 % Tween20
TEM	Transmission electron microscopy
TGN	*Trans*-Golgi network
VAMP4	Vesicle-associated membrane protein 4
Zpbp1	Zona-pellucida binding protein 1

8 Acknowledgements

Completing this thesis was a challenging journey. My advisors provided invaluable guidance, while the support from friends, family, and my partner was crucial in sustaining my momentum. Now, reflecting on this journey, I'm grateful for the collective support that made this achievement possible. This experience was more than an academic task; it was a journey of personal growth and shared success.

Firstly, I must express my profound thanks to Heiko, whose guidance and supervision have been unwavering. His support for my ideas, coupled with his invaluable input, has profoundly shaped my academic journey. To the thesis committee, Prof. Hrabe de Angelis and Dr. Ussar, thank you for the enriching scientific discussions and the constructive ideas and comments that have significantly contributed to the refinement of this work. I would also like to thank all the collaborators who supported and greatly contributed to this thesis.

A special thank you to Donna, whose administrative assistance and friendliness have made navigating the bureaucratic maze a much more pleasant experience. Your support has not gone unnoticed. My appreciation extends to the graduate schools for their meticulous administration and the outstanding education program they offer.

I extend my heartfelt gratitude to our lab managers, Kerstin and Emily, whose leadership and expertise have been pivotal in our lab's success. Additionally, a special thanks to our technicians Timo, Carola, Ines, Jessica, and Lisa, whose dedication and hard work ensure the smooth operation of our lab.

The original members of the inceptor group—Sarah, Ansar, Chirag, Marbod, Katha, and of course Johanna. Your collaboration and support have been a constant source of motivation. Sarah, thank you for introducing me to the basics of inceptor and helping me find my footing in the lab. A special shoutout to Katha, for our great collaboration and her thoughtful feedback on my thesis, as well as for becoming a cherished friend. Johanna, my biggest thanks to you for trusting me with your project, for the incredible partnership in the lab, and for being an extraordinary colleague and friend.

To those who joined the project later—Federico, Prisca, Sreya, Jin, Pei, Weiwei, Carola, Alessandro, and Leo—each of you has made coming to work every day a bit more joyful.

Federico, for being an excellent conference partner and friend, Prisca for your fun and friendly spirit, Pei for your kindness and trust, Jin for your generosity and kindness, Caro for her tender and always ready-to-help spirit, and Alessandro for the laughs and deep conversations. Sreya and Leo, meeting you and sharing countless adventures has been one of the highlights of this journey. A warm welcome to the newest members, Ana, Carolina, and Gea, who I trust will carry the project forward with the same passion and dedication.

To the rest of IDR, your collective efforts create an environment where discovery and innovation can flourish. It has been a great pleasure to work alongside all of you.

To my family, who supported my move to Germany and stayed connected through our weekly long calls—your support has been my pillar of strength.

Last but certainly not least, to my husband, Karsten, the most amazing person I've had the privilege of sharing this journey with. From our days as master's students to the partners we have become, your support, encouragement, and love have been the foundation of my achievements. Thank you for being my partner in every sense of the word.

This acknowledgment, while trying to capture my gratitude, hardly does justice to the depth of my appreciation for each of you. Thank you for being a part of my journey.

9 References

Aaron, L. T., Franco, O. E., & Hayward, S. W. (2016). Review of Prostate Anatomy and Embryology and the Etiology of BPH. *The Urologic Clinics of North America*, *43*(3), 279. https://doi.org/10.1016/J.UCL.2016.04.012

Abate-Shen, C., & de Almeida, F. N. (2022). Establishment of the LNCaP cell line – the dawn of an era for prostate cancer research. *Cancer Research*, *82*(9), 1689. https://doi.org/10.1158/0008-5472.CAN-22-1065

Ahearn, T. U., Peisch, S., Pettersson, A., Ebot, E. M., Zhou, C. K., Graff, R. E., Sinnott, J. A., Fazli, L., Judson, G. L., Bismar, T. A., Rider, J. R., Gerke, T., Chan, J. M., Fiorentino, M., Flavin, R., Sesso, H. D., Finn, S., Giovannucci, E. L., Gleave, M., … Mucci, L. A. (2018). Expression of IGF/insulin receptor in prostate cancer tissue and progression to lethal disease. *Carcinogenesis*, *39*(12), 1431–1437. https://doi.org/10.1093/CARCIN/BGY112

Aldana, A., Carneiro, J., Martínez-Mekler, G., & Darszon, A. (2021). Discrete Dynamic Model of the Mammalian Sperm Acrosome Reaction: The Influence of Acrosomal pH and Physiological Heterogeneity. *Frontiers in Physiology*, *0*, 932. https://doi.org/10.3389/FPHYS.2021.682790

Anakwe, O. O. (1990). Acrosome biogenesis begins during meiosis: evidence from the synthesis and distribution of an acrosomal glycoprotein, acrogranin, during guinea pig spermatogenesis. *Biology of Reproduction*, *42*(2), 317–328. https://doi.org/10.1095/biolreprod42.2.317

Andersen, R. C., Schmidt, J. H., Rombach, J., Lycas, M. D., Christensen, N. R., Lund, V. K., Stapleton, D. S., Pedersen, S. S., Olsen, M. A., Stoklund, M., Noes-Holt, G., Nielsen, T. T. E., Keller, M. P., Jansen, A. M., Herlo, R., Pietropaolo, M., Simonsen, J. B., Kjærulff, O., Holst, B., … Madsen, K. L. (2022). Coding variants identified in patients with diabetes alter PICK1 BAR domain function in insulin granule biogenesis. *The Journal of Clinical Investigation*, *132*(5). https://doi.org/10.1172/JCI144904

Ansarullah, Jain, C., Far, F. F., Homberg, S., Wißmiller, K., von Hahn, F. G., Raducanu, A., Schirge, S., Sterr, M., Bilekova, S., Siehler, J., Wiener, J., Oppenländer, L., Morshedi, A., Bastidas-Ponce, A., Collden, G., Irmler, M., Beckers, J., Feuchtinger, A., … Lickert, H. (2021). Inceptor counteracts insulin signalling in β-cells to control glycaemia. *Nature*, *590*(7845), 326–331. https://doi.org/10.1038/s41586-021-03225-8

Baker, E. N., Blundell, T. L., Cutfield, J. F., Cutfield, S. M., Dodson, E. J., Dodson, G. G., Hodgkin, D. M., Hubbard, R. E., Isaacs, N. W., & Reynolds, C. D. (1988). The structure of 2Zn pig insulin crystals at 1.5 A resolution. *Philosophical Transactions of the Royal Society of London. Series B, Biological Sciences*, *319*(1195), 369–456. https://doi.org/10.1098/RSTB.1988.0058

Bashir, M. N. (2015). Epidemiology of Prostate Cancer. *Asian Pacific Journal of Cancer Prevention : APJCP*, *16*(13), 5137–5141. https://doi.org/10.7314/APJCP.2015.16.13.5137

Belfiore, A., Frasca, F., Pandini, G., Sciacca, L., & Vigneri, R. (2009). Insulin receptor isoforms and insulin receptor/insulin-like growth factor receptor hybrids in physiology and disease. *Endocrine Reviews*, *30*(6), 586–623. https://doi.org/10.1210/ER.2008-0047

Bilekova, S., Garcia-Colomer, B., Cebrian-Serrano, A., Schirge, S., Krey, K., Sterr, M., Kurth, T., Hauck, S. M., & Lickert, H. (2023). Inceptor facilitates acrosomal vesicle formation in

spermatids and is required for male fertility. *Frontiers in Cell and Developmental Biology*, *11*, 1240039. https://doi.org/10.3389/fcell.2023.1240039

Blott, E. J., & Griffiths, G. M. (2002). Secretory lysosomes. In *Nature Reviews Molecular Cell Biology* (Vol. 3, Issue 2, pp. 122–131). Nature Publishing Group. https://doi.org/10.1038/nrm732

Bonifacino, J. S., & Traub, L. M. (2003). Signals for Sorting of Transmembrane Proteins to Endosomes and Lysosomes. *Annual Review of Biochemistry, (Vol. 72, pp. 395–447)*. https://doi.org/10.1146/annurev.biochem.72.121801.161800

Braulke, T., & Bonifacino, J. S. (2009). Sorting of lysosomal proteins. *Biochimica et Biophysica Acta (BBA) - Molecular Cell Research*, *1793*(4), 605–614. https://doi.org/10.1016/j.bbamcr.2008.10.016

Breucker, H., Schäfer, E., & Holstein, A. F. (1985). Morphogenesis and fate of the residual body in human spermiogenesis. *Cell and Tissue Research*, *240*(2), 303–309. https://doi.org/10.1007/BF00222339

Broggi, G., Lo Giudice, A., Di Mauro, M., Pricoco, E., Piombino, E., Ferro, M., Caltabiano, R., Morgia, G., & Russo, G. I. (2021). Insulin signaling, androgen receptor and PSMA immunohistochemical analysis by semi-automated tissue microarray in prostate cancer with diabetes (DIAMOND study). *Translational Research*, *238*, 25–35. https://doi.org/10.1016/J.TRSL.2021.07.002

Buchanan, G., Irvine, R. A., Coetzee, G. A., & Tilley, W. D. (2001). Contribution of the androgen receptor to prostate cancer predisposition and progression. *Cancer Metastasis Reviews*, *20*(3–4), 207–223. https://doi.org/10.1023/A:1015531326689

Cancer.Net. (2023). *Prostate Cancer: Statistics | Cancer.Net*. https://www.cancer.net/cancer-types/prostate-cancer/statistics

Chayko, C. A., & Orgebin-Crist, M. C. (2000). Targeted disruption of the cation-dependent or cation-independent mannose 6-phosphate receptor does not decrease the content of acid glycosidases in the acrosome. *Journal of Andrology*, *21*(6), 944–953. https://doi.org/10.1002/J.1939-4640.2000.TB03426.X

Cheng, C. Y., & Mruk, D. D. (2010). The biology of spermatogenesis: The past, present and future. In *Philosophical Transactions of the Royal Society B: Biological Sciences* (Vol. 365, Issue 1546, pp. 1459–1463). The Royal Society. https://doi.org/10.1098/rstb.2010.0024

Chi, K. N., Gleave, M. E., Fazli, L., Goldenberg, S. L., So, A., Kollmannsberger, C., Murray, N., Tinker, A., & Pollak, M. (2012). A phase II pharmacodynamic study of preoperative figitumumab in patients with localized prostate cancer. *Clinical Cancer Research : An Official Journal of the American Association for Cancer Research*, *18*(12), 3407–3413. https://doi.org/10.1158/1078-0432.CCR-12-0482

Cho, C. J., Park, D., & Mills, J. C. (2022). ELAPOR1 is a secretory granule maturation-promoting factor that is lost during paligenosis. *American Journal of Physiology. Gastrointestinal and Liver Physiology*, *322*(1), G49–G65. https://doi.org/10.1152/AJPGI.00246.2021

Claessens, F., Denayer, S., Van Tilborgh, N., Kerkhofs, S., Helsen, C., & Haelens, A. (2008). Diverse roles of androgen receptor (AR) domains in AR-mediated signaling. *Nuclear Receptor Signaling*, *6*. https://doi.org/10.1621/NRS.06008

Clavijo, R. I., & Hsiao, W. (2018). Update on male reproductive endocrinology. *Translational Andrology and Urology*, *7*(Suppl 3), S367–S372.

https://doi.org/10.21037/TAU.2018.03.25

Cool, D. R., Normant, E., Shen, F. S., Chen, H. C., Pannell, L., Zhang, Y., & Loh, Y. P. (1997). Carboxypeptidase E is a regulated secretory pathway sorting receptor: Genetic obliteration leads to endocrine disorders in Cpe(fat) mice. *Cell*, *88*(1), 73–83. https://doi.org/10.1016/S0092-8674(00)81860-7

Day, K. J., Staehelin, L. A., & Glick, B. S. (2013). A Three-Stage Model of Golgi Structure and Function. *Histochemistry and Cell Biology*, *140*(3), 239. https://doi.org/10.1007/S00418-013-1128-3

Deng, L., Broaddus, R. R., McCampbell, A., Shipley, G. L., Loose, D. S., Stancel, G. M., Pickar, J. H., & Davies, P. J. A. (2005). Identification of a novel estrogen-regulated gene, EIG121, induced by hormone replacement therapy and differentially expressed in type I and type II endometrial cancer. *Clinical Cancer Research : An Official Journal of the American Association for Cancer Research*, *11*(23), 8258–8264. https://doi.org/10.1158/1078-0432.CCR-05-1189

Deng, L., Feng, J., & Broaddus, R. R. (2010). The novel estrogen-induced gene EIG121 regulates autophagy and promotes cell survival under stress. *Cell Death & Disease*, *1*(4), e32. https://doi.org/10.1038/CDDIS.2010.9

Dikeakos, J. D., & Reudelhuber, T. L. (2007). Sending proteins to dense core secretory granules: still a lot to sort out. *Journal of Cell Biology*, *177*(2), 191–196. https://doi.org/10.1083/JCB.200701024

Doi, T., Kuboki, Y., Naito, Y., Ishida, M., Tanaka, T., & Takeuchi, Y. (2022). A phase 1 trial of xentuzumab, an IGF-neutralizing antibody, in Japanese patients with advanced solid tumors. *Cancer Science*, *113*(3), 1010–1017. https://doi.org/10.1111/CAS.15231

Du, Z., & Lovly, C. M. (2018). Mechanisms of receptor tyrosine kinase activation in cancer. *Molecular Cancer 2018 17:1*, *17*(1), 1–13. https://doi.org/10.1186/S12943-018-0782-4

Dymecki, S. M. (1996). Flp recombinase promotes site-specific DNA recombination in embryonic stem cells and transgenic mice. *Proceedings of the National Academy of Sciences of the United States of America*, *93*(12), 6191. https://doi.org/10.1073/PNAS.93.12.6191

Ebina, Y., Ellis, L., Jarnagin, K., Edery, M., Graf, L., Clauser, E., Ou, J. hsiung, Masiarz, F., Kan, Y. W., Goldfine, I. D., Roth, R. A., & Rutter, W. J. (1985). The human insulin receptor cDNA: The structural basis for hormone-activated transmembrane signalling. *Cell*, *40*(4), 747–758. https://doi.org/10.1016/0092-8674(85)90334-4

Escalier, D., Gallo, J. M., Albert, M., Meduri, G., Bermudez, D., David, G., & Schrevel, J. (1991). Human acrosome biogenesis: Immunodetection of proacrosin in primary spermatocytes and of its partitioning pattern during meiosis. *Development*, *113*(3), 779–788. https://doi.org/10.1242/dev.113.3.779

Estrella, J. S., Ma, L. T., Milton, D. R., Yao, J. C., Wang, H., Rashid, A., & Broaddus, R. R. (2014). Expression of estrogen-induced genes and estrogen receptor β in pancreatic neuroendocrine tumors: implications for targeted therapy. *Pancreas*, *43*(7), 996–1002. https://doi.org/10.1097/MPA.0000000000000203

Feldman, B. J., & Feldman, D. (2001). The development of androgen-independent prostate cancer. *Nature Reviews Cancer 2001 1:1*, *1*(1), 34–45. https://doi.org/10.1038/35094009

Feng, Y., He, D., Yao, Z., & Klionsky, D. J. (2013). The machinery of macroautophagy. *Cell Research 2014 24:1*, *24*(1), 24–41. https://doi.org/10.1038/cr.2013.168

Fujihara, Y., Satouh, Y., Inoue, N., Isotani, A., Ikawa, M., & Okabe, M. (2012). SPACA1-deficient male mice are infertile with abnormally shaped sperm heads reminiscent of globozoospermia. *Development*, *139*(19), 3583–3589. https://doi.org/10.1242/dev.081778

Gadila, S. K. G., & Kim, K. (2016). Cargo trafficking from the trans-Golgi network towards the endosome. *Biology of the Cell*, *108*(8), 205–218. https://doi.org/10.1111/BOC.201600001

Gangavarapu, K. J., Jowdy, P. F., Foster, B. A., & Huss, W. J. (2022). Role of prostate stem cells and treatment strategies in benign prostate hyperplasia. *American Journal of Clinical and Experimental Urology*, *10*(3), 154–169. http://www.ncbi.nlm.nih.gov/pubmed/35874288

Gao, J., Chesebrough, J. W., Cartlidge, S. A., Ricketts, S. A., Incognito, L., Veldman-Jones, M., Blakey, D. C., Tabrizi, M., Jallal, B., Trail, P. A., Coats, S., Bosslet, K., & Chang, Y. S. (2011). Dual IGF-I/II-neutralizing antibody MEDI-573 potently inhibits IGF signaling and tumor growth. *Cancer Research*, *71*(3), 1029–1040. https://doi.org/10.1158/0008-5472.CAN-10-2274

Gasmi, A., Roubaud, G., Dariane, C., Barret, E., Beauval, J. B., Brureau, L., Créhange, G., Fiard, G., Fromont, G., Gauthé, M., Ruffion, A., Renard-Penna, R., Sargos, P., Rouprêt, M., Ploussard, G., & Mathieu, R. (2022). Overview of the Development and Use of Akt Inhibitors in Prostate Cancer. *Journal of Clinical Medicine*, *11*(1), 160. https://doi.org/10.3390/JCM11010160

Gerber, S. H., & Südhof, T. C. (2002). Molecular determinants of regulated exocytosis. *Diabetes*, *51 Suppl 1*. https://doi.org/10.2337/DIABETES.51.2007.S3

Germanos, M., Gao, A., Taper, M., Yau, B., & Kebede, M. A. (2021). Inside the insulin secretory granule. In *Metabolites* (Vol. 11, Issue 8). Multidisciplinary Digital Publishing Institute (MDPI). https://doi.org/10.3390/metabo11080515

Goginashvili, A., Zhang, Z., Erbs, E., Spiegelhalter, C., Kessler, P., Mihlan, M., Pasquier, A., Krupina, K., Schieber, N., Cinque, L., Morvan, J., Sumara, I., Schwab, Y., Settembre, C., & Ricci, R. (2015). Insulin secretory granules control autophagy in pancreatic cells. *Science*, *347*(6224), 878–882. https://doi.org/10.1126/science.aaa2628

Grandl, G., Collden, G., Feng, J., Bhattacharya, S., Klingelhuber, F., Schomann, L., Bilekova, S., Ansarullah, Xu, W., Far, F. F., Tost, M., Gruber, T., Bastidas-Ponce, A., Zhang, Q., Novikoff, A., Liskiewicz, A., Liskiewicz, D., Garcia-Caceres, C., Feuchtinger, A., … Müller, T. D. (2024). Global, neuronal or β cell-specific deletion of inceptor improves glucose homeostasis in male mice with diet-induced obesity. *Nature Metabolism 2024*, 1–10. https://doi.org/10.1038/s42255-024-00991-3

Gu, F., Crump, C. M., & Thomas, G. (2001). Trans-Golgi network sorting. *Cellular and Molecular Life Sciences : CMLS*, *58*(8), 1067. https://doi.org/10.1007/PL00000922

Han, F., Liu, C., Zhang, L., Chen, M., Zhou, Y., Qin, Y., Wang, Y., Chen, M., Duo, S., Cui, X., Bao, S., & Gao, F. (2017). Globozoospermia and lack of acrosome formation in GM130-deficient mice. *Cell Death & Disease 2017 8:1*, *8*(1), e2532–e2532. https://doi.org/10.1038/cddis.2016.414

Heni, M., Hennenlotter, J., Scharpf, M., Lutz, S. Z., Schwentner, C., Todenhöfer, T., Schilling, D., Kühs, U., Gerber, V., Machicao, F., Staiger, H., Häring, H. U., & Stenzl, A. (2012). Insulin Receptor Isoforms A and B as well as Insulin Receptor Substrates-1 and -2 Are Differentially Expressed in Prostate Cancer. *PLoS ONE*, *7*(12). https://doi.org/10.1371/JOURNAL.PONE.0050953

Hinners, I., Wendler, F., Fei, H., Thomas, L., Thomas, G., & Tooze, S. A. (2003). AP-1 recruitment to VAMP4 is modulated by phosphorylation-dependent binding of PACS-1. *EMBO Reports*, *4*(12), 1182–1189. https://doi.org/10.1038/sj.embor.7400018

Horoszewicz, J. S., Leong, S. S., Kawinski, E., Karr, J. P., Rosenthal, H., Chu, T. M., Mirand, E. A., & Murphy, G. P. (1983). LNCaP model of human prostatic carcinoma. *Cancer Research*, *43*(4), 1809–1818. http://www.ncbi.nlm.nih.gov/pubmed/6831420

Hoxhaj, G., & Manning, B. D. (2019). The PI3K–AKT network at the interface of oncogenic signalling and cancer metabolism. *Nature Reviews Cancer 2019 20:2*, *20*(2), 74–88. https://doi.org/10.1038/s41568-019-0216-7

Hu, Y. B., Dammer, E. B., Ren, R. J., & Wang, G. (2015). The endosomal-lysosomal system: From acidification and cargo sorting to neurodegeneration. *Translational Neurodegeneration*, *4*(1), 1–10. https://doi.org/10.1186/S40035-015-0041-1

Irminger, J. C., Verchere, C. B., Meyer, K., & Halban, P. A. (1997). Proinsulin targeting to the regulated pathway is not impaired in carboxypeptidase E-deficient Cpe(fat)/Cpe(fat) mice. *Journal of Biological Chemistry*, *272*(44), 27532–27534. https://doi.org/10.1074/jbc.272.44.27532

Ittmann, M. (2018). Anatomy and Histology of the Human and Murine Prostate. *Cold Spring Harbor Perspectives in Medicine*, *8*(5). https://doi.org/10.1101/CSHPERSPECT.A030346

Ittmann, M., Huang, J., Radaelli, E., Martin, P., Signoretti, S., Sullivan, R., Simons, B. W., Ward, J. M., Robinson, B. D., Chu, G. C., Loda, M., Thomas, G., Borowsky, A., & Cardiff, R. D. (2013). Animal models of human prostate cancer: The consensus report of the new york meeting of the mouse models of human cancers consortium prostate pathology committee. *Cancer Research*, *73*(9), 2718–2736. https://doi.org/10.1158/0008-5472.CAN-12-4213

James, E. R., Carrell, D. T., Aston, K. I., Jenkins, T. G., Yeste, M., & Salas-Huetos, A. (2020). The Role of the Epididymis and the Contribution of Epididymosomes to Mammalian Reproduction. *International Journal of Molecular Sciences*, *21*(15), 1–17. https://doi.org/10.3390/IJMS21155377

Kaighn, M. E., Narayan, K. S., Ohnuki, Y., Lechner, J. F., & Jones, L. W. (1979). Establishment and characterization of a human prostatic carcinoma cell line (PC-3). *Investigative Urology*, *17*(1), 16–23. http://www.ncbi.nlm.nih.gov/pubmed/447482

Kang, J. M., Park, S., Kim, S. J., Kim, H., Lee, B., Kim, J., Park, J., Kim, S. T., Yang, H. K., Kim, W. H., & Kim, S. J. (2015). KIAA1324 suppresses gastric cancer progression by inhibiting the oncoprotein GRP78. *Cancer Research*, *75*(15), 3087–3097. https://doi.org/10.1158/0008-5472.CAN-14-3751

Kashiwabara, S., Arai, Y., Kodaira, K., & Baba, T. (1990). Acrosin biosynthesis in meiotic and postmelotic spermatogenic cells. *Biochemical and Biophysical Research Communications*, *173*(1), 240–245. https://doi.org/10.1016/S0006-291X(05)81047-2

Khawar, M. B., Gao, H., & Li, W. (2019). Mechanism of Acrosome Biogenesis in Mammals. In *Frontiers in Cell and Developmental Biology* (Vol. 7, p. 195). Frontiers. https://doi.org/10.3389/fcell.2019.00195

Kienzle, C., & von Blume, J. (2014). Secretory cargo sorting at the trans-Golgi network. *Trends in Cell Biology*, *24*(10), 584–593. https://doi.org/10.1016/j.tcb.2014.04.007

Klumperman, J., Kuliawat, R., Griffith, J. M., Geuze, H. J., & Arvan, P. (1998). Mannose 6-phosphate receptors are sorted from immature secretory granules via adaptor protein

AP-1, clathrin, and syntaxin 6-positive vesicles. *The Journal of Cell Biology*, *141*(2), 359–371. https://doi.org/10.1083/JCB.141.2.359

Kögel, T., & Gerdes, H. H. (2010). Maturation of secretory granules. *Results and Problems in Cell Differentiation*, *50*, 1–20. https://doi.org/10.1007/400_2009_31

Kuliawat, R., Klumperman, J., Ludwig, T., & Arvan, P. (1997). Differential sorting of lysosomal enzymes out of the regulated secretory pathway in pancreatic β-cells. In *Journal of Cell Biology* (Vol. 137, Issue 3, pp. 595–608). J Cell Biol. https://doi.org/10.1083/jcb.137.3.595

Leenders, A. G. M., Lopes da Silva, F. H., Ghijsen, W. E. J. M., & Verhage, M. (2001). Rab3A Is Involved in Transport of Synaptic Vesicles to the Active Zone in Mouse Brain Nerve Terminals. *Molecular Biology of the Cell*, *12*(10), 3095. https://doi.org/10.1091/MBC.12.10.3095

Leibiger, B., Leibiger, I. B., Moede, T., Kemper, S., Kulkarni, R. N., Kahn, C. R., De Vargas, L. M., & Berggren, P. O. (2001). Selective insulin signaling through A and B insulin receptors regulates transcription of insulin and glucokinase genes in pancreatic beta cells. *Molecular Cell*, *7*(3), 559–570. https://doi.org/10.1016/S1097-2765(01)00203-9

Lemmon, M. A., & Schlessinger, J. (2010). Cell Signaling by Receptor Tyrosine Kinases. *Cell*, *141*(7), 1117–1134. https://doi.org/10.1016/J.CELL.2010.06.011

LeRoith, D., Holly, J. M. P., & Forbes, B. E. (2021). Insulin-like growth factors: Ligands, binding proteins, and receptors. *Molecular Metabolism*, *52*, 101245. https://doi.org/10.1016/J.MOLMET.2021.101245

Li, M., Feng, F., Feng, H., Hu, P., Xue, Y., Xu, T., & Song, E. (2022). VAMP4 regulates insulin levels by targeting secretory granules to lysosomes. *Journal of Cell Biology*, *221*(10). https://doi.org/10.1083/jcb.202110164

Lin, Y.-N., Roy, A., Yan, W., Burns, K. H., & Matzuk, M. M. (2007). Loss of Zona Pellucida Binding Proteins in the Acrosomal Matrix Disrupts Acrosome Biogenesis and Sperm Morphogenesis. *Molecular and Cellular Biology*, *27*(19), 6794. https://doi.org/10.1128/MCB.01029-07

Litwin, M. S., & Tan, H. J. (2017). The diagnosis and treatment of prostate cancer: A review. *JAMA - Journal of the American Medical Association*, *317*(24), 2532–2542. https://doi.org/10.1001/jama.2017.7248

Liu, G., Zhu, M., Zhang, M., & Pan, F. (2023). Emerging Role of IGF-1 in Prostate Cancer: A Promising Biomarker and Therapeutic Target. *Cancers*, *15*(4). https://doi.org/10.3390/CANCERS15041287

Lonergan, P. E., & Tindall, D. J. (2011). *Androgen receptor signaling in prostate cancer development and progression*. https://doi.org/10.4103/1477-3163.83937

Loy, C. J., Sim, K. S., & Yong, E. L. (2003). Filamin-A fragment localizes to the nucleus to regulate androgen receptor and coactivator functions. *Proceedings of the National Academy of Sciences of the United States of America*, *100*(8), 4562–4567. https://doi.org/10.1073/PNAS.0736237100

Lutz, S. Z., Todenhöfer, T., Wagner, R., Hennenlotter, J., Ferchl, J. M., Scharpf, M. O., Martus, P., Staiger, H., Fritsche, A., Stenzl, A., Häring, H. U., & Heni, M. (2018). Higher prevalence of lymph node metastasis in prostate cancer in patients with diabetes. *Endocrine-Related Cancer*, *25*(3), L19–L22. https://doi.org/10.1530/ERC-17-0465

Margolis, B. (1999). The PTB Domain: The Name Doesn't Say It All. *Trends in Endocrinology & Metabolism*, *10*(7), 262–267. https://doi.org/10.1016/S1043-

2760(99)00168-X

Marsh, B. J., Soden, C., Alarcón, C., Wicksteed, B. L., Yaekura, K., Costin, A. J., Morgan, G. P., & Rhodes, C. J. (2007). Regulated autophagy controls hormone content in secretory-deficient pancreatic endocrine beta-cells. *Molecular Endocrinology (Baltimore, Md.)*, *21*(9), 2255–2269. https://doi.org/10.1210/ME.2007-0077

Martínez-Menárguez, J. A., Geuze, H. J., & Ballesta, J. (1996). Evidence for a nonlysosomal origin of the acrosome. *Journal of Histochemistry and Cytochemistry*, *44*(4), 313–320. https://doi.org/10.1177/44.4.8601690

McNeal, J. E. (1981). The zonal anatomy of the prostate. *The Prostate*, *2*(1), 35–49. https://doi.org/10.1002/PROS.2990020105

Meseure, D., Drak Alsibai, K., Vacher, S., Hatem, R., Nicolas, A., Callens, C., Lerebours, F., & Bieche, I. (2020). Altered Expression of Three EGFR Posttranslational Regulators MDGI, MIG6, and EIG121 in Invasive Breast Carcinomas. *Analytical Cellular Pathology (Amsterdam)*, *2020*. https://doi.org/10.1155/2020/9268236

Moreno, R. D. (2003). Differential expression of lysosomal associated membrane protein (LAMP-1) during mammalian spermiogenesis. *Molecular Reproduction and Development*, *66*(2), 202–209. https://doi.org/10.1002/MRD.10342

Moreno, R. D., & Alvarado, C. P. (2006). The mammalian acrosome as a secretory lysosome: New and old evidence. *Molecular Reproduction and Development*, *73*(11), 1430–1434. https://doi.org/10.1002/MRD.20581

Moreno, R. D., Ramalho-Santos, J., Sutovsky, P., Chan, E. K. L., & Schatten, G. (2000). Vesicular traffic and golgi apparatus dynamics during mammalian spermatogenesis: implications for acrosome architecture. *Biology of Reproduction*, *63*(1), 89–98. https://doi.org/10.1095/BIOLREPROD63.1.89

Mullock, B. M., Smith, C. W., Ihrke, G., Bright, N. A., Lindsay, M., Parkinson, E. J., Brooks, D. A., Parton, R. G., James, D. E., Luzio, J. P., & Piper, R. C. (2000). Syntaxin 7 Is Localized to Late Endosome Compartments, Associates with Vamp 8, and Is Required for Late Endosome–Lysosome Fusion. *Molecular Biology of the Cell*, *11*(9), 3137. https://doi.org/10.1091/MBC.11.9.3137

O'Donnell, L., Smith, L. B., & Rebourcet, D. (2022). Sertoli cells as key drivers of testis function. *Seminars in Cell & Developmental Biology*, *121*, 2–9. https://doi.org/10.1016/J.SEMCDB.2021.06.016

Oakberg, E. F. (1956). A description of spermiogenesis in the mouse and its use in analysis of the cycle of the seminiferous epithelium and germ cell renewal. *American Journal of Anatomy*, *99*(3), 391–413. https://doi.org/10.1002/AJA.1000990303

Omar-Hmeadi, M., & Idevall-Hagren, O. (2021). Insulin granule biogenesis and exocytosis. *Cellular and Molecular Life Sciences*, *78*(5), 1957–1970. https://doi.org/10.1007/S00018-020-03688-4

Orci, L., Ravazzola, M., Amherdt, M., Yanaihara, C., Yanaihara, N., Halban, P., Renold, A. E., & Perrelet, A. (1984). Insulin, not C-peptide (proinsulin), is present in crinophagic bodies of the pancreatic B-cell. *Journal of Cell Biology*, *98*(1), 222–228. https://doi.org/10.1083/jcb.98.1.222

Orci, L., Ravazzola, M., Storch, M. J., Anderson, R. G. W., Vassalli, J. D., & Perrelet, A. (1987). Proteolytic maturation of insulin is a post-Golgi event which occurs in acidifying clathrin-coated secretory vesicles. *Cell*, *49*(6), 865–868. https://doi.org/10.1016/0092-8674(87)90624-6

Ozanne, D. M., Brady, M. E., Cook, S., Gaughan, L., Neal, D. E., & Robson, C. N. (2000). Androgen receptor nuclear translocation is facilitated by the f-actin cross-linking protein filamin. *Molecular Endocrinology (Baltimore, Md.)*, *14*(10), 1618–1626. https://doi.org/10.1210/MEND.14.10.0541

Parchure, A., Tian, M., Stalder, D., Boyer, C. K., Bearrows, S. C., Rohli, K. E., Zhang, J., Rivera-Molina, F., Ramazanov, B. R., Mahata, S. K., Wang, Y., Stephens, S. B., Gershlick, D. C., & von Blume, J. (2022). Liquid-liquid phase separation facilitates the biogenesis of secretory storage granules. *The Journal of Cell Biology*, *221*(12). https://doi.org/10.1083/JCB.202206132

Pasquier, A., Vivot, K., Erbs, E., Spiegelhalter, C., Zhang, Z., Aubert, V., Liu, Z., Senkara, M., Maillard, E., Pinget, M., Kerr-Conte, J., Pattou, F., Marciniak, G., Ganzhorn, A., Ronchi, P., Schieber, N. L., Schwab, Y., Saftig, P., Goginashvili, A., & Ricci, R. (2019). Lysosomal degradation of newly formed insulin granules contributes to β cell failure in diabetes. *Nature Communications*, *10*(1), 3312. https://doi.org/10.1038/s41467-019-11170-4

Pawson, T., Gish, G. D., & Nash, P. (2001). SH2 domains, interaction modules and cellular wiring. *Trends in Cell Biology*, *11*(12), 504–511. https://doi.org/10.1016/S0962-8924(01)02154-7

Pienta, K. J., & Bradley, D. (2006). Mechanisms underlying the development of androgen-independent prostate cancer. *Clinical Cancer Research : An Official Journal of the American Association for Cancer Research*, *12*(6), 1665–1671. https://doi.org/10.1158/1078-0432.CCR-06-0067

Pierre, V., Martinez, G., Coutton, C., Delaroche, J., Yassine, S., Novella, C., Pernet-Gallay, K., Hennebicq, S., Ray, P. F., & Arnoult, C. (2012). Absence of Dpy19l2, a new inner nuclear membrane protein, causes globozoospermia in mice by preventing the anchoring of the acrosome to the nucleus. *Development*, *139*(16), 2955–2965. https://doi.org/10.1242/dev.077982

Pollak, M. (2008). Insulin and insulin-like growth factor signalling in neoplasia. *Nature Reviews Cancer 2008 8:12*, *8*(12), 915–928. https://doi.org/10.1038/nrc2536

Ran, X., Zhou, P., & Zhang, K. (2017). Autophagy plays an important role in stemness mediation and the novel dual function of EIG121 in both autophagy and stemness regulation of endometrial carcinoma JEC cells. *International Journal of Oncology*, *51*(2), 644–656. https://doi.org/10.3892/ijo.2017.4047

Rehfeld, A., Nylander, M., & Karnov, K. (2017). Glandular Epithelium and Glands. *Compendium of Histology*, 101–120. https://doi.org/10.1007/978-3-319-41873-5_6

Riahi, Y., Wikstrom, J. D., Bachar-Wikstrom, E., Polin, N., Zucker, H., Lee, M. S., Quan, W., Haataja, L., Liu, M., Arvan, P., Cerasi, E., & Leibowitz, G. (2016). Autophagy is a major regulator of beta cell insulin homeostasis. *Diabetologia*, *59*(7), 1480–1491. https://doi.org/10.1007/s00125-016-3868-9

Roudsari, N. M., Lashgari, N. A., Momtaz, S., Abaft, S., Jamali, F., Safaiepour, P., Narimisa, K., Jackson, G., Bishayee, A., Rezaei, N., Abdolghaffari, A. H., & Bishayee, A. (2021). Inhibitors of the PI3K/Akt/mTOR Pathway in Prostate Cancer Chemoprevention and Intervention. *Pharmaceutics*, *13*(8). https://doi.org/10.3390/PHARMACEUTICS13081195

Ruizeveld De Winter, J. A., Trapman, J., Vermey, M., Mulder, E., Zegers, N. D., & Van der Kwast, T. H. (1991). Androgen receptor expression in human tissues: An immunohistochemical study. *Journal of Histochemistry and Cytochemistry*, *39*(7), 927–936. https://doi.org/10.1177/39.7.1865110

Schindelin, J., Arganda-Carreras, I., Frise, E., Kaynig, V., Longair, M., Pietzsch, T., Preibisch, S., Rueden, C., Saalfeld, S., Schmid, B., Tinevez, J. Y., White, D. J., Hartenstein, V., Eliceiri, K., Tomancak, P., & Cardona, A. (2012). Fiji: an open-source platform for biological-image analysis. *Nature Methods*, *9*(7), 676–682. https://doi.org/10.1038/NMETH.2019

Schlessinger, J. (2000). Cell Signaling by Receptor Tyrosine Kinases. *Cell*, *103*(2), 211–225. https://doi.org/10.1016/S0092-8674(00)00114-8

Schlumbrecht, M. P., Xie, S.-S., Shipley, G. L., Urbauer, D. L., & Broaddus, R. R. (2011). Molecular clustering based on ERα and EIG121 predicts survival in high-grade serous carcinoma of the ovary/peritoneum. *Modern Pathology : An Official Journal of the United States and Canadian Academy of Pathology, Inc*, *24*(3), 453–462. https://doi.org/10.1038/modpathol.2010.211

Siehler, J. (2023). *Characterizing the function of inceptor and ELAPOR2 in human stem cell-derived pancreatic beta cells*. Doctoral thesis.

Siehler, J., Bilekova, S., Chapouton, P. Dema, A., Albanese, P., Tamara, S., Jain, C., Sterr, M., Enos, S.J., Chen, C., Malhotra, C., Villalba, A,., Schomann, L., Bhattacharya, S., Feng, J., Akgün, M., Ribaudo, F., Ansarullah, Burtscher, I., … Lickert, H. Inceptor binds and directs insulin to lysosomal degradation in β-cells. *In revision*

Soriano, P. (1999). Generalized lacZ expression with the ROSA26 Cre reporter strain. *Nature Genetics*, *21*(1), 70–71. https://doi.org/10.1038/5007

Stinnesbeck, M., Kristiansen, A., Ellinger, J., Hauser, S., Egevad, L., Tolkach, Y., & Kristiansen, G. (2021). Prognostic role of TSPAN1, KIAA1324 and ESRP1 in prostate cancer. *APMIS : Acta Pathologica, Microbiologica, et Immunologica Scandinavica*, *129*(4), 204–212. https://doi.org/10.1111/APM.13117

Tang, B. L., Tan, A. E. H., Lim, L. K., Lee, S. S., Low, D. Y. H., & Hong, W. (1998). Syntaxin 12, a member of the syntaxin family localized to the endosome. *The Journal of Biological Chemistry*, *273*(12), 6944–6950. https://doi.org/10.1074/JBC.273.12.6944

Tang, T., Li, L., Tang, J., Li, Y., Lin, W. Y., Martin, F., Grant, D., Solloway, M., Parker, L., Ye, W., Forrest, W., Ghilardi, N., Oravecz, T., Platt, K. A., Rice, D. S., Hansen, G. M., Abuin, A., Eberhart, D. E., Godowski, P., … De Sauvage, F. J. (2010). A mouse knockout library for secreted and transmembrane proteins. *Nature Biotechnology*, *28*(7), 749–755. https://doi.org/10.1038/nbt.1644

Taylor, B. S., Schultz, N., Hieronymus, H., Gopalan, A., Xiao, Y., Carver, B. S., Arora, V. K., Kaushik, P., Cerami, E., Reva, B., Antipin, Y., Mitsiades, N., Landers, T., Dolgalev, I., Major, J. E., Wilson, M., Socci, N. D., Lash, A. E., Heguy, A., … Gerald, W. L. (2010). Integrative genomic profiling of human prostate cancer. *Cancer Cell*, *18*(1), 11–22. https://doi.org/10.1016/J.CCR.2010.05.026

Tissue Cell Type - ELAPOR1 - The Human Protein Atlas. Retrieved April 6, 2023, from https://www.proteinatlas.org/ENSG00000116299-ELAPOR1/tissue+cell+type

Tortorella, E., Giantulli, S., Sciarra, A., & Silvestri, I. (2023). AR and PI3K/AKT in Prostate Cancer: A Tale of Two Interconnected Pathways. *International Journal of Molecular Sciences 2023, Vol. 24, Page 2046*, *24*(3), 2046. https://doi.org/10.3390/IJMS24032046

Tulsiani, D. R. P., Abou-Haila, A., Loeser, C. R., & Pereira, B. M. J. (1998). The biological and functional significance of the sperm acrosome and acrosomal enzymes in mammalian fertilization. *Experimental Cell Research*, *240*(2), 151–164. https://doi.org/10.1006/EXCR.1998.3943

Ullrich, A., Bell, J. R., Chen, E. Y., Herrera, R., Petruzzelli, L. M., Dull, T. J., Gray, A., Coussens, L., Liao, Y. C., Tsubokawa, M., Mason, A., Seeburg, P. H., Grunfeld, C., Rosen, O. M., & Ramachandran, J. (1985). Human insulin receptor and its relationship to the tyrosine kinase family of oncogenes. *Nature 1985 313:6005*, *313*(6005), 756–761. https://doi.org/10.1038/313756a0

Van Bokhoven, A., Varella-Garcia, M., Korch, C., Johannes, W. U., Smith, E. E., Miller, H. L., Nordeen, S. K., Miller, G. J., & Lucia, M. S. (2003). Molecular characterization of human prostate carcinoma cell lines. *The Prostate*, *57*(3), 205–225. https://doi.org/10.1002/PROS.10290

Velazco-Cruz, L., Song, J., Maxwell, K. G., Goedegebuure, M. M., Augsornworawat, P., Hogrebe, N. J., & Millman, J. R. (2019). Acquisition of Dynamic Function in Human Stem Cell-Derived β Cells. *Stem Cell Reports*, *12*(2), 351–365. https://doi.org/10.1016/j.stemcr.2018.12.012

Vivot, K., Pasquier, A., Goginashvili, A., & Ricci, R. (2020). Breaking Bad and Breaking Good: β-Cell Autophagy Pathways in Diabetes. *Journal of Molecular Biology*, *432*(5), 1494–1513. https://doi.org/10.1016/J.JMB.2019.07.030

Wang, H., Wan, H., Li, X., Liu, W., Chen, Q., Wang, Y., Yang, L., Tang, H., Zhang, X., Duan, E., Zhao, X., Gao, F., & Li, W. (2014). Atg7 is required for acrosome biogenesis during spermatogenesis in mice. *Cell Research 2014 24:7*, *24*(7), 852–869. https://doi.org/10.1038/cr.2014.70

Wei, Z., & Liu, H. T. (2002). MAPK signal pathways in the regulation of cell proliferation in mammalian cells. *Cell Research 2002 12:1*, *12*(1), 9–18. https://doi.org/10.1038/sj.cr.7290105

Wilhelmi, I., Grunwald, S., Gimber, N., Popp, O., Dittmar, G., Arumughan, A., Wanker, E. E., Laeger, T., Schmoranzer, J., Daumke, O., & Schürmann, A. (2021). The ARFRP1-dependent Golgi scaffolding protein GOPC is required for insulin secretion from pancreatic β-cells. *Molecular Metabolism*, *45*. https://doi.org/10.1016/J.MOLMET.2020.101151

Wissmiller, K. (2021). *The role of IGFR-L1 in Insulin Signalling of Pancreatic β-cells and Hormone-dependent Cancers*. Doctoral thesis.

Wissmiller, K., Bilekova, S., Franko, A., Lutz, S. Z., Katsburg, M., Gulde, S., Pellegata, N. S., Stenzl, A., Heni, M., Berti, L., Häring, H.-U., & Lickert, H. (2023). Inceptor correlates with markers of prostate cancer progression and modulates insulin/IGF1 signaling and cancer cell migration. *Molecular Metabolism*, *71*, 101706. https://doi.org/10.1016/J.MOLMET.2023.101706

Wright, A. S., Thomas, L. N., Douglas, R. C., Lazier, C. B., & Rittmaster, R. S. (1996). Relative potency of testosterone and dihydrotestosterone in preventing atrophy and apoptosis in the prostate of the castrated rat. *The Journal of Clinical Investigation*, *98*(11), 2558–2563. https://doi.org/10.1172/JCI119074

Wu, H. -C, Hsieh, J. -T, Gleave, M. E., Brown, N. M., Pathak, S., & Chung, L. W. K. (1994). Derivation of androgen-independent human LNCaP prostatic cancer cell sublines: role of bone stromal cells. *International Journal of Cancer*, *57*(3), 406–412. https://doi.org/10.1002/IJC.2910570319

Xiao, N., Kam, C., Shen, C., Jin, W., Wang, J., Kwong, M. L., Jiang, L., & Xia, J. (2009). PICK1 deficiency causes male infertility in mice by disrupting acrosome formation. *The Journal of Clinical Investigation*, *119*(4), 802. https://doi.org/10.1172/JCI36230

Xue, R., Meng, H., Yin, J., Xia, J., Hu, Z., & Liu, H. (2021). The Role of Calmodulin vs.

Synaptotagmin in Exocytosis. *Frontiers in Molecular Neuroscience*, *14*, 691363. https://doi.org/10.3389/FNMOL.2021.691363/BIBTEX

Yaekura, K., Julyan, R., Wicksteed, B. L., Hays, L. B., Alarcon, C., Sommers, S., Poitout, V., Baskin, D. G., Wang, Y., Philipson, L. H., & Rhodes, C. J. (2003). Insulin secretory deficiency and glucose intolerance in Rab3A null mice. *The Journal of Biological Chemistry*, *278*(11), 9715–9721. https://doi.org/10.1074/JBC.M211352200

Yamamoto, S., Kuramoto, K., Wang, N., Cordoba-Chacon, J., & Layden, B. T. (2018). Autophagy Differentially Regulates Insulin Production and Insulin Sensitivity. *Cell Reports*, *23*, 3286–3299. https://doi.org/10.1016/j.celrep.2018.05.032

Yao, R., Ito, C., Natsume, Y., Sugitani, Y., Yamanaka, H., Kuretake, S., Yanagida, K., Sato, A., Toshimori, K., & Noda, T. (2002). Lack of acrosome formation in mice lacking a Golgi protein, GOPC. *Proceedings of the National Academy of Sciences*, *99*(17), 11211–11216. https://doi.org/10.1073/pnas.162027899

Yu, E. Y., Li, H., Higano, C. S., Agarwal, N., Pal, S. K., Alva, A., Heath, E. I., Lam, E. T., Gupta, S., Lilly, M. B., Inoue, Y., Chi, K. N., Vogelzang, N. J., Quinn, D. I., Cheng, H. H., Plymate, S. R., Hussain, M., Tangen, C. M., & Thompson, I. M. (2015). SWOG S0925: A Randomized Phase II Study of Androgen Deprivation Combined With Cixutumumab Versus Androgen Deprivation Alone in Patients With New Metastatic Hormone-Sensitive Prostate Cancer. *Journal of Clinical Oncology : Official Journal of the American Society of Clinical Oncology*, *33*(14), 1601–1608. https://doi.org/10.1200/JCO.2014.59.4127

Zhou, S., Shoelson, S. E., Chaudhuri, M., Gish, G., Pawson, T., Haser, W. G., King, F., Roberts, T., Ratnofsky, S., Lechleider, R. J., Neel, B. G., Birge, R. B., Fajardo, J. E., Chou, M. M., Hanafusa, H., Schaffhausen, B., & Cantley, L. C. (1993). SH2 domains recognize specific phosphopeptide sequences. *Cell*, *72*(5), 767–778. https://doi.org/10.1016/0092-8674(93)90404-E

Zhou, Y., Liu, Z., Zhang, S., Zhuang, R., Liu, H., Liu, X., Qiu, X., Zhang, M., Zheng, Y., Li, L., Hong, W., & Wang, T. (2020). RILP restricts insulin secretion through mediating lysosomal degradation of proinsulin. *Diabetes*, *69*(1), 67–82. https://doi.org/10.2337/db19-0086

Zhou, Z. X., Lane, M. V., Kemppainen, J. A., French, F. S., & Wilson, E. M. (1995). Specificity of ligand-dependent androgen receptor stabilization: receptor domain interactions influence ligand dissociation and receptor stability. *Molecular Endocrinology*, *9*(2), 208–218. https://doi.org/10.1210/mend.9.2.7776971

Zhu, M. L., & Kyprianou, N. (2008). Androgen receptor and growth factor signaling cross-talk in prostate cancer cells. *Endocrine-Related Cancer*, *15*(4), 841. https://doi.org/10.1677/ERC-08-0084

Zlotta, A. R., Egawa, S., Pushkar, D., Govorov, A., Kimura, T., Kido, M., Takahashi, H., Kuk, C., Kovylina, M., Aldaoud, N., Fleshner, N., Finelli, A., Klotz, L., Sykes, J., Lockwood, G., & Van Der Kwast, T. H. (2013). Prevalence of Prostate Cancer on Autopsy: Cross-Sectional Study on Unscreened Caucasian and Asian Men. *JNCI: Journal of the National Cancer Institute*, *105*(14), 1050–1058. https://doi.org/10.1093/JNCI/DJT151

frontiers | Frontiers in Cell and Developmental Biology

TYPE Original Research
PUBLISHED 24 August 2023
DOI 10.3389/fcell.2023.1240039

OPEN ACCESS

EDITED BY
Ricardo Daniel Moreno,
Pontificia Universidad Católica de Chile, Chile

REVIEWED BY
Su-Ren Chen,
Beijing Normal University, China
Julio Castaneda,
Osaka University, Japan

*CORRESPONDENCE
Heiko Lickert,
heiko.lickert@helmholtz-muenchen.de

RECEIVED 14 June 2023
ACCEPTED 07 August 2023
PUBLISHED 24 August 2023

CITATION
Bilekova S, Garcia-Colomer B, Cebrian-Serrano A, Schirge S, Krey K, Sterr M, Kurth T, Hauck SM and Lickert H (2023), Inceptor facilitates acrosomal vesicle formation in spermatids and is required for male fertility.
Front. Cell Dev. Biol. 11:1240039.
doi: 10.3389/fcell.2023.1240039

Inceptor facilitates acrosomal vesicle formation in spermatids and is required for male fertility

Sara Bilekova[1,2,3], Balma Garcia-Colomer[2,4], Alberto Cebrian-Serrano[2,4], Silvia Schirge[1,2], Karsten Krey[3,5], Michael Sterr[1,2], Thomas Kurth[6], Stefanie M. Hauck[2,7] and Heiko Lickert[1,2,3]*

[1]Helmholtz Center Munich, German Research Center for Environmental Health GmbH, Institute of Diabetes and Regeneration Research, Neuherberg, Germany, [2]German Center for Diabetes Research (DZD), Neuherberg, Germany, [3]School of Medicine, Technical University of Munich, Munich, Germany, [4]Helmholtz Center Munich, Institute for Diabetes and Obesity, Neuherberg, Germany, [5]Institute of Virology, Technical University of Munich, Munich, Germany, [6]Center for Molecular and Cellular Bioengineering (CMCB), Technology Platform, Core Facility Electron Microscopy and Histology, Dresden University of Technology, Dresden, Germany, [7]Metabolomics and Proteomics Core, Helmholtz Center Munich, German Research Center for Environmental Health GmbH, Munich, Germany

Spermatogenesis is a crucial biological process that enables the production of functional sperm, allowing for successful reproduction. Proper germ cell differentiation and maturation require tight regulation of hormonal signals, cellular signaling pathways, and cell biological processes. The acrosome is a lysosome-related organelle at the anterior of the sperm head that contains enzymes and receptors essential for egg-sperm recognition and fusion. Even though several factors crucial for acrosome biogenesis have been discovered, the precise molecular mechanism of pro-acrosomal vesicle formation and fusion is not yet known. In this study, we investigated the role of the insulin inhibitory receptor (inceptor) in acrosome formation. Inceptor is a single-pass transmembrane protein with similarities to mannose-6-phosphate receptors (M6PR). Inceptor knockout male mice are infertile due to malformations in the acrosome and defects in the nuclear shape of spermatozoa. We show that inceptor is expressed in early spermatids and mainly localizes to vesicles between the Golgi apparatus and acrosome. Here we show that inceptor is an essential factor in the intracellular transport of *trans*-Golgi network-derived vesicles which deliver acrosomal cargo in maturing spermatids. The absence of inceptor results in vesicle-fusion defects, acrosomal malformation, and male infertility. These findings support our hypothesis of inceptor as a universal lysosomal or lysosome-related organelle sorting receptor expressed in several secretory tissues.

KEYWORDS

acrosome, differentiation, male fertility, spermatogenesis, vesicle, localization

1 Introduction

Murine male germ cells show a marked upregulation of over 1500 genes at the onset of meiosis and the expression of around 350 of these genes is restricted to the male germ line, many of them directly necessary for the fertility of sperm (Schultz et al., 2003). However, many testis-specific genes have been found to be dispensable, most likely due to the

robustness and redundancy of the system (Miyata et al., 2016; Lu et al., 2019; Park et al., 2020). This illustrates the complexity and evolutionary necessity of the tight regulation of spermatogenesis. Even though the cell biology of spermatogenesis has been well described, the molecular mechanism and variety of involved factors remain poorly characterized.

Spermatogenesis takes place in the seminiferous tubules of the testis. The spermatogonia undergo mitosis and develop into spermatocytes. In meiotic spermatocytes of humans and mice, heavily glycosylated soluble hydrolases, zymogens, transmembrane proteins, and other acrosome-specific cargo mature through the ER-Golgi networks and are packed into proacrosomal vesicles (pro-AVs) (Anakwe, 1990; Kashiwabara et al., 1990; Escalier et al., 1991). In mice, after the completion of meiosis, spermatids develop in a 16-step process (Oakberg, 1956). In steps 1-3, pro-AVs fuse and attach to the nuclear membrane (Escalier et al., 1991; Bermudez et al., 1994). How this process is initiated and how premature fusion is inhibited, is so far unknown. Trafficking between the Golgi apparatus and the acrosome is dynamic and bidirectional, with several Golgi proteins found on acrosomes that are later retrieved (Moreno et al., 2000). In steps 3-4, F-actin forms the acroplaxome adjacent to the nuclear membrane to which keratin V is added in steps 4–5. This cytoskeletal structure forms the site of pro-AV attachment to the nuclear lamina, initiating acrosome formation (Kierszenbaum et al., 2004). Adaptor protein 1 (AP-1) has been proposed to be the clathrin-adaptor protein mediating pro-AV trafficking towards the acrosome (Kang-Decker et al., 2001). However, it is unknown if AP-1 is present at the time of fusion and how the pro-AVs merge. Clathrin and adaptins are expressed in steps 1-5, whereas syntaxins and vesicle-associated membrane proteins (VAMPs) which mediate membrane fusion, have been found to localize to the pro-AVs in steps 1-2 and later to the acrosome (Ramalho-Santos et al., 2001). The acrosomal shape has been used to describe the characteristic spermatid development stages: the Golgi phase, when the acrosomal material is located near the Golgi apparatus, the cap phase, when the acrosome grows and spreads onto the nuclear surface, the acrosomal stage, when the nucleus and acrosome elongate, and finally the maturation stage. The spermatozoon continues to mature throughout its passage through the epididymis and female reproductive tract.

The insulin inhibitory receptor (in short: inceptor, gene *Iir*, also known as Elapor1) has been previously described in the context of cancer prognosis and progression (Deng et al., 2005; Kang et al., 2015; Stinnesbeck et al., 2021; Wissmiller et al., 2023). Moreover, we have shown that inceptor desensitizes insulin and insulin-like growth factor (IGF) receptor signaling in pancreatic beta cells (Ansarullah et al., 2021). Inceptor contains an adaptor protein 2 (AP-2) sorting signal and interacts with the μ subunit of AP-2 (Ansarullah et al., 2021). From our most recent findings in pancreatic beta cells, we propose that inceptor is a sorting and degradation receptor found in clathrin-coated vesicles budding from the plasma membrane and *trans*-Golgi membrane that routes insulin and proinsulin to lysosomal degradation (Siehler et al., unpublished results). Additionally, inceptor has been found to regulate secretory granule formation in zymogenic cells in the stomach (Cho et al., 2022). Early spermatids also express inceptor, and interestingly, the acrosome formation process has similarities with both regulated secretion and lysosome biogenesis (Khawar et al., 2019). Therefore, we hypothesized that inceptor might play a role in acrosomal trafficking and acrosome formation.

The acrosome is a large granule at the anterior end of the sperm head essential for sperm-oocyte recognition and fusion (Khawar et al., 2019). It is a low-pH organelle that contains Golgi-derived cargo, which is either acrosome-specific or lysosome-like. Therefore, the acrosome has been proposed to be a lysosome-related organelle (Berruti et al., 2010). It contains several enzymes, zymogens, and receptors necessary for oocyte recognition. At the time of oocyte-sperm contact, the acrosome is exocytosed as the outer acrosomal membrane fuses with the plasma membrane, enabling the sperm to penetrate the *zona pellucida* around the oocyte. Then, the inner acrosomal membrane fuses with the oocyte's plasma membrane. The acrosome reaction has been reviewed in detail (Aldana et al., 2021).

Some of the factors which play a role in insulin granule formation or secretion are also essential for acrosome formation, such as Protein interacting with C kinase 1 (PICK1), Golgi-associated PDZ- and coiled-coil motif-containing protein (GOPC), or Mysoin Va (Yao et al., 2002; Kierszenbaum et al., 2003; Varadi et al., 2005; Xiao et al., 2009; Wilhelmi et al., 2021; Andersen et al., 2022). Moreover, Golgi and lysosomal proteins are retrieved from acrosomes in pathways resembling retrieval from maturing secretory granules in neuroendocrine cells, mediated by AP-1 and STX6 (Klumperman et al., 1998). The acrosome also displays similarities with the lysosome, but it is unknown whether it can carry out lysosomal metabolic functions in sperm. Even though the acrosome contains several unique proteins, it also contains typical lysosomal proteins, such as cathepsin D and H (Moreno and Alvarado, 2006). In addition to the acrosome's similarities to lysosomes and secretory granules, recent studies point to mitochondrial engagement in acrosome formation. Condensed mitochondria were found to act as donors to the AV, and several mitochondrial enzymes were shown to localize to the acrosome (Ren et al., 2019; 2022; Otčenášková et al., 2023). Altogether, this shows that there is a substantial gap in knowledge regarding the acrosomal origin and the molecular mechanism of its biogenesis.

Here, we demonstrate the importance of inceptor in male fertility in a whole-body inceptor knockout (KO) mouse model, showing that inceptor is essential for the formation of morphologically normal sperm. Inceptor KO spermatids are characterized by acrosomal malformation, an irregular or round nucleus, and reduced motility. We propose that inceptor is tightly involved in acrosome development in early spermatids and is directly involved in cargo transport and delivery to the forming AV.

2 Materials and methods

2.1 Mouse models

Animal experiments were carried out in compliance with the German Animal Protection Act and with the approved guidelines of the Society of Laboratory Animals (GV-SOLAS) and of the Federation of Laboratory Animal Science Associations (FELASA). Whole-body $Iir^{-/-}$ mice were generated from the previously described GeneTrap allele (Ansarullah et al., 2021). $Iir^{-/-}$:

5330417C22Rik$^{tm1a(EUCOMM)Hmgu}$ embryonic stem cells were aggregated with CD1 morula to generate chimeric mice. For critical exon deletion, the GeneTrap mice were crossed with FLPe mice (Dymecki, 1996) to generate a floxed allele (*Iir*^{fl}). *Iir*$^{fl/fl}$ mice were crossed with Rosa26R-Cre mice (Soriano, 1999) to generate heterozygous *Iir*$^{+/-}$ mice. *Iir*$^{+/-}$ mice were backcrossed to a C57BL/6 J (Charles River) background. Genotyping has been performed with the following primers: 5′-CCAAGGCCAGCGATACAACC-3′, 5′-GGAACTTCGTCGAGATAACTTCGTATAG-3′, 5′-GTGCAC TCTGGGTAGTGTTC-3'. Tissues of males between 9–12 weeks of age were used.

2.2 Caudal sperm isolation

The epididymis was isolated, weighed, and cut between the corpus and cauda. The cauda was cut open with several incisions and incubated in HEPES-balanced salt solution (114 mM NaCl, 4.7 mM KCl, 1.2 mM KH_2PO_4, 1.16 mM $MgSO_4$, 2.5 mM $CaCl_2$, 25.5 mM $NaHCO_3$, 20 mM HEPES pH 7.2) for 15 min at 37°C. A sperm sample from this suspension was heat-inactivated for 2 minutes at 60°C and loaded on a hemocytometer to calculate the total sperm count per cauda epididymis.

2.3 Sperm motility assay

Isolated caudal sperm was assessed for motility in pre-warmed M2 medium (Sigma-Aldrich) using a Zeiss Axio Vert. A1 microscope with a 20 × objective. Five different fields of approximately 5 s were recorded by the STC-MC152USB camera (Sentech) in the XYClone software (Hamilton Thorne, V5.12.0.32243) and assessed for moving sperm (motility) and progressing sperm (progressive motility). A minimum of 130 cells were evaluated for each animal.

2.4 Immunofluorescence

Isolated testes were fixed in 4% paraformaldehyde (PFA) at 4°C overnight. The fixed tissue was dehydrated in sucrose (10% and 30%) and embedded in tissue freezing medium (Leica). Sections of 10 µm thickness were cut at −20°C, dried at room temperature, and kept frozen at −20°C. Frozen sections were thawed at room temperature, washed with PBS, and permeabilized with 0.2% Triton-X100, followed by blocking with 3% donkey serum, 10% fetal calf serum (FCS), and 0.1% bovine serum albumin (BSA) in PBS-T. Primary antibodies were incubated at 4°C overnight (anti-TGN38, 1:50, NBP1-03495SS, Novus Biologicals; anti-GATA-4, 1:200, 14–9980–80, Thermo Fisher Scientific; anti-DDX4, 1:200, 8761S, Cell Signaling Technology; anti-LAMP2, 1:200, ab13524, anti-CI-M6PR, 1:200, PA3-850, ThermoFisher Scientific; Abcam; anti-inceptor, 1:250, 2G6 (Ansarullah et al., 2021)). Secondary antibodies were used at 1:600 with 4',6-diamidino-2-phenylindole (DAPI) at 1 µg/mL for 2 hours at room temperature (anti-rat-Alexa Fluor™ 488, A-21208, Thermo Fisher Scientific; anti-rat-Cy3, 712–165–153, Jackson ImmunoResearch; anti-rabbit-Alexa Fluor™ 488, A21206, Thermo Fisher Scientific). Peanut agglutinin (PNA)-CY5 (CL-1075–1, Vector Laboratories) was used at 1:1000 added to the secondary antibody mix. The slides were mounted with coverslips in Elvanol and imaged on Zeiss LSM 880 with or without Airyscan Fast mode with a 20 × or 63 × objective. Images were analyzed by Fiji (Schindelin et al., 2012) and treated equally within one experiment, unless stated otherwise, by adjusting brightness, and contrast, and for Figures 2B, D, E, noise was reduced by removing outliers with a two-pixel radius. Maximum intensity projection is shown when stated in the respective figure legend.

For mitochondria staining in caudal sperm, live sperm suspensions were incubated with 100 nM MitoTracker™ Red FM (Invitrogen) and 2.5 ng/mL Hoechst 33342 dye (Invitrogen) for 15 min at 37°C. Samples were centrifuged for 5 min at 600 g and the pellet was resuspended in 100 µL pre-warmed M2 media. Epifluorescence images were taken with a Keyence BZ-9000E microscope with a 20 × objective and captured in the BZ-II Viewer software (Keyence). The channels were merged in Fiji.

2.5 Transmission electron microscopy (TEM)

Isolated murine testes were fixed in 4% PFA in 100 mM phosphate buffer pH 7.4 at room temperature for 30 min, then cut in half and fixed for another 1.5 h. For embedding into epoxy resin, the fixed tissue was kept in 4% PFA, for Tokuyasu cryo-sectioning, the tissue was transferred to 1% PFA until further processing. For epoxy resin embedding, the samples were processed according to a modified protocol using osmium tetroxide (OsO_4), thiocarbohydrazide (TCH), and again OsO_4 to generate enhanced membrane contrast (Hanker et al., 1966; Deerinck et al., 2010; Völkner et al., 2022). In brief, samples were postfixed overnight in modified Karnovsky fixative (2% glutaraldehyde/2% formaldehyde in 50 mM HEPES, pH 7.4), followed by post-fixation in a 2% aqueous OsO_4 solution containing 1.5% potassium ferrocyanide and 2 mM $CaCl_2$ (30 min on ice), washes in water, 1% TCH in water (20 min at room temperature), washes in water and a second osmium contrasting step in 2% OsO_4/water (30 min on ice). Samples were washed in water and *en-bloc* contrasted with 1% uranyl acetate/water for 2 h on ice, washed again in water, and dehydrated in a graded series of ethanol/water mixtures (30%, 50%, 70%, 90%, 96%), followed by three changes in pure ethanol on molecular sieve. Samples were infiltrated into EMBed 812 (resin/ethanol mixtures: 1:3, 1:1, 3:1 for 1 h each, followed by pure resin overnight and for 5 h), embedded in flat embedding molds, and cured at 65°C overnight. Ultrathin sections (70 nm) were prepared with a Leica UC6 ultramicrotome (Leica Microsystems) using a diamond knife (Diatome), collected on formvar-coated slot grids, and stained with lead citrate (Venable and Coggeshall, 1965) and uranyl acetate. For Tokuyasu-cryosectioning and immunogold labeling, the samples were processed as described previously (Tokuyasu, 1980; Slot and Geuze, 2007; Völkner et al., 2022). First, they were washed in phosphate buffer, infiltrated stepwise into 10% gelatin (1% for 30 min, 3% for 45 min, 7% for 1 h, 10% for 2 h) at 37°C, cooled down on ice, cut into small blocks, incubated in 2.3 M sucrose/water for 24 h at 4°C, mounted on pins (Leica # 16701950), and plunge frozen in liquid nitrogen. 70–100 nm sections were cut on a Leica UC6+FC6 cryo-ultramicrotome (Leica Microsystems) and picked

up in methyl cellulose/sucrose (1 part 2% methyl cellulose (MC, Sigma M-6385, 25 centipoises +1 part 2.3 M sucrose) using a perfect loop. Gelatin, sucrose, and methyl cellulose were removed by placing the grids on 37°C warm PBS for 3 × 20 min, followed by washes with 0.1% glycin/PBS (5 × 1 min), blocking with 1% BSA/PBS (2 × 5 min) and incubation with the primary antibody (rat anti-inceptor 16F6 (Ansarullah et al., 2021), 1:100) for 1 h. The sections were washed in PBS (4 × 2 min) and incubated with bridging antibodies (rabbit-anti-mouse or rabbit-anti-rat IgGs, 1:100), followed by washes in PBS (4 × 2 min), and incubation with protein A conjugated to 10 nm gold (1:25, UMC) for 1 h. Then, the grids were washed in PBS (3 × 5 s, 4 × 2 min), post-fixed in 1% glutaraldehyde (5 min), thoroughly washed in water to get rid of the PBS (10 × 1 min) and contrasted with neutral uranyl oxalate (2% uranyl acetate (UA) in 0.15 M oxalic acid, pH 7.0) for 5 min, washed in water and incubated in MC containing 0.4% UA for 5 min. Grids were looped out with a perfect loop, the MC/UA film was reduced to an even thin film and air dried. All sections were analyzed on a JEM 1400PLus transmission electron microscope (JEOL) at 80 kV and images were taken with a Ruby digital camera (JEOL).

2.6 Co-immunoprecipitation (co-IP) and western blotting

Isolated murine testes (n = 6) were homogenized in a Potter-Elvehjem homogenizer in 125 mM KCl, 10 mM EDTA, 20 mM HEPES (pH 7.2), 1% protease inhibitor cocktail (Sigma). The protein concentration was measured by BCA Protein Assay Kit (Thermo Scientific Pierce). Western blot samples were prepared by adding Laemmli buffer and boiling. For co-IP, the homogenate was centrifuged at 2000 *g* for 10 min. To the supernatant, 1% NP-40 alternative (Merck Millipore) was added. For mass spectrometry, the lysate was added to anti-Inceptor antibodies or isotype control antibodies (2G6 and 11A7, respectively (Ansarullah et al., 2021)) coupled to protein G SureBeads (BioRad). For co-IP followed by Western blotting, the following antibodies were coupled to protein G beads: anti-AP1M1 (PA5104319, Thermo Fisher Scientific), anti-AP2B1 (ab205014, Abcam), anti-AP3D1 (anti-delta SA4, DSHB), rabbit control (3900, Cell Signaling Technology), mouse control (5415, Cell Signaling Technology), anti-STX7 (12322-1-AP, Proteintech), anti-LYZL4 (17443-1-AP, Proteintech), anti-MAP1B (ab224115, Abcam), anti-Cathepsin Z (ab182575, Abcam). The co-immunoprecipitated protein was eluted into Laemmli buffer at 99°C for Western blotting or at 60°C for mass spectrometry. The samples were loaded on a 10% or 4%–20% gradient SDS-polyacrylamide gel. The separated protein was transferred to a PVDF membrane with 0.2 µm pore-size by semi-dry transfer (BioRad). Blotted membranes were blocked in 5% milk in TBS-T, incubated with primary antibodies at 4°C overnight (anti-SPACA1, 1:1000, ab191843, Abcam; anti-γ-tubulin, 1:2000, T5326, Sigma-Aldrich; anti-β-adaptin, 1:1000, 610382, BD Biosciences; anti-GAPDH, 1:4000, 2118L, Cell Signaling Technology; anti-inceptor, 1:1000, 16F6 (Ansarullah et al., 2021); anti-LYZL4, 1:1000, 17443-1-AP, Proteintech; anti-HSP90, 1:5000, 4874S, Cell Signaling Technology) and with secondary antibodies 1:5000 for 1 h at room temperature (anti-rat-HRP, 112-035-175, Jackson ImmunoResearch; anti-mouse-HRP, 115-035-146, Jackson ImmunoResearch; anti-rabbit-HRP, 111-035-144, Jackson ImmunoResearch). The chemiluminescence signal was detected by ChemStudio2A (Analytik Jena) using Clarity Western ECL Substrate (Bio-Rad).

2.7 Mass spectrometry

For total proteome, 1% NP-40 alternative (Merck Millipore) was added to homogenized testis, prepared as described above. For the interactome analysis, the eluate from the co-IP described above was used. The samples were further proteolyzed with LysC and trypsin as described (Wiśniewski et al., 2009; Grosche et al., 2016). Acidified eluted peptides were analyzed on a Q Exactive HF-X mass spectrometer (Thermo Fisher Scientific) online coupled to a UItimate 3000 RSLC nano-HPLC (Dionex) on a C18 analytical column, separated by a 90-min non-linear acetonitrile gradient at a flow rate of 250 nL/min. MS spectra were recorded at a resolution of 60000 with an AGC target of 3 x 1e6 and a maximum injection time of 30 ms from 300 to 1500 m/z. From the MS scan, the 15 most abundant peptide ions were selected for fragmentation via HCD with a normalized collision energy of 28, an isolation window of 1.6 m/z, and a dynamic exclusion of 30 s. MS/MS spectra were recorded at a resolution of 15000 with a AGC target of 1e5 and a maximum injection time of 50 ms. Unassigned charges, and charges of +1 and >8 were excluded from precursor selection.

Acquired raw data of the total testis proteome samples was analyzed in the Proteome Discoverer 2.4 SP1 software (Thermo Fisher Scientific; version 2.4.1.15) for peptide and protein identification via a database search (Sequest HT search engine) against the SwissProt Mouse database (Release 2020_02, 17061 sequences), considering full tryptic specificity, allowing for up to one missed tryptic cleavage site. The Percolator algorithm (Käll et al., 2007) was used for validating peptide spectrum matches and peptides. The final list of proteins satisfying the strict parsimony principle included only protein groups passing an additional protein confidence false discovery rate <5% (target/decoy concatenated search validation). Protein groups with ≥50% missing values were disregarded. In the remaining protein groups, missing values were imputed by GMSimpute (Li et al., 2020). The *p* values were adjusted according to Hochberg (Hochberg, 1988), and we deemed proteins with an adjusted *p* value <0.05 significant. Significant hits were analyzed for gene ontology (GO) term enrichment via the g:Profiler tool g:GOSt (Raudvere et al., 2019) against the custom reference gene list containing all detected proteins after imputation and filtration in the total proteome sample.

Raw data for the interactome analysis was imported into Progenesis QI software (version 4.1). After feature alignment and normalization, spectra were exported as Mascot Generic files and searched against SwissProt Mouse database (Release 2020_02, 17061 sequences) with Mascot (Matrix Science, version 2.8.2) with the following search parameters: 10 ppm peptide mass tolerance and 20 mmu fragment mass tolerance, one missed cleavage allowed, carbamidomethylation was set as fixed modification, methionine oxidation, and asparagine or glutamine deamidation were allowed as variable modifications. A Mascot-integrated decoy database search calculated an average false discovery rate <0.5% for PSMs when searches were performed

applying the mascot percolator score and a significance threshold $p < 0.05$. Peptide assignments were re-imported into the Progenesis QI software and the abundances of all unique peptides allocated to each protein were summed up. The resulting normalized abundances of the individual proteins were used for calculation of fold-changes of protein ratios between experimental conditions and statistical analysis was performed on log2 transformed normalized abundance values using one-way ANOVA. Values are corrected for multiple testing by an optimized FDR approach (q value). Potential interactors with a q value <0.05, a fold change between inceptor and control IP > 2, and less than seven missing values (corresponding to 60%) were selected and a GO:term analysis was performed. GO:BP terms were reduced with the rrvgo R package 1.10.0 (Sayols, 2020) with a threshold of 0.6. The mass spectrometry proteomics data have been deposited to the ProteomeXchange Consortium via the PRIDE (Perez-Riverol et al., 2022) partner repository with the dataset identifier PXD043946.

2.8 *Iir* expression across cell types

Normalized transcripts per million (nTPM) data from scRNA-seq datasets were downloaded from The Human Protein Atlas and the 20 cell types with nTPM >20 were plotted for *Elapor1* expression. Cell type group information was manually added.

2.9 Statistical analysis and software

Statistical analysis and the generation of bar plots were performed in GraphPad Prism 9.5.1, using unpaired *t*-test. Bar plots are shown as mean ± SD. Mass spectrometry raw data were analyzed in Proteome Discoverer 2.4 SP1 (Thermo Fisher Scientific; version 2.4.1.15) and Progenesis QI software (version 4.1). GO term annotation was performed by g:Profiler (Raudvere et al., 2019) and GO:BP term reduction was done by the rrvgo R package 1.10.0 (Sayols, 2020). The volcano plot and GO term bar plots were generated in RStudio (2022.12.0 + 353, R version 4.2.2) by ggplot2. Image acquisition was done by ZEN 2.3 (black edition, Zeiss), XYClone (Hamilton Thorne), and BZ-II Viewer (Keyence) and image processing was done in Fiji (ImageJ 1.53o) (Schindelin et al., 2012). Figures were generated in Inkscape 1.2.1.

3 Results

Inceptor is highly expressed in several tissues, such as the digestive tract, pancreas, prostate, female reproductive tract, lung, brain, and testis, specifically enriched in glandular cell types, endocrine cells, and early spermatids (Supplementary Figure S1A) (The Human Protein Atlas). We confirmed inceptor protein expression in the stomach, salivary gland, colon, and lung by immunofluorescence (Supplementary Figure S1B).

To analyze the function of inceptor, we generated the $Iir^{+/-}$ mouse line by crossing the previously generated GeneTrap line (Ansarullah et al., 2021) to FLPe and RosaCre animals to obtain a germline deletion of exon 3 (Supplementary Figure S1C). By heterozygous intercrossing of the $Iir^{+/-}$ mouse line, Mendelian ratios of offspring genotypes were observed at weaning age (Supplementary Figure S1D). We confirmed the absence of inceptor in $Iir^{-/-}$ testis lysates by Western blotting (Supplementary Figure S1E). Intriguingly, the $Iir^{-/-}$ genotype could not be maintained on a homozygous background. While $Iir^{-/-}$ females delivered similar litter sizes as $Iir^{+/-}$ females with $Iir^{+/-}$ males, matings with $Iir^{-/-}$ males were unsuccessful (Figure 1A). These results are consistent with previously described infertility of $Iir^{-/-}$ males (Tang et al., 2010; Cho et al., 2022), however, the underlying cellular and molecular mechanism was unknown.

To further investigate the function of inceptor in male fertility, we analyzed testis sections in $Iir^{+/+}$ and $Iir^{-/-}$ mice. Interestingly, we noticed partially or totally missing PNA staining, indicating failure in acrosome formation (Figure 1B). The round nuclei of $Iir^{-/-}$ spermatozoa are indicative of a condition referred to as globozoospermia (Figure 1C). Globozoospermia and acrosome malformation are often accompanied by motility and mitochondria defects (Xiao et al., 2009; Han et al., 2017). Indeed, $Iir^{-/-}$ spermatozoa are characterized by reduced motility, as well as defective mitochondrial organization (Figures 1D–F).

$Iir^{+/+}$ and in $Iir^{-/-}$ males did not differ in body weight (Supplementary Figure S2A), while $Iir^{-/-}$ males had a slightly increased testis weight without a significant difference in caudal sperm count (Supplementary Figures S2B, C). There was no difference in gross morphology of the testis and epididymis (Supplementary Figure S2D). By analyzing testicular cross sections by immunofluorescence, there were no differences between $Iir^{+/+}$ and $Iir^{-/-}$ testes in germ cells marked by DDX4 and Sertoli cells marked by GATA-4 (Supplementary Figure S2E), as well as tubule diameter (Supplementary Figure S2F).

In the seminiferous tubules of the testis, inceptor is expressed in spermatocytes and in Golgi-phase and cap-phase spermatids but not in elongated spermatids in the acrosomal phase (Figure 2A). By confocal microscopy, we found inceptor in the vesicles of pachytene spermatocytes when the pro-AVs are harbored close to the Golgi apparatus and not yet attached to the nuclear membrane (Figure 2B). After meiosis, spermatids develop in 16 steps into spermatozoa (Oakberg, 1956; Wakayama et al., 2022) (Figure 2C). Confocal microscopy and TEM of immunogold labeled Tokuyasu-cryosections showed that inceptor is localized to pro-AVs and other vesicles before stage 3 (S3), before the pro-AVs attach to the nucleus (Figure 2D). Next, pro-AVs start to fuse into a cap-like structure (up to S7), when inceptor is predominantly present in the vesicles trafficking between the Golgi and the AV, and to a lesser extent in the inner and outer acrosomal membranes (Figures 2E, F). Then, the nucleus starts to elongate while the AV expands to cover most of the nuclear surface. The cell discards the Golgi apparatus and other organelles at this stage, while the inceptor immunosignal is completely lost (Figure 2G). In conclusion, in the early stages of acrosome formation, inceptor is localized to trafficking vesicles, pro-AVs, and the inner and outer acrosomal membranes of the developing AV.

As inceptor expression coincides with the early steps of acrosome formation, we used TEM to visualize the acrosomal shape in $Iir^{+/+}$ and $Iir^{-/-}$ mice. As expected, in $Iir^{+/+}$ mice, we observed electron-dense pro-AVs before acrosome formation, that are around 200-µm large in diameter (Figure 3A, white arrowhead). During pro-AV fusion, the single AV attaches to the

10.3389/fcell.2023.1240039

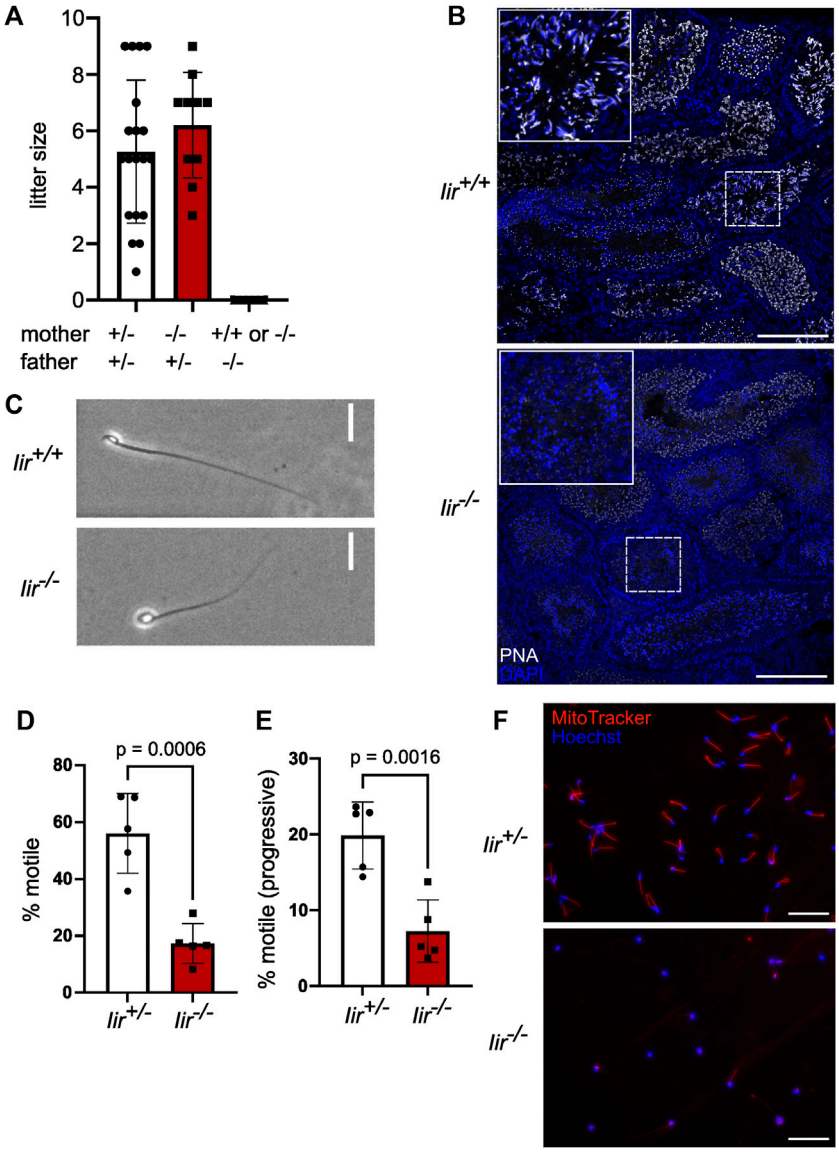

FIGURE 1
lir$^{-/-}$ male mice are infertile and *lir*$^{-/-}$ spermatids show acrosome malformation and a globular shape. **(A)** Litter size of crossing *lir*$^{+/-}$ and *lir*$^{-/-}$ mice. **(B)** Representative PNA marking acrosomes and DAPI staining marking nuclei in testis sections of *lir*$^{+/+}$ and *lir*$^{-/-}$ mice. Maximum-intensity projection. Scale bar 150 µm. **(C)** Representative phase-contrast image of isolated caudal sperm. Scale bar 20 µm. **(D–E)** percentage of motile **(D)** and progressive-motile **(E)** isolated caudal sperm. Each dot represents sperm isolated from one mouse consisting of five measurements per mouse **(F)** Representative MitoTracker staining with Hoechst 33342 counterstain of isolated caudal sperm from *lir*$^{+/-}$ and *lir*$^{-/-}$ mice. Scale bar 100 µm.

nucleus at the beginning of the cap phase. At the nuclear membrane and AV contact site, the electron-dense acroplaxome is visible (Figure 3B, black arrows). As the AV expands and covers more nuclear surface, the acroplaxome also grows along the contact site (Figure 3C). After that, the nucleus and AV elongate, and the nucleus becomes more electron-dense (Supplementary Figures S3A–C). In *Iir*$^{-/-}$ testis, pro-AVs localize to the *trans*-Golgi network as in the *Iir*$^{+/+}$ controls before acrosome formation (Figure 3D). At the beginning of the cap phase, however, pro-AVs do not form one large AV but remain segregated into around 200-µm large vesicles (Figure 3E). These vesicles are in close proximity to the nucleus, suggesting the correct delivery but failure to fuse at the acroplaxome. In later stages, the electron-dense acroplaxome expands around the nucleus, but the AV consists of small, irregularly distributed electron-dense vesicles in *Iir*$^{-/-}$ mice (Figure 3F). In further stages of acrosome formation, the nucleus fails to elongate and remains round or irregular in shape (Supplementary Figures S3D–F). By immunofluorescence, we observed some of the scattered acrosomal content marked by PNA localized to LAMP2-positive lysosomes, whereas in *Iir*$^{+/+}$ cap-phase spermatids, LAMP2-positive lysosomes mainly localized to the posterior side of the spermatid (Figure 3G). Due to the similarity between inceptor and M6PRs, we investigated the localization of the cation-independent (CI-)M6PR and confirmed

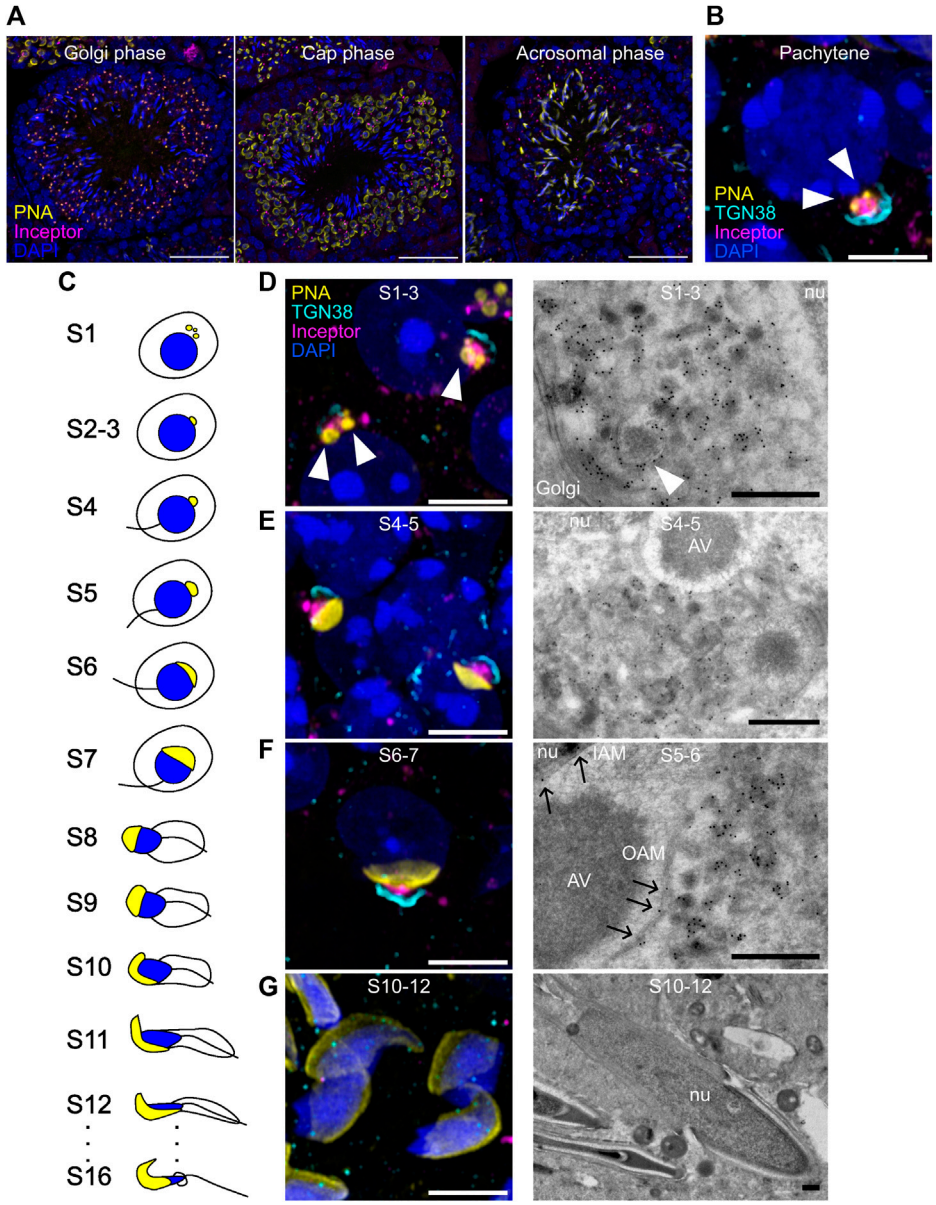

FIGURE 2
Inceptor localizes to the pro-AVs and acrosome in early-stage spermatids. **(A)** Representative immunofluorescence images of inceptor co-stained with PNA and DAPI, maximum intensity projection. Scale bar 50 µm. **(B)** Representative immunofluorescence images of inceptor and TGN38 co-stained with PNA and DAPI in the pachytene stage. **(C)** Schematic overview of spermatid development **(D–G)** Representative immunofluorescence images for stages S1-3, **(E)** S4-5, **(F)** S6-7, **(G)** S10-12 (left panels) and immunogold labeling of inceptor (right panels). **(B,D–G)** Airyscan acquisition and processing, maximum intensity projection. Scale bar 10 µm for immunofluorescence images, scale bar 2 µm for TEM images. nu, nucleus; AV, acrosomal vesicle; IAM, inner acrosomal membrane; OAM, outer acrosomal membrane. White arrowheads: pro-AVs, black arrows: inceptor localization to the acrosomal membrane.

that CI-M6PR localization resembles a more diffuse vesicular localization than inceptor, with occasional colocalization with LAMP2-positive lysosomes (Figure 3H, white arrows).

As we observed small, deformed, or lacking acrosomes in *Iir*$^{-/-}$ spermatids, we performed whole-testis proteome analysis on *Iir*$^{+/+}$ and *Iir*$^{-/-}$ testes to provide an unbiased picture of differential regulation of spermatocyte development. For the analysis, we considered 5389 considered protein groups, from which there were 28 significantly downregulated and one significantly upregulated protein (Figure 4A, Supplementary Table S1). We performed a GO term analysis of the significant hits on the background of all 5389 considered protein groups, which shows significantly deregulated terms related to acrosomes, secretion, and fertilization (Figure 4B). Specifically, we see significant downregulation of proteins localized to the acrosome, either soluble or transmembrane proteins. Many well-known proteins essential for fertilization are strongly downregulated in *Iir*$^{-/-}$ testes. Among these proteins were Acrosin (ACR), Acrosin-binding

10.3389/fcell.2023.1240039

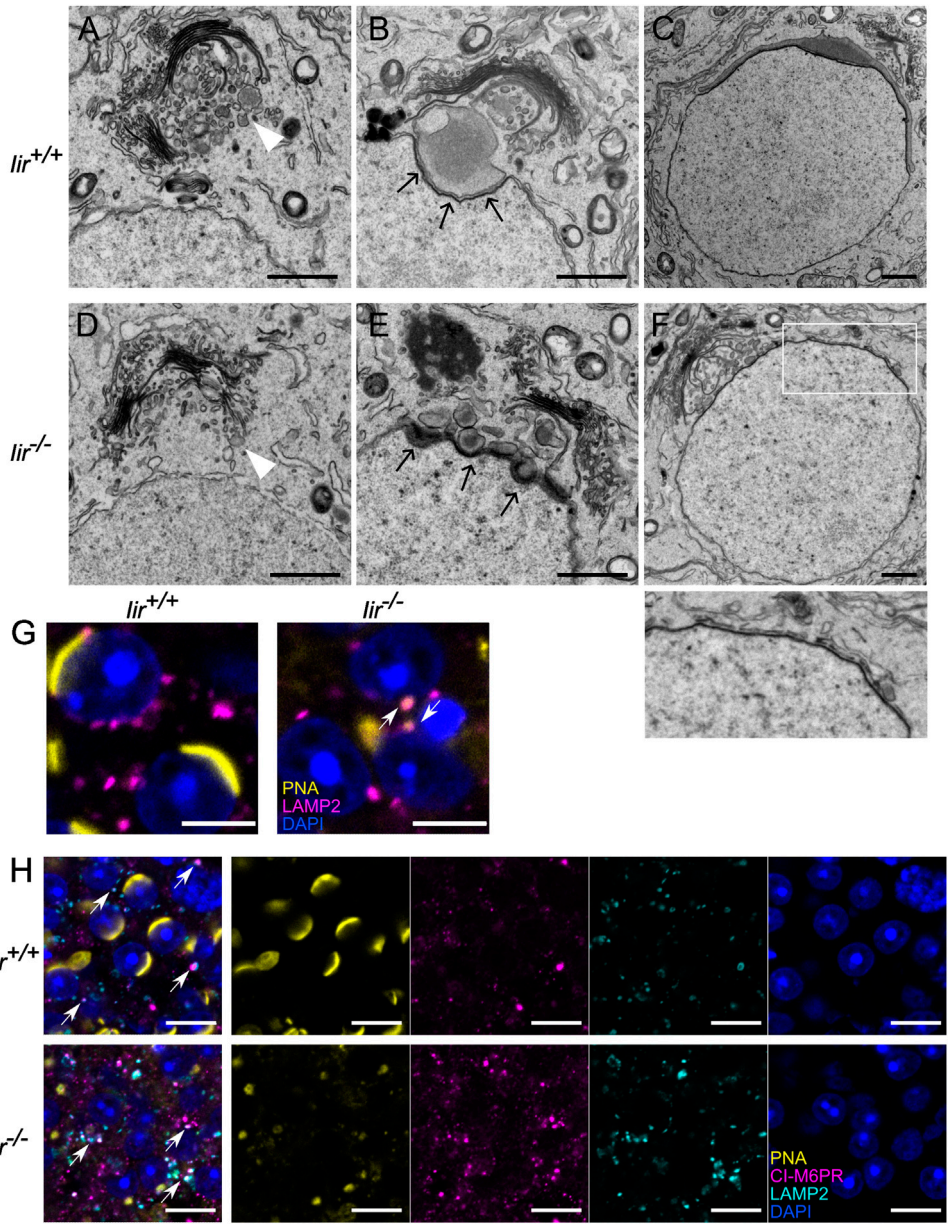

FIGURE 3
Pro-AVs do not fuse in *lir*$^{-/-}$ spermatids, resulting in a scrambled acrosome **(A–F)** Representative electron micrographs of early-stage spermatids. Scale bars 1 µm. White arrowheads: pro-AVs, black arrows: acroplaxome **(G)** Example immunofluorescence image of LAMP2 and PNA overlapping in *lir*$^{+/+}$ and *lir*$^{-/-}$ spermatids. Scale bar 5 µm. White arrows point at PNA-positive lysosomes **(H)** Representative immunofluorescence image of CI-M6PR and LAMP2-positive vesicle localization in *lir*$^{+/+}$ and *lir*$^{-/-}$ spermatids and PNA and DAPI counterstain. Scale bar 10 µm. White arrows point at LAMP2 and CI-M6PR colocalization.

protein (ACRBP), Acrosomal vesicle protein 1 (ACRV1), Sperm acrosome membrane-associated 1 (SPACA1), and Equatorin (EQTN), which are among the main constituents of the acrosome. Additionally, Izumo sperm-egg fusion protein 4 (IZUMO4), and the *Zona-pellucida* binding protein (ZPBP), which have direct functions in sperm-egg fusion, were also downregulated. CD46 and TMEM190 are proteins specifically localized to the inner acrosomal membrane and we also found them downregulated in *Iir*$^{-/-}$ testes. Interestingly, Insulin-like factor 6 (INSL6) is also downregulated, a member of the insulin superfamily expressed specifically in the testis with expression onset in pachytene spermatocytes (Burnicka-Turek et al., 2009). We confirmed the downregulation of SPACA1 and Lysozyme-like 4 (LYZL4) by Western blot (Figure 4C).

As inceptor localizes between the Golgi and AV and in its absence the acrosome does not fully develop, we hypothesized that inceptor is necessary for trafficking between the Golgi and AV in developing spermatids. Therefore, the interaction partners and potential cargo of inceptor became of interest in deciphering the underlying mechanism of inceptor's role in acrosome formation. We

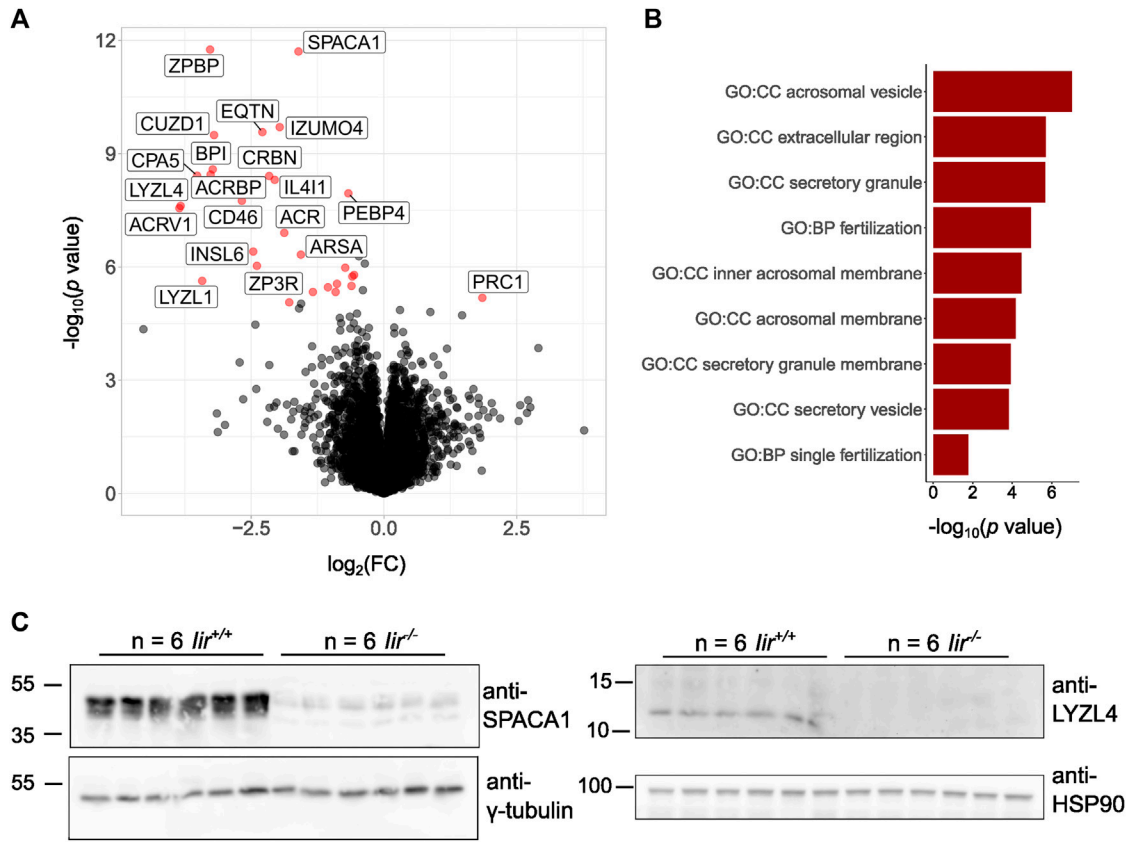

FIGURE 4
lir$^{-/-}$ testes lack acrosomal proteins essential for fertilization. **(A)** Volcano plot of the total testis proteome of *lir*$^{-/-}$ vs *lir*$^{+/+}$ mice. Red dots highlight significant hits. **(B)** Significant GO terms from significant hits from **(A)** against all proteins detected in **(A)**. **(C)** Validation of the downregulation of SPACA1 and LYZL4 by Western blot.

performed an inceptor co-IP experiment followed by mass spectrometry analysis (Figure 5A). We analyzed GO terms related to biological processes (GO:BP) on the 128 potential interactors (Supplementary Table S2). The significant GO:BP terms were reduced to eleven parental terms (Supplementary Figure S4). This GO:BP enrichment analysis revealed that inceptor interacts with proteins related to protein localization, organelle organization, catabolic process and vesicle-mediated transport (Figure 5B). From the list of candidate interactors, we validated the binding of inceptor to proteins that are well-known for their function in vesicle trafficking and fusion, such as syntaxin 7 (STX7) and microtubule-associated protein 1B (MAP1B) (Figure 5C). We also confirmed the interaction with the significantly downregulated LYZL4 and the M6P-containing cathepsin Z (Figure 5C). We have previously shown inceptor's YXXθ to bind the μ subunit of AP-2 in pancreatic beta cells (Ansarullah et al., 2021), as this motif is known to bind the μ subunits of AP1-4 (Braulke and Bonifacino, 2009). Interestingly, we found the adaptor protein 3 μ2 subunit (AP3M2) to interact with inceptor (Supplementary Table S1), so we investigated adaptor protein and inceptor's interaction in testes. We found that inceptor is bound by the AP complexes 1, 2, and 3, which likely mediate its subcellular localization and trafficking (Figure 5D). In summary, we propose that inceptor mediates vesicle trafficking between the Golgi and AV compartments and facilitates the transport and function of various proteins involved in cellular trafficking, such as proteins involved in vesicle fusion (Figure 5E).

4 Discussion

Around seven percent of the human male population has a form of infertility but the underlying disease mechanism remains unknown in most cases (Krausz and Riera-Escamilla, 2018). Moreover, discovering factors that could serve as targets for on-demand male contraception is sought after (Kent et al., 2020). For this purpose, factors essential for spermatogenesis specifically expressed in spermatocytes and spermatids but not in spermatogonia are promising candidates.

Here, we described inceptor expression, localization, and function in the murine testis. Inceptor is essential for the development of morphologically intact, motile, and fertile spermatozoa. Inceptor's expression onset is in primary spermatocytes, which arise from germ cells by meiosis. The expression is retained until the elongation stage of maturing spermatids. By immunofluorescence and immunogold labeling, we found that inceptor localizes to vesicles shuttling between the Golgi and acrosome compartments, and in its absence, pro-AVs do

10.3389/fcell.2023.1240039

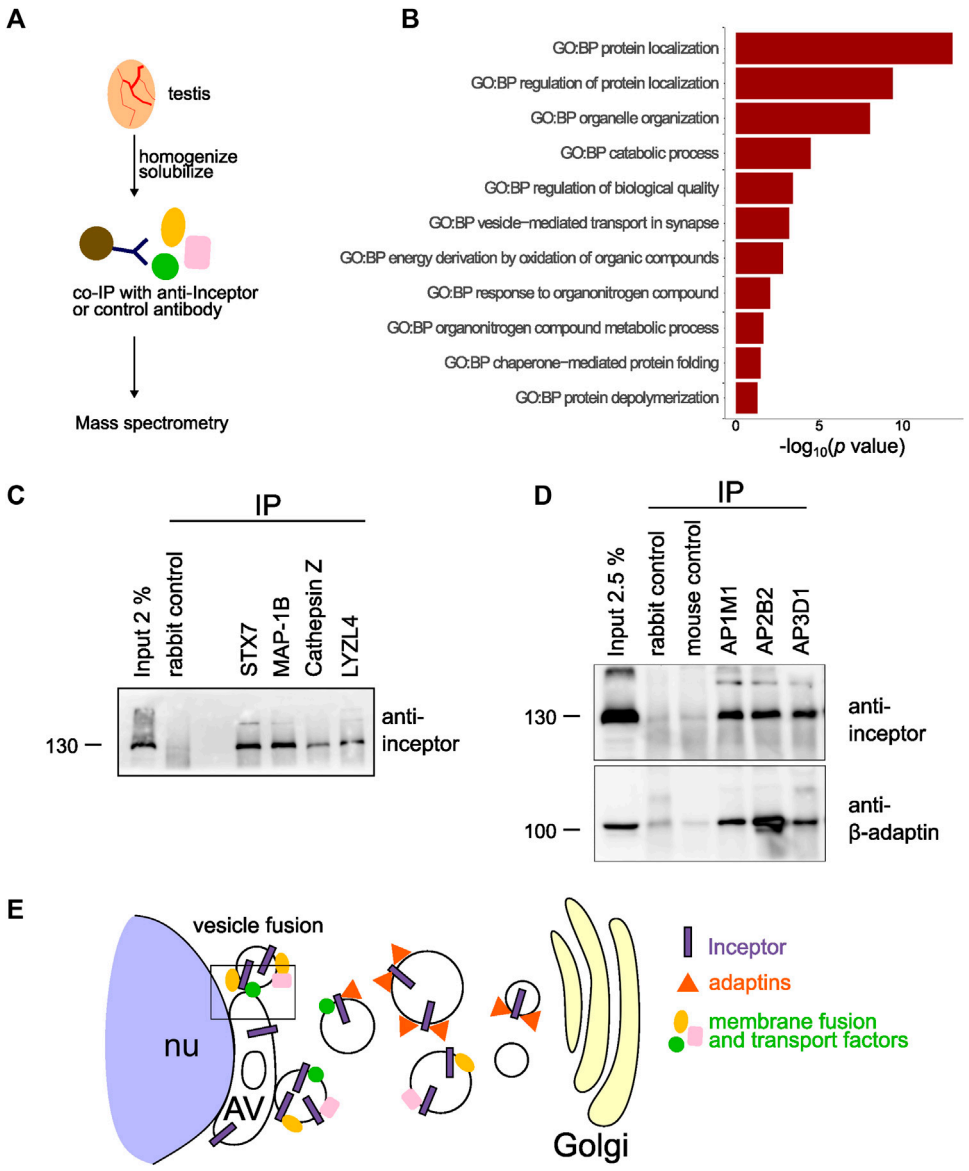

FIGURE 5
Inceptor mediates subcellular localization and transport in maturing spermatids **(A)** Schematic representation of the experimental setup. **(B)** Parental GO:BP terms of co-immunoprecipitated proteins with inceptor in whole testis. **(C)** Validation of the mass spectrometry results by co-IP of potential interactors. **(D)** Western blot of adaptor protein co-IP for inceptor and β-adaptin. **(E)** Schematic overview of inceptor localization and function in early-stage spermatids.

not fuse to form the acrosome. Together with the downregulation of proteins localized to the acrosome in *Iir*$^{-/-}$ testes and the enrichment of transport and localization-related proteins in inceptor's interactome, these results indicate, that inceptor mediates intracellular transport to ensure pro-AV fusion. Indeed, we confirm inceptor to bind membrane-fusion and vesicle-trafficking factors, such as STX7 and MAP1B. As inceptor likely does not contain catalytically active domains and we described domains important for interacting with other proteins (Ansarullah et al., 2021), we propose that inceptor does not mediate the membrane fusion of the pro-AVs directly, but has a function in delivering factors that aid the membrane fusion and cargo delivery to the acrosome.

Interestingly, *Pick1*$^{-/-}$ and *Gopc*$^{-/-}$ mice also show defects in acrosome formation and a failure of pro-AV fusion, similarly to *Iir*$^{-/-}$ mice (Yao et al., 2002; Xiao et al., 2009). From these published immunofluorescence images, PICK1 and GOPC seem to localize more broadly in spermatids compared to inceptor and the TEM images suggest that inceptor and PICK1 could be present in the same vesicles. Other mouse KOs also show globozoospermia and defects in acrosome formation, albeit with some differences. For example, *Gm130*$^{-/-}$ spermatids form an AV which then fails to grow, whereas *Dpy19l2*$^{-/-}$ spermatids show a destabilized nuclear membrane (Pierre et al., 2012; Han et al., 2017). *Spaca1*$^{-/-}$ spermatids have a destabilized AV and lack the acroplaxome, whereas *Zpbp*$^{-/-}$ mice have a fragmented acrosome due to failure

in acrosome compaction (Lin et al., 2007; Fujihara et al., 2012). These functional studies suggest, that each step of acrosome formation is tightly regulated by a variety of proteins. However, these regulatory steps seem to interconnected, as *Gopc*$^{-/-}$ mice also show reduced ZPBP1 and SPACA1 proteins, and *Zpbp*$^{-/-}$ mice also show a reduction in SPACA1 (Fujihara et al., 2012). Interestingly, neither PICK1, GOPC, nor DPY19L2 levels were changed in *Iir*$^{-/-}$ testes, whereas SPACA1 and ZPBP1 were among the most significantly downregulated proteins compared to *Iir*$^{+/+}$ testes (Supplementary Table S1).

Inceptor binds insulin and proinsulin in pancreatic beta cells and regulates their degradation (Siehler et al., unpublished results). Intriguingly, INSL6, a relaxin-like protein and one of insulin-like factors specifically expressed in testes, was also downregulated in testes of *Iir*$^{-/-}$ mice. INSL6 levels have been found to correlate positively with male fertility in humans (Ivell and Grutzner, 2009; Chen et al., 2011; Ivell et al., 2017; Gumus et al., 2022). Inceptor also shares similarities to CI-M6PR, which transports IGF2 towards lysosomes, as well as acts as transport receptors for hydrolases toward late endosomes and lysosomes. As the acrosome shares similarities in origin and content to lysosomes, one hypothesis could be that M6PRs also contribute towards regulating the acrosomal content. Interestingly, the CI- and cation-dependent (CD)-M6PR have only been found to associate with LAMP1-positive lysosomes and not with acrosin-containing vesicles or acrosomes in spermatids (Martínez-Menárguez et al., 1996), similarly to our results (Figure 3H). In later stages, CI-M6PR has been found to transiently co-localize with acrosomes and has been proposed to contribute to shaping the acrosome (Moreno, 2003). However, in CI- and CD-M6PR mutants, the acrosomal content of selected hydrolases was not affected (Chayko and Orgebin-Crist, 2000). We have confirmed that the M6PR colocalizes with LAMP2-positive lysosomes rather than the acrosome, whereas inceptor is more closely located to the acrosome. In summary, we propose that inceptor is an important lysosomal trafficking receptor in different cell types, and an acrosomal trafficking receptor in developing spermatids.

Data availability statement

The datasets presented in this study can be found in online repositories. The names of the repository/repositories and accession number(s) can be found in the article/Supplementary Material.

Ethics statement

Animal experiments were carried out in compliance with the German Animal Protection Act and with the approved guidelines of the Society of Laboratory Animals (GV-SOLAS) and of the Federation of Laboratory Animal Science Associations (FELASA).

Author contributions

SB and HL conceived the idea and designed the study. SB wrote the manuscript. SB, BG-C, AC-S, TK, and SH performed experiments and analyzed data. SS generated the mouse line and oversaw the animal experiment. KK contributed to the analysis and interpretation of the mass spectrometry data. MS plotted the scRNA-seq data from the Human Protein Atlas. HL supervised the study. All authors contributed to the article and approved the submitted version.

Acknowledgments

The authors would like to thank T. Öztürk, L. Appel, K. Diemer, and S. Kretschmar for technical assistance. We thank A. Dema and V. Grass for the helpful comments on the manuscript.

Conflict of interest

HL is the inventor of patent "Novel IGFR-like receptor and uses thereof" held by the Helmholtz Zentrum München GmbH (WO2017042242) and co-inventor of the pending patent application filed by the Helmholtz Zentrum München GmbH "Novel IGFR-like 1 monoclonal antibodies and uses thereof" (WO2023002060).

The remaining authors declare that the research was conducted in the absence of any commercial or financial relationships that could be construed as a potential conflict of interest.

Publisher's note

Supplementary material

The Supplementary Material for this article can be found online at: https://www.frontiersin.org/articles/10.3389/fcell.2023.1240039/full#supplementary-material

References

Aldana, A., Carneiro, J., Martínez-Mekler, G., and Darszon, A. (2021). Discrete dynamic model of the mammalian sperm acrosome reaction: the influence of acrosomal pH and physiological heterogeneity. *Front. Physiol.* 0, 682790. doi:10.3389/FPHYS.2021.682790

Anakwe, O. O., and Gerton, G. L. (1990). Acrosome biogenesis begins during meiosis: evidence from the synthesis and distribution of an acrosomal glycoprotein, acrogranin, during Guinea pig spermatogenesis. *Biol. Reprod.* 42, 317–328. doi:10.1095/biolreprod42.2.317

Andersen, R. C., Schmidt, J. H., Rombach, J., Lycas, M. D., Christensen, N. R., Lund, V. K., et al. (2022). Coding variants identified in patients with diabetes alter PICK1 BAR domain function in insulin granule biogenesis. *J. Clin. Invest.* 132, e144904. doi:10.1172/JCI144904

Ansarullah, G., Jain, C., Far, F. F., Homberg, S., Wißmiller, K., von Hahn, F. G., et al. (2021). Inceptor counteracts insulin signalling in β-cells to control glycaemia. *Nature* 590, 326–331. doi:10.1038/s41586-021-03225-8

Bermudez, D., Escalier, D., Gallo, J. M., Viellefond, A., Rius, F., Perez de Vargas, I., et al. (1994). Proacrosin as a marker of meiotic and post-meiotic germ cell differentiation: quantitative assessment of human spermatogenesis with a monoclonal antibody. *J. Reprod. Fertil.* 100, 567–575. doi:10.1530/JRF.0.1000567

Berruti, G., Ripolone, M., and Ceriani, M. (2010). USP8, a regulator of endosomal sorting, is involved in mouse acrosome biogenesis through interaction with the spermatid ESCRT-0 complex and microtubules. *Biol. Reprod.* 82, 930–939. doi:10.1095/BIOLREPROD.109.081679

Braulke, T., and Bonifacino, J. S. (2009). Sorting of lysosomal proteins. *Biochim. Biophys. Acta - Mol. Cell. Res.* 1793, 605–614. doi:10.1016/j.bbamcr.2008.10.016

Burnicka-Turek, O., Shirneshan, K., Paprotta, I., Grzmil, P., Meinhardt, A., Engel, W., et al. (2009). Inactivation of insulin-like factor 6 disrupts the progression of spermatogenesis at late meiotic prophase. *Endocrinology* 150, 4348–4357. doi:10.1210/EN.2009-0201

Chayko, C. A., and Orgebin-Crist, M. C. (2000). Targeted disruption of the cation-dependent or cation-independent mannose 6-phosphate receptor does not decrease the content of acid glycosidases in the acrosome. *J. Androl.* 21, 944–953. doi:10.1002/J.1939-4640.2000.TB03426.X

Chen, G. W., Luo, X., Liu, Y. L., Jiang, Q., Qian, X. M., and Guo, Z. Y. (2011). R171H missense mutation of INSL6 in a patient with spermatogenic failure. *Eur. J. Med. Genet.* 54, e455–e457. doi:10.1016/j.ejmg.2011.04.008

Cho, C. J., Park, D., and Mills, J. C. (2022). ELAPOR1 is a secretory granule maturation-promoting factor that is lost during paligenosis. *Am. J. Physiol. Gastrointest. Liver Physiol.* 322, G49–G65. doi:10.1152/AJPGI.00246.2021

Deerinck, T., Bushong, E., Thor, A., and Ellisman, M. (2010). SBEM protocol v7_01_10. NCMIR methods for 3D EM: a new protocol for preparation of biological specimens for serial blockface scanning electron microscopy national center for microscopy and imaging research. Available at: https://ncmir.ucsd.edu/sbem-protocol (Accessed March 7, 2023).

Deng, L., Broaddus, R. R., McCampbell, A., Shipley, G. L., Loose, D. S., Stancel, G. M., et al. (2005). Identification of a novel estrogen-regulated gene, EIG121, induced by hormone replacement therapy and differentially expressed in type I and type II endometrial cancer. *Clin. Cancer Res.* 11, 8258–8264. doi:10.1158/1078-0432.CCR-05-1189

Dymecki, S. M. (1996). Flp recombinase promotes site-specific DNA recombination in embryonic stem cells and transgenic mice. *Proc. Natl. Acad. Sci. U. S. A.* 93, 6191–6196. doi:10.1073/PNAS.93.12.6191

Escalier, D., Gallo, J. M., Albert, M., Meduri, G., Bermudez, D., David, G., et al. (1991). Human acrosome biogenesis: immunodetection of proacrosin in primary spermatocytes and of its partitioning pattern during meiosis. *Development* 113, 779–788. doi:10.1242/dev.113.3.779

Fujihara, Y., Satouh, Y., Inoue, N., Isotani, A., Ikawa, M., and Okabe, M. (2012). SPACA1-deficient male mice are infertile with abnormally shaped sperm heads reminiscent of globozoospermia. *Development* 139, 3583–3589. doi:10.1242/dev.081778

Grosche, A., Hauser, A., Lepper, M. F., Mayo, R., Von Toerne, C., Merl-Pham, J., et al. (2016). The proteome of native adult müller glial cells from murine retina. *Mol. Cell. Proteomics* 15, 462–480. doi:10.1074/MCP.M115.052183

Gumus, K., Demir, M., and Dag, I. (2022). Insulin-like peptide-6 levels in non-obstructive azoospermia. *J. Coll. Physicians Surg. Pak.* 32, 1238–1241. doi:10.29271/jcpsp.2022.10.1238

Han, F., Liu, C., Zhang, L., Chen, M., Zhou, Y., Qin, Y., et al. (2017). Globozoospermia and lack of acrosome formation in GM130-deficient mice. *Cell. Death Dis.* 8, e2532. doi:10.1038/cddis.2016.414

Hanker, J. S., Deb, C., Wasserkrug, H. L., and Seligman, A. M. (1966). Staining tissue for light and electron microscopy by bridging metals with multidentate ligands. *Sci.* 152, 1631–1634. doi:10.1126/science.152.3729.1631

Hochberg, Y. (1988). A sharper Bonferroni procedure for multiple tests of significance. *Biometrika* 75, 800–802. doi:10.1093/BIOMET/75.4.800

Ivell, R., Agoulnik, A. I., and Anand-Ivell, R. (2017). Relaxin-like peptides in male reproduction – A human perspective. *Br. J. Pharmacol.* 174, 990–1001. doi:10.1111/bph.13689

Ivell, R., and Grutzner, F. (2009). Evolution and male fertility: lessons from the insulin-like factor 6 gene (Insl6). *Endocrinology* 150, 3986–3990. doi:10.1210/en.2009-0691

Käll, L., Canterbury, J. D., Weston, J., Noble, W. S., and MacCoss, M. J. (2007). Semi-supervised learning for peptide identification from shotgun proteomics datasets. *Nat. Methods* 4, 923–925. doi:10.1038/nmeth1113

Kang, J. M., Park, S., Kim, S. J., Kim, H., Lee, B., Kim, J., et al. (2015). KIAA1324 suppresses gastric cancer progression by inhibiting the oncoprotein GRP78. *Cancer Res.* 75, 3087–3097. doi:10.1158/0008-5472.CAN-14-3751

Kang-Decker, N., Mantchev, G. T., Juneja, S. C., McNiven, M. A., and van Deursen, J. M. A. (2001). Lack of acrosome formation in hrb-deficient mice. *Science* 294, 1531–1533. doi:10.1126/science.1063665

Kashiwabara, S., Arai, Y., Kodaira, K., and Baba, T. (1990). Acrosin biosynthesis in meiotic and postmeiotic spermatogenic cells. *Biochem. Biophys. Res. Commun.* 173, 240–245. doi:10.1016/S0006-291X(05)81047-2

Kent, K., Johnston, M., Strump, N., and Garcia, T. X. (2020). Toward development of the male pill: a decade of potential non-hormonal contraceptive targets. *Front. Cell. Dev. Biol.* 8, 61. doi:10.3389/fcell.2020.00061

Khawar, M. B., Gao, H., and Li, W. (2019). Mechanism of acrosome biogenesis in mammals. *Front. Cell. Dev. Biol.* 7, 195. doi:10.3389/fcell.2019.00195

Kierszenbaum, A. L., Rivkin, E., and Tres, L. L. (2003). The actin-based motor myosin Va is a component of the acroplaxome, an acrosome-nuclear envelope junctional plate, and of manchette-associated vesicles. *Cytogenet. Genome Res.* 103, 337–344. doi:10.1159/000076822

Kierszenbaum, A. L., Tres, L. L., Rivkin, E., Kang-Decker, N., and Van Deursen, J. M. A. (2004). The acroplaxome is the docking site of golgi-derived myosin va/rab27a/b-containing proacrosomal vesicles in wild-type and hrb mutant mouse spermatids. *Biol. Reprod.* 70, 1400–1410. doi:10.1095/BIOLREPROD.103.025346

Klumperman, J., Kuliawat, R., Griffith, J. M., Geuze, H. J., and Arvan, P. (1998). Mannose 6-phosphate receptors are sorted from immature secretory granules via adaptor protein AP-1, clathrin, and syntaxin 6-positive vesicles. *J. Cell. Biol.* 141, 359–371. doi:10.1083/JCB.141.2.359

Krausz, C., and Riera-Escamilla, A. (2018). Genetics of male infertility. *Nat. Rev. Urol.* 15, 369–384. doi:10.1038/S41585-018-0003-3

Li, Q., Fisher, K., Meng, W., Fang, B., Welsh, E., Haura, E. B., et al. (2020). GMSimpute: a generalized two-step lasso approach to impute missing values in label-free mass spectrum analysis. *Bioinformatics* 36, 257–263. doi:10.1093/BIOINFORMATICS/BTZ488

Lin, Y. N., Roy, A., Yan, W., Burns, K. H., and Matzuk, M. M. (2007). Loss of zona pellucida binding proteins in the acrosomal matrix disrupts acrosome biogenesis and sperm morphogenesis. *Mol. Cell. Biol.* 27, 6794–6805. doi:10.1128/MCB.01029-07

Lu, Y., Oura, S., Matsumura, T., Oji, A., Sakurai, N., Fujihara, Y., et al. (2019). CRISPR/Cas9-mediated genome editing reveals 30 testis-enriched genes dispensable for male fertility in mice. *Biol. Reprod.* 101, 501–511. doi:10.1093/BIOLRE/IOZ103

Martínez-Menárguez, J. A., Geuze, H. J., and Ballesta, J. (1996). Evidence for a nonlysosomal origin of the acrosome. *J. Histochem. Cytochem.* 44, 313–320. doi:10.1177/44.4.8601690

Miyata, H., Castaneda, J. M., Fujihara, Y., Yu, Z., Archambeault, D. R., Isotani, A., et al. (2016). Genome engineering uncovers 54 evolutionarily conserved and testis-enriched genes that are not required for male fertility in mice. *Proc. Natl. Acad. Sci.* 113, 7704–7710. doi:10.1073/pnas.1608458113

Moreno, R. D., and Alvarado, C. P. (2006). The mammalian acrosome as a secretory lysosome: new and old evidence. *Mol. Reprod. Dev.* 73, 1430–1434. doi:10.1002/MRD.20581

Moreno, R. D. (2003). Differential expression of lysosomal associated membrane protein (LAMP-1) during mammalian spermiogenesis. *Mol. Reprod. Dev.* 66, 202–209. doi:10.1002/MRD.10342

Moreno, R. D., Ramalho-Santos, J., Sutovsky, P., Chan, E. K. L., and Schatten, G. (2000). Vesicular traffic and golgi apparatus dynamics during mammalian spermatogenesis: implications for acrosome architecture. *Biol. Reprod.* 63, 89–98. doi:10.1095/BIOLREPROD63.1.89

Oakberg, E. F. (1956). A description of spermiogenesis in the mouse and its use in analysis of the cycle of the seminiferous epithelium and germ cell renewal. *Am. J. Anat.* 99, 391–413. doi:10.1002/AJA.1000990303

Otčenášková, T., Macíčková, E., Vondráková, J., Frolíková, M., Komrskova, K., Stopková, R., et al. (2023). Proteomic analysis of the mouse sperm acrosome - towards an understanding of an organelle with diverse functionality. *Eur. J. Cell. Biol.* 102, 151296. doi:10.1016/J.EJCB.2023.151296

Park, S., Shimada, K., Fujihara, Y., Xu, Z., Shimada, K., Larasati, T., et al. (2020). CRISPR/Cas9-mediated genome-edited mice reveal 10 testis-enriched genes are dispensable for male fecundity. *Biol. Reprod.* 103, 195–204. doi:10.1093/BIOLRE/IOAA084

Perez-Riverol, Y., Bai, J., Bandla, C., García-Seisdedos, D., Hewapathirana, S., Kamatchinathan, S., et al. (2022). The PRIDE database resources in 2022: a hub for mass spectrometry-based proteomics evidences. *Nucleic Acids Res.* 50, D543–D552. doi:10.1093/nar/gkab1038

Pierre, V., Martinez, G., Coutton, C., Delaroche, J., Yassine, S., Novella, C., et al. (2012). Absence of Dpy19l2, a new inner nuclear membrane protein, causes globozoospermia in mice by preventing the anchoring of the acrosome to the nucleus. *Development* 139, 2955–2965. doi:10.1242/dev.077982

Ramalho-Santos, J., Moreno, R. D., Wessel, G. M., Chan, E. K. L., and Schatten, G. (2001). Membrane trafficking machinery components associated with the mammalian acrosome during spermiogenesis. *Exp. Cell. Res.* 267, 45–60. doi:10.1006/EXCR.2000.5119

Raudvere, U., Kolberg, L., Kuzmin, I., Arak, T., Adler, P., Peterson, H., et al. (2019). g:Profiler: a web server for functional enrichment analysis and conversions of gene lists (2019 update). *Nucleic Acids Res.* 47, W191–W198. doi:10.1093/NAR/GKZ369

Ren, M., Xu, Y., Erdjument-Bromage, H., Donelian, A., Phoon, C. K. L., Terada, N., et al. (2019). Extramitochondrial cardiolipin suggests a novel function of mitochondria in spermatogenesis. *J. Cell. Biol.* 218, 1491–1502. doi:10.1083/JCB.201808131

Ren, M., Xu, Y., Phoon, C. K. L., Erdjument-Bromage, H., Neubert, T. A., Rajan, S., et al. (2022). Condensed mitochondria assemble into the acrosomal matrix during spermiogenesis. *Front. Cell. Dev. Biol.* 10, 867175. doi:10.3389/FCELL.2022.867175

Sayols, S. (2020). rrvgo: a Bioconductor package for interpreting lists of Gene Ontology terms. *Micropubl. Biol.* 10, 881. doi:10.17912/micropub.biology.000811

Schindelin, J., Arganda-Carreras, I., Frise, E., Kaynig, V., Longair, M., Pietzsch, T., et al. (2012). Fiji: an open-source platform for biological-image analysis. *Nat. Methods* 9, 676–682. doi:10.1038/NMETH.2019

Schultz, N., Hamra, F. K., and Garbers, D. L. (2003). A multitude of genes expressed solely in meiotic or postmeiotic spermatogenic cells offers a myriad of contraceptive targets. *Proc. Natl. Acad. Sci.* 100, 12201–12206. doi:10.1073/pnas.1635054100

Slot, J. W., and Geuze, H. J. (2007). Cryosectioning and immunolabeling. *Nat. Protoc.* 2, 2480–2491. doi:10.1038/nprot.2007.365

Soriano, P. (1999). Generalized lacZ expression with the ROSA26 Cre reporter strain. *Nat. Genet.* 21, 70–71. doi:10.1038/5007

Stinnesbeck, M., Kristiansen, A., Ellinger, J., Hauser, S., Egevad, L., Tolkach, Y., et al. (2021). Prognostic role of TSPAN1, KIAA1324 and ESRP1 in prostate cancer. *APMIS* 129, 204–212. doi:10.1111/APM.13117

Tang, T., Li, L., Tang, J., Li, Y., Lin, W. Y., Martin, F., et al. (2010). A mouse knockout library for secreted and transmembrane proteins. *Nat. Biotechnol.* 28, 749–755. doi:10.1038/nbt.1644

Tokuyasu, K. T. (1980). Immunochemistry on ultrathin frozen sections. *Histochem. J.* 12, 381–403. doi:10.1007/BF01011956

Varadi, A., Tsuboi, T., and Rutter, G. A. (2005). Myosin Va transports dense core secretory vesicles in pancreatic MIN6 beta-cells. *Mol. Biol. Cell.* 16, 2670–2680. doi:10.1091/MBC.E04-11-1001

Venable, J. H., and Coggeshall, R. (1965). A simplified lead citrate stain for use in electron microscopy. *J. Cell. Biol.* 25, 407–408. doi:10.1083/jcb.25.2.407

Völkner, M., Wagner, F., Steinheuer, L. M., Carido, M., Kurth, T., Yazbeck, A., et al. (2022). HBEGF-TNF induce a complex outer retinal pathology with photoreceptor cell extrusion in human organoids. *Nat. Commun.* 131, 6183–6222. doi:10.1038/s41467-022-33848-y

Wakayama, T., Yokota, S., Noguchi, K., Sugawara, T., Sonoda, K., and Wanta, A. (2022). Quantitative evaluation of spermatogenesis by fluorescent histochemistry. *Histochem. Cell. Biol.* 157, 287–295. doi:10.1007/s00418-022-02080-6

Wilhelmi, I., Grunwald, S., Gimber, N., Popp, O., Dittmar, G., Arumughan, A., et al. (2021). The ARFRP1-dependent Golgi scaffolding protein GOPC is required for insulin secretion from pancreatic β-cells. *Mol. Metab.* 45, 101151. doi:10.1016/J.MOLMET.2020.101151

Wiśniewski, J. R., Zougman, A., Nagaraj, N., and Mann, M. (2009). Universal sample preparation method for proteome analysis. *Nat. Methods* 65, 359–362. doi:10.1038/nmeth.1322

Wissmiller, K., Bilekova, S., Franko, A., Lutz, S. Z., Katsburg, M., Gulde, S., et al. (2023). Inceptor correlates with markers of prostate cancer progression and modulates insulin/IGF1 signaling and cancer cell migration. *Mol. Metab.* 71, 101706. doi:10.1016/J.MOLMET.2023.101706

Xiao, N., Kam, C., Shen, C., Jin, W., Wang, J., Kwong, M. L., et al. (2009). PICK1 deficiency causes male infertility in mice by disrupting acrosome formation. *J. Clin. Invest.* 119, 802–812. doi:10.1172/JCI36230

Yao, R., Ito, C., Natsume, Y., Sugitani, Y., Yamanaka, H., Kuretake, S., et al. (2002). Lack of acrosome formation in mice lacking a Golgi protein, GOPC. *Proc. Natl. Acad. Sci.* 99, 11211–11216. doi:10.1073/pnas.162027899

Supplementary Table 2 - Candidate interactors of inceptor from the mass spectrometry analysis. Arranged from top to bottom by descending fold change compared to a co-IP with a control antibody. The candidates have been filtered for $q < 0.05$, fold change > 2, and < 60 % missing values.

	Gene	Description	Fold change	*q* value
1	Nudt21	Cleavage and polyadenylation specificity factor subunit 5	Inf	0.00024
2	Ap3m2	AP-3 complex subunit mu-2	Inf	0.00881
3	Sh3bgrl	SH3 domain-binding glutamic acid-rich-like protein	Inf	0.00999
4	Gorasp2	Golgi reassembly-stacking protein 2	97159.2	0.01328
5	Epb41	Protein 4.1	20328.8	0.00002
6	Pdk1	[Pyruvate dehydrogenase (acetyl-transferring)] kinase isozyme 1, mitochondrial	448.3	0.00398
7	Hephl1	Ferroxidase HEPHL1	405.4	0.03284
8	Map1a	Microtubule-associated protein 1A	281.1	0.01887
9	Ranbp1	Ran-specific GTPase-activating protein	250.7	0.03524
10	Pycr3	Pyrroline-5-carboxylate reductase 3	235.0	0.03564
11	Snx3	Sorting nexin-3	144.7	0.00103
12	Dlg4	Disks large homolog 4	141.9	0.02217
13	Rpe65	Retinoid isomerohydrolase	141.8	0.04080
14	Nucks1	Nuclear ubiquitous casein and cyclin-dependent kinase substrate 1	133.6	0.02184
15	Tmem190	Transmembrane protein 190	114.7	0.00103
16	Gpm6b	Neuronal membrane glycoprotein M6-b	112.4	0.00467
17	Pdxk	Pyridoxal kinase	83.3	0.00618
18	Dctn5	Dynactin subunit 5	76.0	0.00233
19	Pgm2	Phosphoglucomutase-2	69.9	0.00176
20	Basp1	Brain acid soluble protein 1	68.6	0.02720
21	Septin6	Septin-6	55.7	0.02944
22	Dnajb2	DnaJ homolog subfamily B member 2	51.4	0.00854
23	Tax1bp1	Tax1-binding protein 1 homolog	47.6	0.02445
24	Msn	Moesin	41.9	0.01004
25	Gnb5	Guanine nucleotide-binding protein subunit beta-5	41.0	0.01762
26	Arhgdia	Rho GDP-dissociation inhibitor 1	36.4	0.00036
27	Atp5md	ATP synthase membrane subunit DAPIT, mitochondrial	35.2	0.02846
28	Eprs1	Bifunctional glutamate/proline--tRNA ligase	32.7	0.04879
29	Pcmt1	Protein-L-isoaspartate(D-aspartate) O-methyltransferase	32.7	0.02360
30	Pgm1	Phosphoglucomutase-1	32.5	0.00000
31	Nrbp1	Nuclear receptor-binding protein	32.1	0.01056
32	Syngr1	Synaptogyrin-1	31.5	0.00704
33	Syn1	Synapsin-1	30.9	0.00803
34	Stx7	Syntaxin-7	30.6	0.00557
35	Psmc6	26S proteasome regulatory subunit 10B	28.3	0.04948
36	Pacs1	Phosphofurin acidic cluster sorting protein 1	27.8	0.04763
37	Kiaa0753	Protein moonraker	27.7	0.00054
38	Pkp3	Plakophilin-3	27.5	0.04959
39	Pafah1b1	Platelet-activating factor acetylhydrolase IB subunit alpha	27.4	0.00104
40	Dnajb6	DnaJ homolog subfamily B member 6	25.6	0.01016
41	Arl6	ADP-ribosylation factor-like protein 6	25.2	0.04948
42	Slc25a11	Mitochondrial 2-oxoglutarate/malate carrier protein	24.8	0.01371

43	Capg	Macrophage-capping protein	22.0	0.02720
44	Psmg3	Proteasome assembly chaperone 3	21.4	0.04059
45	Auh	Methylglutaconyl-CoA hydratase, mitochondrial	21.2	0.03994
46	Ncam2	Neural cell adhesion molecule 2	21.0	0.03524
47	Uqcrfs1	Cytochrome b-c1 complex subunit Rieske, mitochondrial	19.6	0.02846
48	Atp2a2	Sarcoplasmic/endoplasmic reticulum calcium ATPase 2	19.2	0.00621
49	Dctn1	Dynactin subunit 1	17.6	0.02293
50	Immt	MICOS complex subunit Mic60	17.6	0.02918
51	Hdgfl3	Hepatoma-derived growth factor-related protein 3	16.7	0.02846
52	Arf3	ADP-ribosylation factor 3	16.3	0.00927
53	Snx27	Sorting nexin-27	16.2	0.03645
54	Scamp1	Secretory carrier-associated membrane protein 1	15.6	0.03524
55	Otub1	Ubiquitin thioesterase OTUB1	15.0	0.02431
56	Gucy2e	Retinal guanylyl cyclase 1	14.7	0.02937
57	Hnrnpdl	Heterogeneous nuclear ribonucleoprotein D-like	14.4	0.01045
58	Dlst	Dihydrolipoyllysine-residue succinyltransferase component of 2-oxoglutarate dehydrogenase complex, mitochondrial	14.3	0.03672
59	Chn2	Beta-chimaerin	14.2	0.00293
60	Kiaa1324	UPF0577 protein KIAA1324	13.3	0.00003
61	Kif2c	Kinesin-like protein KIF2C	13.1	0.04959
62	Snap25	Synaptosomal-associated protein 25	13.0	0.01904
63	Psmd12	26S proteasome non-ATPase regulatory subunit 12	12.7	0.00396
64	Pgrmc2	Membrane-associated progesterone receptor component 2	12.7	0.01721
65	Rlbp1	Retinaldehyde-binding protein 1	12.5	0.03284
66	Nipsnap1	Protein NipSnap homolog 1	12.5	0.03524
67	Prdx6	Peroxiredoxin-6	11.9	0.01381
68	Uba1	Ubiquitin-like modifier-activating enzyme 1	11.9	0.02459
69	Stx12	Syntaxin-12	11.8	0.00740
70	Cadps	Calcium-dependent secretion activator 1	11.7	0.00060
71	Crk	Adapter molecule crk	11.7	0.03990
72	Tubb2a	Tubulin beta-2A chain	11.5	0.03054
73	Appl1	DCC-interacting protein 13-alpha	11.3	0.02316
74	Amph	Amphiphysin	11.2	0.00370
75	Prdx3	Thioredoxin-dependent peroxide reductase, mitochondrial	11.0	0.01328
76	Nptn	Neuroplastin	10.6	0.03883
77	Impdh1	Inosine-5'-monophosphate dehydrogenase 1	9.9	0.02426
78	Psme3ip1	PSME3-interacting protein	8.2	0.00175
79	Cs	Citrate synthase, mitochondrial	8.2	0.03054
80	Hprt1	Hypoxanthine-guanine phosphoribosyltransferase	8.1	0.00054
81	Chchd3	MICOS complex subunit Mic19	7.5	0.03564
82	Hpca	Neuron-specific calcium-binding protein hippocalcin	7.5	0.03284
83	Pea15	Astrocytic phosphoprotein PEA-15	7.0	0.04009
84	Rpsa	40S ribosomal protein SA	7.0	0.04053
85	Gstp2	Glutathione S-transferase P 2	6.2	0.00048
86	Rab3a	Ras-related protein Rab-3A	6.2	0.03564
87	Ptgfrn	Prostaglandin F2 receptor negative regulator	6.1	0.00523
88	Snrpa1	U2 small nuclear ribonucleoprotein A'	5.9	0.02217
89	Sae1	SUMO-activating enzyme subunit 1	5.8	0.00483
90	Pygl	Glycogen phosphorylase, liver form	5.6	0.00103
91	Glud1	Glutamate dehydrogenase 1, mitochondrial	5.5	0.04879
92	Sptbn1	Spectrin beta chain, non-erythrocytic 1	4.8	0.00005
93	Ccdc90b	Coiled-coil domain-containing protein 90B, mitochondrial	4.8	0.00008

94	Atp1a1	Sodium/potassium-transporting ATPase subunit alpha-1	4.7	0.00995
95	Eef1a2	Elongation factor 1-alpha 2	4.4	0.03424
96	Qars1	Glutamine--tRNA ligase	4.3	0.04879
97	Acp1	Low molecular weight phosphotyrosine protein phosphatase	4.3	0.04111
98	Ppp2cb	Serine/threonine-protein phosphatase 2A catalytic subunit beta isoform	4.2	0.00483
99	Ube2v2	Ubiquitin-conjugating enzyme E2 variant 2	4.2	0.00740
100	Lmna	Prelamin-A/C	4.2	0.00654
101	Psmd13	26S proteasome non-ATPase regulatory subunit 13	4.1	0.00043
102	Smc1a	Structural maintenance of chromosomes protein 1A	4.1	0.00704
103	Psmd2	26S proteasome non-ATPase regulatory subunit 2	3.9	0.02445
104	Eif2s2	Eukaryotic translation initiation factor 2 subunit 2	3.8	0.04797
105	Eif3e	Eukaryotic translation initiation factor 3 subunit E	3.7	0.04220
106	Ncl	Nucleolin	3.7	0.02108
107	Erlin2	Erlin-2	3.6	0.02513
108	Aifm1	Apoptosis-inducing factor 1, mitochondrial	3.5	0.04051
109	Nop53	Ribosome biogenesis protein NOP53	3.4	0.00498
110	Cse1l	Exportin-2	3.4	0.00621
111	Acly	ATP-citrate synthase	3.2	0.04202
112	Arf4	ADP-ribosylation factor 4	3.2	0.04959
113	Igsf3	Immunoglobulin superfamily member 3	3.2	0.00999
114	Hk1	Hexokinase-1	3.1	0.00112
115	Cct3	T-complex protein 1 subunit gamma	3.0	0.01604
116	Arpc2	Actin-related protein 2/3 complex subunit 2	3.0	0.00897
117	Lrrc59	Leucine-rich repeat-containing protein 59	3.0	0.04202
118	Pfkm	ATP-dependent 6-phosphofructokinase, muscle type	2.8	0.00740
119	Cct6a	T-complex protein 1 subunit zeta	2.8	0.02426
120	Uba3	NEDD8-activating enzyme E1 catalytic subunit	2.5	0.01698
121	Plec	Plectin	2.5	0.04343
122	Rps6	40S ribosomal protein S6	2.5	0.01160
123	Atp6v0a1	V-type proton ATPase 116 kDa subunit a isoform 1	2.2	0.03969
124	Psmc2	26S proteasome regulatory subunit 7	2.2	0.03284
125	Ipo5	Importin-5	2.2	0.02184
126	Tcp1	T-complex protein 1 subunit alpha	2.0	0.03564
127	Ift122	Intraflagellar transport protein 122 homolog	2.0	0.03120
128	Eftud2	116 kDa U5 small nuclear ribonucleoprotein component	2.0	0.01964

Supplementary Figure S1. Inceptor expression and *Iir*$^{-/-}$ mouse line generation. (A) Cell type-specific *Iir* expression (normalized transcripts per million TPM) in Human Protein Atlas scRNA-seq data. Shown are the top 20 cell types with highest *Iir* expression. Cell type groups, sharing common functional features, are shown in different colors. (B) Representative immunostaining confocal images of inceptor expression in various tissues. The image brightness setting is not maintained between images. The images of the stomach, salivary gland, and colon are maximum-intensity projections. Scale bar 25 μm. (C) schematic representation of the *Iir*$^{-}$ allele generation in mice. (D) percentage of the genotypes at weaning age of litters from *Iir*$^{+/-}$ intercrosses, n = 132. (E) Western blot of testis lysates from *Iir*$^{+/+}$ and *Iir*$^{-/-}$ mice.

Supplementary Figure S2. *Iir*$^{-/-}$ mice show normal testis gross morphology. (A) Body weight, (B) testis weight, and (C) caudal sperm count of 9–12-week-old *Iir*$^{+/+}$ and *Iir*$^{-/-}$ mice. (D) testis (T) and epididymis (epi) of *Iir*$^{+/+}$ and *Iir*$^{-/-}$ mice. Tick marks 1 mm. (E) Representative immunofluorescence images of the germ cells (DDX4) and Sertoli cells (GATA-4) in the seminiferous tubules. Image brightness has been adjusted to match DAPI intensity between images. Scale bar 50 μm. (F) Quantification of seminiferous tubule diameter at the narrowest section. Each dot represents a tubule measurement from a total of 87 and 66 tubules in *Iir*$^{+/+}$ and *Iir*$^{-/-}$ testes sections, respectively, n = 3 for both genotypes.

Supplementary Figure S3. *Iir*$^{-/-}$ spermatids have morphological defects in later stages of development. (A-C) Electron micrographs of *Iir*$^{+/+}$ elongated spermatid development and (D-F) *Iir*$^{-/-}$ elongated spermatid development. Scale bar 2 μm.

Supplementary Figure S4. Tree map of the reduction of GO:BP terms of the inceptor interactome. Schematic representation of the reduction of GO:BP terms into eleven parental terms.

Supplementary Table 1. Data used for plotting the log2(FC) and *p* value of the testis proteome. The *p* value was adjusted according to Hochberg. The hits are listed by descending -log10(*p* value).

Supplementary Table 2. Candidate interactors of inceptor from the mass spectrometry analysis. Arranged from top to bottom by descending fold change compared to a co-IP with a control antibody. The candidates have been filtered for $q < 0.05$, fold change > 2, and < 60 % missing values.

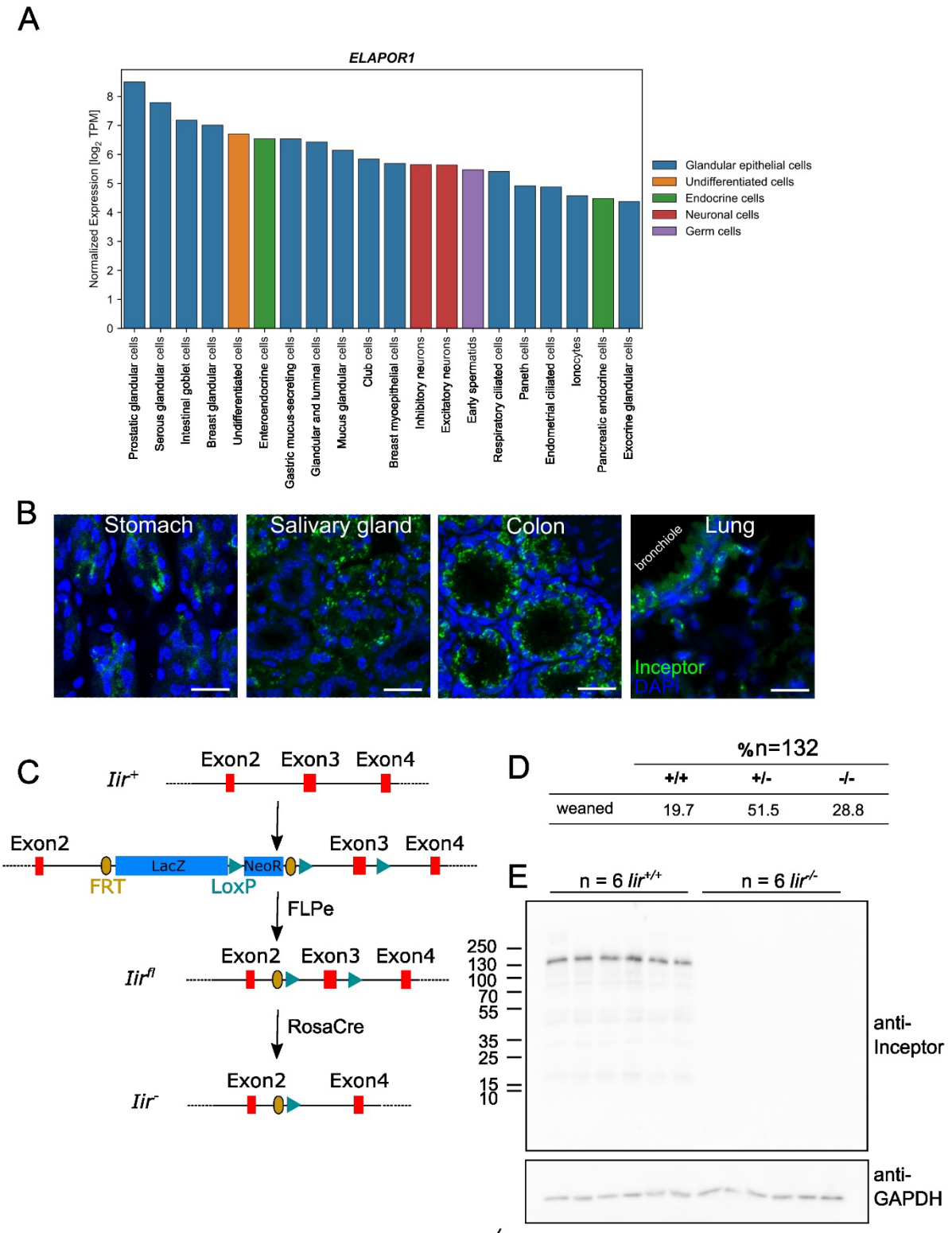

Supplementary figure S1 Inceptor expression and *lir*$^{-/-}$ mouse line generation.

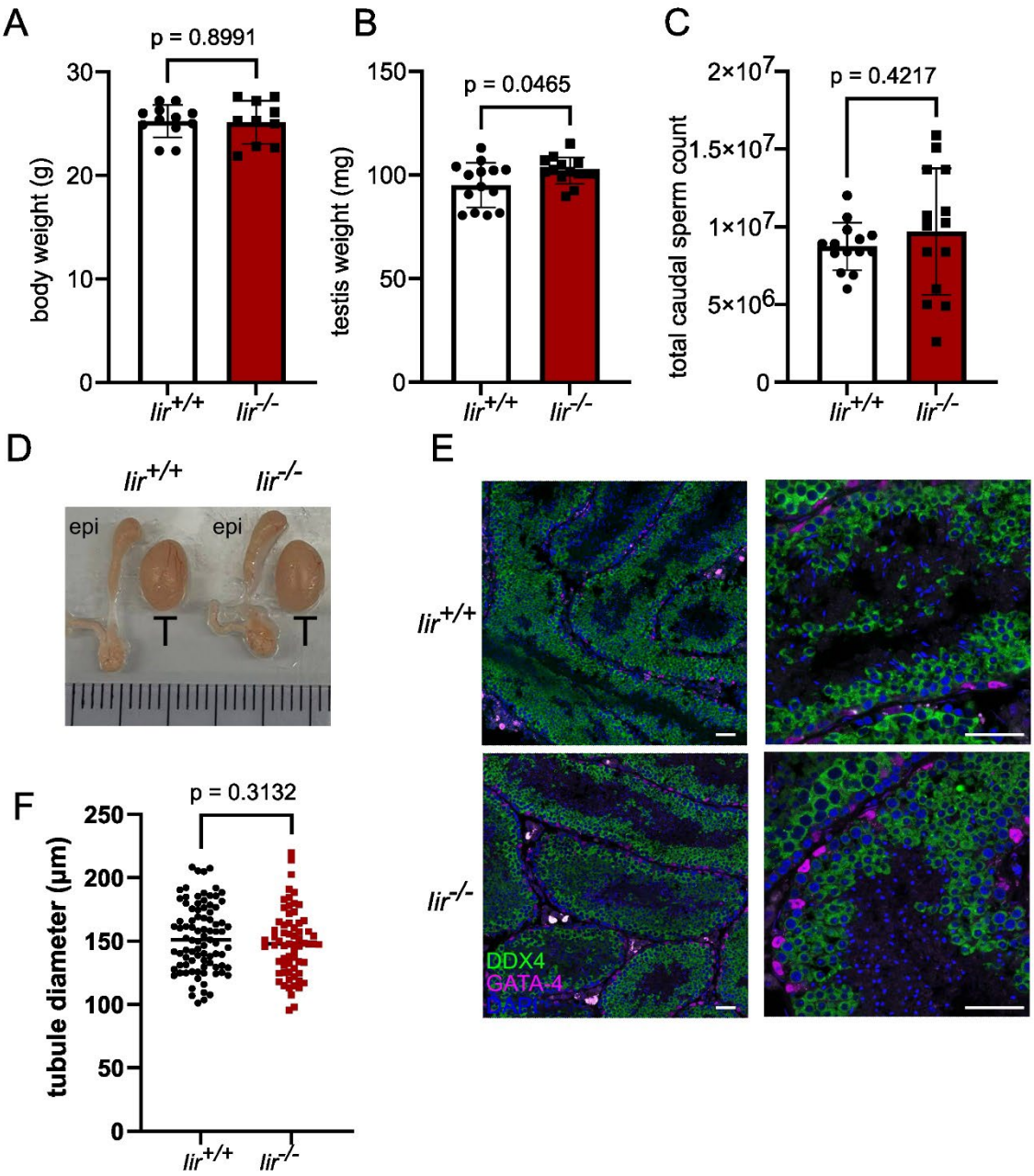

Supplementary figure S2 *lir*$^{-/-}$ mice show normal testis gross morphology.

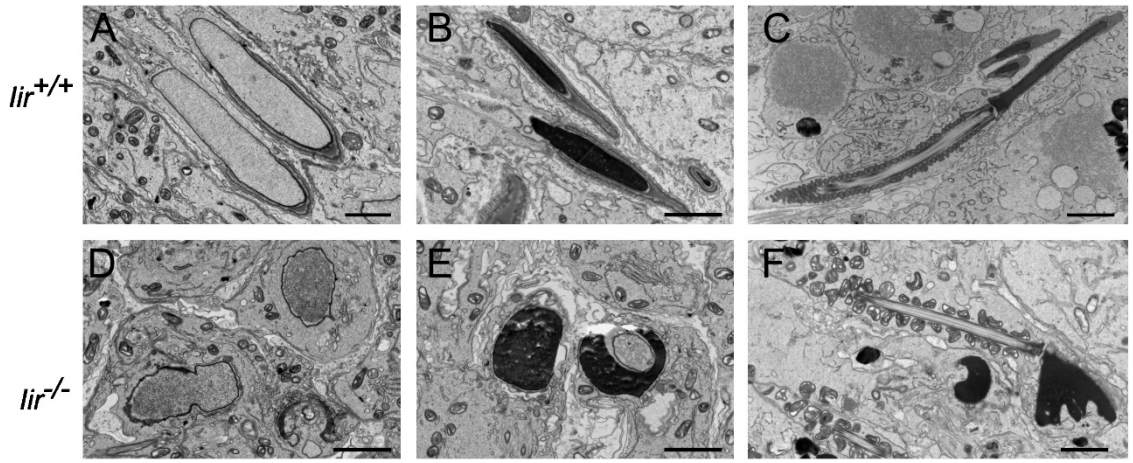

Supplementary figure S3 *lir*$^{-/-}$ spermatids have morphological defects in later stages of development.

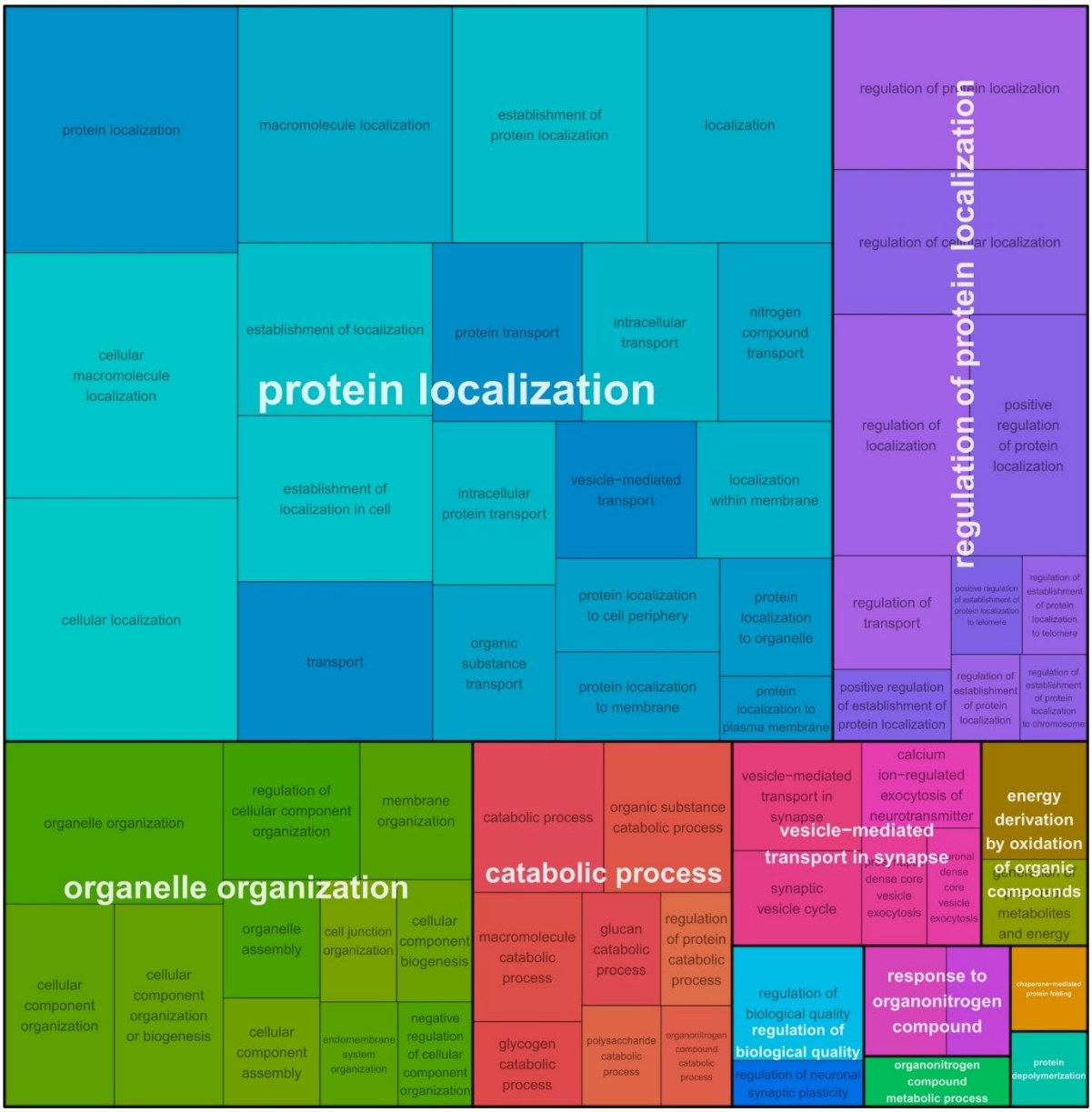

Supplementary figure S4 Tree map of the reduction of GO:BP terms of the inceptor interactome.

Original Article

MOLECULAR METABOLISM

Inceptor correlates with markers of prostate cancer progression and modulates insulin/IGF1 signaling and cancer cell migration

Katharina Wissmiller [1,2,3,10], Sara Bilekova [1,2,3,10], Andras Franko [2,4,5], Stefan Z. Lutz [5,6], Miriam Katsburg [1], Sebastian Gulde [7], Natalia S. Pellegata [7], Arnulf Stenzl [8], Martin Heni [2,4,5,9], Lucia Berti [2,4], Hans-Ulrich Häring [2,4,5], Heiko Lickert [1,2,3,*]

ABSTRACT

Objective: The insulin/insulin-like growth factor 1 (IGF1) pathway is emerging as a crucial component of prostate cancer progression. Therefore, we investigated the role of the novel insulin/IGF1 signaling modulator inceptor in prostate cancer.

Methods: We analyzed the expression of inceptor in human samples of benign prostate epithelium and prostate cancer. Further, we performed signaling and functional assays using prostate cancer cell lines.

Results: We found that inceptor was expressed in human benign and malignant prostate tissue and its expression positively correlated with various genes of interest, including genes involved in androgen signaling. *In vitro,* total levels of inceptor were increased upon androgen deprivation and correlated with high levels of androgen receptor in the nucleus. Inceptor overexpression was associated with increased cell migration, altered IGF1R trafficking and higher IGF1R activation.

Conclusions: Our *in vitro* results showed that inceptor expression was associated with androgen status, increased migration, and IGF1R signaling. In human samples, inceptor expression was significantly correlated with markers of prostate cancer progression. Taken together, these data provide a basis for investigation of inceptor in the context of prostate cancer.

Keywords Insulin; IGF1R; Androgen; Signaling; Trafficking

1. INTRODUCTION

Hyperinsulinemia is known to increase the risk for many cancer types [1], thus the potential link between diabetes and cancer is of interest in exploring diagnosis and treatment options. While the risk for prostate cancer is not increased in patients with diabetes mellitus [2], the prognosis for prostate cancer patients with diabetes is worse [3–6]. This goes along with altered carcinogenic pathways [7]. Prostate cancer is the third most frequent type of cancer among males worldwide [8]. The initial treatment for localized prostate cancer includes radical prostatectomy, radiation and chemotherapy [9]. As prostate tumor growth is highly dependent on androgens, the chemotherapeutical treatment of choice is androgen deprivation therapy via antiandrogens [10]. These substances block the androgen receptor (AR), which is a transcription factor that is dimerized after binding to androgen and translocated to the nucleus, where it binds to androgen response elements and modulates gene expression [11].

However, during the course of androgen deprivation therapy patients often become resistant to treatment and develop androgen-independent tumors. There is currently no effective treatment for this highly invasive and metastatic form of prostate cancer. Several pathways contribute to the progression towards androgen-independent prostate cancer [12]. For instance, the AR can become hypersensitive to residual androgen through gene duplication [13], or it can become promiscuous and recognize other steroids or even anti-androgens [14]. Some tumors switch to bypass pathways that activate proliferation via entirely different mechanisms [15]. Finally, AR downstream signaling can be cross-activated by other pathways, e.g.

[1]Institute of Diabetes and Regeneration Research at the Helmholtz Center Munich, Ingolstaedter Landstr. 1, 85764, Neuherberg, Germany [2]German Center for Diabetes Research (DZD), Ingolstaedter Landstr. 1, 85764, Neuherberg, Germany [3]Technical University of Munich, School of Medicine, Ismaninger Str. 22, 81675, Munich, Germany [4]Institute of Diabetes and Metabolic Disease at the Helmholtz Center Munich, Ottfried-Müller-Str. 10, 72076, Tübingen, Germany [5]Department of Internal Medicine, Division of Endocrinology, Diabetology and Nephrology, University Hospital Tübingen, Ottfried-Müller-Str. 10, 72076, Tübingen, Germany [6]Clinic for Geriatric and Orthopedic Rehabilitation Bad Sebastiansweiler, Hechinger Str. 26, 72116, Mössingen, Germany [7]Institute of Diabetes and Cancer at the Helmholtz Center Munich, Ingolstaedter Landstr. 1, 85764, Neuherberg, Germany [8]Department of Urology, University Hospital Tübingen, Hoppe-Seyler-Str. 3, 72076, Tübingen, Germany [9]Department for Diagnostic Laboratory Medicine, Institute for Clinical Chemistry and Pathobiochemistry, University Hospital Tübingen, Hoppe-Seyler-Str. 3, 72076, Tübingen, Germany

[10] These authors contributed equally to this work.

*Corresponding author: Institute of Diabetes and Regeneration Research at the Helmholtz Center Munich, Ingolstaedter Landstr. 1, 85764, Neuherberg, Germany E-mail: heiko.lickert@helmholtz-munich.de (H. Lickert).

Received December 1, 2022 • Revision received February 21, 2023 • Accepted March 9, 2023 • Available online 15 March 2023

https://doi.org/10.1016/j.molmet.2023.101706

Abbreviations

5-HT	5-hydroxytryptamine (serotonin)
AR	Androgen Receptor
ARE	Androgen Response Element
BMI	Body Mass Index
CK	Cytokeratin
EdU	5-ethynyl-2′-deoxyuridine
DAPI	4′,6-diamidino-2-phenylindole
EGF	Epidermal Growth Factor
EGFR	Epidermal Growth Factor Receptor
ER	Estrogen Receptor
ERE	Estrogen Response Element
FBS	Fetal Bovine Serum
HPA	Human Protein Atlas
HPEC	Human Primary Prostate Epithelial Cells
Ins	Insulin
IGF1	Insulin-like growth factor 1
IGF1R	Insulin-like growth factor 1 receptor
IgG	Immunoglobulin G
IIR/inceptor	Insulin Inhibitory Receptor
IP	Immunoprecipitation
IR	Insulin Receptor
LAMP1	Lysosomal-associated membrane protein 1
PBS	Phosphate-Buffered Saline
PI3K	Phosphoinositide 3-kinase
PSA	Prostate-Specific Antigen (aka KLK3)
PSMA	Prostate-Specific Membrane Antigen (aka FOLH1)
(q)PCR	(quantitative) Polymerase Chain Reaction
TCGA	The Cancer Genome Atlas
WT	Wildtype

the insulin-like growth factor 1 receptor (IGF1R) pathway [16]. Immunohistochemical staining of human tissue samples has shown that IGF1R is upregulated in prostate cancer during androgen-independent progression [17,18]. As a potential mechanism, it has been suggested that IGF1R signaling induces phosphorylation of Foxo1, which subsequently leaves the nucleus and loses its ability to block AR [19].

The PI3K/Akt pathway, which is downstream of insulin receptor (IR), IGF1R and epidermal growth factor receptor (EGFR), is highly relevant in the context of cancer initiation and progression [20,21]. The combined inhibition of AR and PI3K proved effective in an animal model of androgen-independent prostate cancer [22]. Inhibitors of mTOR, which is activated by Akt, have been implicated in prostate cancer therapy in multiple studies [23,24]. Direct inhibition of IGF1R has shown promising results in androgen-independent prostate cancer as monotherapy [25] or in combination with the cytotoxic agent docetaxel [26]. IR acts via the same downstream pathways as IGF1R. Specifically the isoform IRa, which is mainly important during embryonic development and in various malignancies, has a high affinity for IGF1 and IGF2. In contrast to the more common isoform IRb, IRa predominantly activates proliferative rather than metabolic pathways [27]. It is therefore not surprising that IR activation can compensate for IGF1R inhibition in prostate cancer cells [28]. Likewise, a recent study revealed that insulin can reactivate the loss of PI3K signaling achieved by PI3K inhibitors [29]. Further, it was shown that AR signaling is elevated in prostate cancer patients with diabetes [30]. In addition to these findings, there is evidence that hyperinsulinemia can be a major driver for prostate cancer progression [31,32]. Thus, targeting the insulin/IGF1 axis might be beneficial in the treatment of metastatic prostate cancer. We have previously found that a novel receptor, namely insulin inhibitory receptor (gene name: *IIR*/short form: inceptor), is a negative regulator of insulin and IGF1 signaling in pancreatic β-cells. We showed that inceptor knockout in β-cells led to increased IR and IGF1R activation *in vitro* and *in vivo*, and that inceptor desensitized IR and IGF1R by facilitating clathrin-mediated receptor endocytosis [33]. In earlier studies, inceptor was associated with various cancers. Initially, it was described as a biomarker in estrogen-related endometrial carcinoma and therefore termed estrogen-induced gene 121 (*EIG121*) [34]. Later it was shown that expression of this gene, also referred to as *KIAA1324*, was correlated to favorable prognosis in pancreatic neuroendocrine tumors and suppressed gastric cancer growth [35,36]. However, inceptor induced progression of endometrial cancer *in vitro* and *in vivo* [37] and was associated with poor prognosis in ovarian cancer [38]. The expression of inceptor in healthy tissues according to the Human Protein Atlas [39] is highest in the prostate, along with uterus, stomach and salivary glands. Further, it is expressed in the pituitary gland and other reproductive organs, i.e., testis, breast, endometrium and fallopian tube [39]. Thus, we hypothesize that due to its interaction with insulin/IGF1 signaling and its potential link to sex hormone signaling inceptor might be a drug target candidate in prostate cancer. For this reason, we investigated the expression of inceptor in benign and malignant prostate tissues and examined its potential role in prostate cancer cell lines.

2. MATERIAL AND METHODS

2.1. Animal breeding

Mouse breeding was performed in compliance with the German Animal Protection Act and with the approved guidelines of the Society of Laboratory Animals (GV-SOLAS) and the Federation of Laboratory Animal Science Associations (FELASA). The male mice (strain: CD1xC57BL) were 4 months old and fed ad libitum.

2.2. Cell culture

LNCaP and LNCaP C4-2 cells were purchased from ATCC (CRL-1740, CRL-3314) and routinely cultured in RPMI 1640 with L-Glutamine (Gibco, 21875034), supplemented with 10% fetal bovine serum (FBS) (Pan, P40-37500). For androgen deprivation, the cells were maintained in RPMI 1640 without phenol red (Gibco, 11835030), supplemented with 10% charcoal-stripped FBS (Sigma–Aldrich, F6765). As a control, 10 nM dihydrotestosterone (DHT) (Sigma–Aldrich, D-073) was added to the charcoal-stripped medium. The medium was changed every 2 days. BPH-1 cells were purchased from DSMZ (ACC 143) and cultured in RPMI 1640 + 20% FBS + 20 ng/ml testosterone + 5 μg/ml transferrin +5 ng/ml sodium selenite + 5 μg/ml insulin. Human Prostate Epithelial cells (HPEC) (Merck Millipore, SCCE019) were cultivated using the Prostate Epithelia Complete Culture Kit (Merck Millipore, SCMP001) and PC3 cells (CLS, 300,312) were grown in DMEM F-12 (Gibco, 11,039, +5% FBS).

2.3. Cell line generation

The stable cell lines overexpressing inceptor-venus or venus only were generated by transfection of LNCaP cells using Lipofectamine 2000 (Thermo Fisher, 11668027) and selection with 1 μg/ml puromycin (Thermo Fisher, A1113803) for approx. 4 weeks. The cells were then sorted according to expression levels via fluorescence-activated cell

sorting (FACS) to ensure that clones with similar expression levels were analyzed. The construct pCAG-inceptor-venus was generated as described before [33].

2.4. Immunohistochemistry

Cells were seeded in μ-slide 8 well chambers (Ibidi, 80,826) at a density of 25,000 cells per well and after 3 days were fixed in 4% PFA for 10 min at room temperature and permeabilized in 0.25% Triton-X100, 100 mM glycine for 15 min at room temperature.

Isolated mouse prostates were dehydrated in a sucrose gradient (7.5—30% sucrose in phosphate-buffered saline [PBS]) after overnight fixation in 4% PFA at 4 °C and embedded in tissue freezing medium (Leica, 14020108926) before cutting 10 μm sections. The frozen sections were rehydrated in PBS and permeabilized in 0.5% Triton-X100 for 20 min at room temperature.

Human prostate paraffin sections were deparaffinized in xylol, rehydrated in an ethanol series (100%—40%) and boiled in 100 mM sodium citrate, pH 6.0.

The cells or sections were blocked in 0.1% Tween-20, 10% FCS, 0.1% BSA and 3% donkey serum for 1 h at room temperature and incubated with the following primary antibodies overnight at 4 °C: rat anti-inceptor #16F6 or #2G6, or mouse anti-inceptor #31A11 (unpurified antibody in 1:10 dilution), rabbit anti-Cytokeratin 5 (Abcam, ab53121, 1:400), guinea pig anti-Cytokeratin 8/18 (OriGene, BP5007, 1:200), rabbit anti-AR (Abcam, ab133273, 1:200), rabbit anti-5HT/Serotonin (Neuromics, RA20080, 1:1000), rabbit anti-E-cadherin (Cell Signaling 24E10, 3195, 1:100), mouse anti-GM130 (BD, 610,822, 1:400), rabbit anti-Giantin (BioLegend, 924,302, 1:400), rat anti-LAMP1 (BD, 553,792, 1:100), rabbit anti-IR beta (SantaCruz, sc-711, 1:2000), rabbit anti-IGF1R (Cell Signaling, 3024, 1:100), rabbit anti-EGFR (Cell Signaling, 4267, 1:400). The inceptor antibodies #16F6 and #31A11 were previously validated in a murine β-cell line [33], and the validation of #2G6 is shown in Fig. S4. All inceptor antibodies were provided by Regina Feederle, Monoclonal Antibody Core Facility, Helmholtz-Zentrum München).

After washing with PBS-T (PBS + 0.1% Tween-20), the secondary antibodies were added in 1:800 dilution for 2 h at room temperature: donkey anti-rabbit immunoglobulin G (IgG) Alexa Fluor® 555 (Invitrogen, A31572); donkey anti-mouse IgG Alexa Fluor® 488 (Invitrogen, A21202); donkey anti-rabbit IgG Alexa Fluor® 488 (Invitrogen, A21206); donkey anti-guinea pig IgG Alexa Fluor® 488 (Dianova, 706-545-148); donkey anti-rat IgG Alexa Fluor® 488 (Invitrogen, A21208); donkey anti-rat IgG Alexa Fluor®647 (Dianova, 712-605-150). For subsequent nuclear counterstaining, 4′,6-diamidino-2-phenylindole (DAPI) (Sigma, 32,670) was used. Samples were stored in an aqueous embedding medium (25% Glycerol, 10% Polyvinyl alcohol, 2% 1,4-Diazabicyclo [2.2.2]octan, 100 mM Tris) and imaged on a Zeiss LSM 880 AiryScan.

The colocalization of inceptor with GM130, Giantin, LAMP1 and IGF1R/EGFR with E-cadherin was calculated using the ImageJ plugin Coloc2, using automatic threshold adjustment (Costes). The fluorescence intensity of AR and inceptor was quantified by hand-drawing regions of interest around single cells in ImageJ.

2.5. Western blot

Cells were lysed in RIPA buffer (150 mM NaCl, 1% NP-40, 0.5% sodium deoxycholate, 0.1% SDS, 25 mM Tris pH 8) supplemented with protease inhibitor cocktail (Sigma, P8340, 1:100 dilution), phosphatase inhibitor cocktail 2 (Sigma, P5726, 1:100) and phosphatase inhibitor cocktail 3 (Sigma, P0044, 1:100). Protein concentrations were determined with the Pierce™ BCA protein assay kit (Thermo Fisher, 23,225). For SDS-PAGE, 20—25 μg protein were loaded in 6.5% or 7.5% acrylamide gels, and immunoblot on PVDF membrane was carried out in a Bio-Rad electrophoresis chamber and transfer system. The membranes were blocked in 5% milk powder in TBS-T for 1 h at room temperature and incubated with the following primary antibodies overnight at 4 °C: rat anti-inceptor #16F6 (1:1000 dilution), mouse anti-prostate-specific membrane antigen (PSMA) (Abcam, ab19071, 1:1000), mouse anti-AR (Santa Cruz, sc-7305, 1:500), mouse anti-IR (Cell Signaling, 3020, 1:1000), rabbit anti-IGF1R (Cell Signaling, 9750, 1:1000), rabbit anti-IGF1R phospho/IR phospho (Cell Signaling, 3024, 1:1000), rabbit anti-EGFR (Cell Signaling, 4267, 1:1000), rabbit anti-EGFR phospho (Cell Signaling, 3777, 1:1000) mouse anti-tubulin-gamma (Sigma, T5326, 1:5000), rabbit anti-prostate-specific antigen (PSA) (Abcam, ab53774, 1:5000), rabbit anti-heat shock protein 90 (Hsp90) (Cell signaling, 4874 S, 1:5000).

After washing with TBS-T, membranes were incubated for 2 h at room temperature with the secondary, horseradish peroxidase (HRP)-conjugated antibodies (1: 10,000 dilution) goat anti-mouse IgG (Dianova, 115-036-062), goat anti-rabbit IgG (Dianova, 111-036-045) or goat anti-rat IgG (Dianova, 112-035-175). The bands were detected using Clarity Western ECL Substrate (Bio-Rad, 1705061) in a ChemStudio2A (Analytik Jena). Quantification via densitometric analysis (normalized to tubulin as loading control) was performed in ImageJ.

2.6. Co-immunoprecipitation

LNCaP cells overexpressing inceptor-venus were seeded 3 days before in LNCaP medium. The confluent cultures were lysed in immunoprecipitation (IP) lysis buffer (1% Triton-X-100, 20 mM Tris—HCl pH 7.5, 150 mM NaCl, 1 mM EDTA) and centrifuged in a tabletop centrifuge at 14,000 rpm, 4 °C for 10 min; protein concentrations were determined via the Pierce™ BCA protein assay kit. SureBeads Protein G magnetic beads (Bio-Rad, 161—4021) were incubated with IR or IGF1R antibody (see Section 2.5) for 30 min at room temperature under rotation, then washed three times with PBS-T (PBS with 0.1% Tween20). Around 400 μl lysate (concentration adjusted to 1 μg/μl) were added to the antibody-conjugated SureBeads for overnight incubation at 4 °C (10 μl beads/100 μg protein). Beads were washed 3*x* with 500 μl lysis PBS-T and eluted with Laemmli-buffer for 10 min at 95 °C for subsequent Western blot analysis.

2.7. Proliferation assay

To assess the proliferation of LNCaP cells, they were seeded in 384-well clear bottom plates (Corning, 3770), after 2 days incubated with 10 μM 5-ethynyl-2′-deoxyuridine (EdU) for 8 h, fixated with 4% PFA and stored in PBS at 4 °C. The EdU was labeled using the Click-iT™ EdU Cell Proliferation Kit for Imaging with Alexa Fluor™ 647 (Invitrogen, C10340). Images were taken on a Zeiss Axio Observer Z1 and counted using an ImageJ Macro.

2.8. Endocytosis assay

To visualize the endocytosis of inceptor, LNCaP cells expressing inceptor-venus in μ-slide 8 well chambers (Ibidi, 80,826) were incubated with 10 μg/ml AlexaFluor555-conjugated rat anti-inceptor antibody. The cells were then observed for 5—60 min using a Zeiss LSM 880 AiryScan with incubation at 37 °C and 5% CO_2 supply.

To analyze co-endocytosis of insulin/EGF and inceptor, LNCaP cells in μ-slide 8 well chambers (Ibidi, 80,826) were incubated with 100 nM AlexaFluor546-labeled insulin (provided by Oliver Plettenburg, Institute for Medicinal Chemistry, Helmholtz-Zentrum München) or 1 μg/ml AlexaFluor488-labeled EGF (Life Technologies, E13345), along with 10 μg/ml rat anti-inceptor antibody (#2G6) in normal growth medium

(see Section 2.2) for 60 min at 37 °C. The cells were then fixated with 4% PFA for 10 min and permeabilized in 0.25% Triton-X100, 100 mM glycine for 15 min at room temperature. To visualize the inceptor antibody, secondary anti-rat IgG Alexa Fluor® 488 (Invitrogen, A21208) was added for 2 h at room temperature, along with SiR-Actin (Cytoskeleton, Inc., #CY-SC001, 1:1000 dilution) and DAPI for counterstaining. The samples were imaged on a Zeiss LSM 880 AiryScan and colocalization of the inceptor antibody with labeled insulin/EGF was calculated using the ImageJ Plugin JaCoP with manual thresholding.

2.9. Migration assay

To form LNCaP spheroids, the AggreWell™ 400 24 well plates (STEMCELL, Cat. No. 34411) were used. For each condition one well was rinsed using AggreWell Rinsing Solution (STEMCELL, Cat. No. 07010) and centrifuged at 1300 rcf for 5 min. Each well was washed with RPMI 1640 and filled with 1 ml prewarmed LNCaP medium (see Section 2.2) before adding the cell suspension (1.2 million cells in 1 ml) to form spheroids containing approx. 1000 cells. The plate was centrifuged at 100 rcf for 3 min and incubated for 48 h. The spheroids were then carefully collected via a 37 μm reversible cell strainer, sedimented by gravity and resuspended in 1.2 ml of a 10 μM collagen solution (Collagen type I, Sigma—Aldrich, Cat. No. C4243) buffered with 10 mM HEPES and approx. 15 mM NaOH to reach a neutral pH. The cell suspension was distributed between 4 wells of a 24-well plate (Thermo Scientific, 142,475) and incubated for 4 h. After the collagen had solidified, 1 ml of LNCaP medium (see Section 2.2) and 200 μl of mineral oil to prevent evaporation (Sigma—Aldrich, M5310) were added to each well and the plate was mounted on a Zeiss Axio Observer Z1 using incubation at 37 °C and 5% CO_2 supply for live cell imaging. The area of the migrating cells was measured by hand-drawing regions of interest in ImageJ. Statistical analysis for all *in vitro* experiments was performed using GraphPad Prism 8 (GraphPad Software, Inc.).

2.10. Human samples

We selected 121 newly diagnosed male prostate cancer patients with a mean age of 64 years and mean body mass index (BMI) of kg/m^2, who were recruited prior to radical prostatectomy. None of the patients received hormone-altering therapy prior to inclusion. Tissue sampling was performed by an experienced uropathologist. Prostate cancer (n = 50) as well as benign prostate tissues (n = 71) were immediately snap-frozen in liquid nitrogen and stored at −80 °C. For histological confirmation, hematoxylin and eosin stainings were performed on paraffinized samples and Gleason scores were determined. The tumor contents of the specimen were very variable among the patients (5%—90%). Patient characteristics are provided in Supplementary Table S2. To analyze cell types in human prostate sections, we used paraffin sections taken from prostate cancer patients aged 55—76 years with Gleason score 3—4.

Informed written consent was obtained from all participants and the Ethics Committee of the University of Tübingen approved the protocol according to the Declaration of Helsinki.

Multivariate linear regression models adjusted for age and BMI were performed using the JMP statistical software package (JMP 14.2, SAS Institute Inc.).

2.11. Real-time PCR

Total RNA from prostate cell lines and human prostate tissues was isolated using the Allprep RNA/DNA/protein kit (Qiagen) according to the manufacturer's description and cDNA was synthesized (Transcriptor First Strand cDNA synthesis kit, Roche). Real-time PCRs were performed with LightCycler 480 Probes Master (Roche) with universal probe library using LightCycler 480 (Roche) as previously described [40]. Delta—delta crossing-point (Cp) values were calculated and values were normalized to the housekeeping gene *ubiquitin c* (*UBC*) [41]. For real-time PCR analysis the following primers and probes were applied: *UBC* 5′-GGAAGGCATTCCTCCTGAT and 3′-CCCACCTCTGAGACGGAGTA (probe nr 11), *EGFR* 5′-GTGGATGGCATTGGAATCA and 3′-CAAAGGTCATCAACTCCCAAA (probe nr 50), *inceptor* 5′-CAGGTGCAGTCCACAGAAAA and 3′-GCCATCACAGGTCCCATC (probe nr 74) and *MDM2* 5′-CCATGATCTACAGGAACTTGGTAGTA and 3′-TCACTCACAGATGTACCTGAGTCC (probe nr 18). Primer sequences for *AR, PSA, PSMA, IRa, IRb, IGF1R, CYP7B1* and *ERb* were previously published [30].

2.12. Bioinformatic analyses

Tissue expression of inceptor was extracted from the Human Protein Atlas (HPA) [39] (https://www.proteinatlas.org/ENSG00000116299-KIAA1324/tissue, last accessed on 18.09.2020). Data for the HPA dataset was collected by Illumina RNA-seq of specimen from the Uppsala Biobank. The protein sequence of inceptor was analyzed using the ENSEMBL database [42] (https://www.ensembl.org, reference ENSG00000116299, last accessed on 18.09.2020). The predicted domains were selected for the 1013aa transcript and annotated in SnapGene Viewer for visualization (Insightful Science; available at snapgene.com). The gene expression data in Figure 2 was extracted from the TCGA dataset using the GEPIA web server [43] (http://gepia.cancer-pku.cn/detail.php?gene=KIAA1324, last accessed on 18.09.2020). Mutation data in the TCGA and Neuroendocrine Prostate Cancer [44] datasets were obtained from CBioPortal [45] (https://www.cbioportal.org, last accessed on 18.09.2020). The DNA sequence of *IIR* was copied from the National Center for Biotechnology Information (NCBI) (available from https://www.ncbi.nlm.nih.gov/, 20.11.2020).

3. RESULTS

3.1. Inceptor expression in healthy prostate epithelium and prostate cancer cell lines

Database searches revealed that *IIR* mRNA (also known as *EIG121/KIAA1324*) is highly expressed in human prostate (Fig. S1a). To confirm the protein expression and to identify the cell type and tissue distribution of inceptor, we used our previously generated specific monoclonal antibodies against inceptor [33] and performed immunohistochemistry on adult mouse prostate sections (Figure 1a) and on sections of human prostate biopsies (Fig. 1b). We observed inceptor in all luminal cells of the murine and human prostate epithelium, which are marked by presence of Cytokeratin 8/18 and absence of Cytokeratin 5. Moreover, the prostate epithelium contains a subset of cells that expresses both Cytokeratin 5 and Cytokeratin 8/18, usually referred to as intermediate cells [46]. We found that intermediate cells expressed inceptor, while Cytokeratin 8/18 negative basal cells did not (Figure 1a,b). There was no or only very low inceptor expression in neuroendocrine cells (Fig. 1c), which regulate growth and differentiation of the prostate epithelium by secreting peptide hormones, such as serotonin (5-HT), calcitonin and somatostatin [47].

To analyze the expression of *IIR* in various androgen-dependent and independent cell lines, we performed qPCR and Western blot analyses. In qPCR, we detected *IIR* mRNA expression in the primary HPEC line, as well as in the androgen-dependent prostate cancer cell line LNCaP and the androgen-independent prostate cancer cell line PC3 (Fig. 1d). In Western blot we additionally analyzed the immortalized cell line BPH-1,

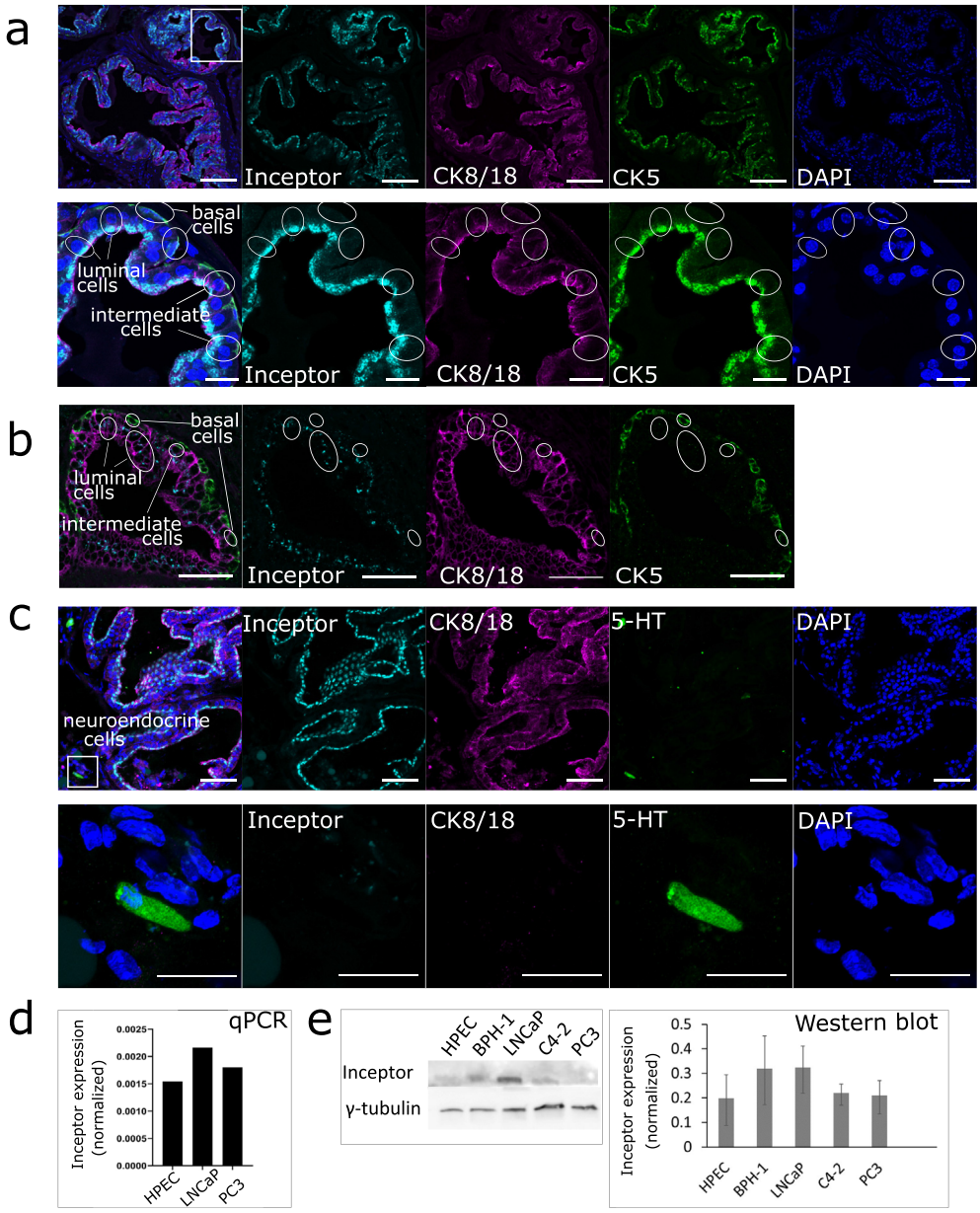

Figure 1: Inceptor is expressed in healthy murine prostate epithelium and human prostate cancer cell lines. a. Immunohistochemical staining of WT mouse prostate with antibodies against inceptor, Cytokeratin 8/18 marking luminal cells and Cytokeratin 5 marking basal cells. Image shows a section of dorsal prostate, representative of 14 slices from two mice, taken from the dorsal, ventral or anterior prostate. Scale bar: 100 μm (upper row), 20 μm (lower row, zoomed in). b. Immunohistochemical staining of human prostate with antibodies against inceptor (cyan), Cytokeratin 8/18 (magenta), and Cytokeratin 5 (red). Scale bar: 50 μm. c. WT mouse prostate stained for inceptor, Cytokeratin 8/18 and Serotonin (5-HT) expressed in neuroendocrine cells. Image shows a section of dorsal prostate, representative of 8 slices from teo mice, taken from the dorsal, ventral or anterior prostate. Scale bar: 100 μm (upper row), 20 μm (lower row, zoomed in). d,e. Expression levels of inceptor in different human prostate cancer cell lines, determined by qPCR and Western blot. Densitometric quantification of the Western blot is shown on the right, values are normalized on γ-tubulin as loading control (n = 3).

which is a model for benign prostate hyperplasia, as well as the androgen-independent LNCaP derivative LNCaP C4-2 (Fig. 1e). For further experiments we chose LNCaP cells, which showed reliable *IIR* mRNA and protein expression.

3.2. Correlation of inceptor expression with carcinogenic markers in human prostate samples

To evaluate the relevance of inceptor in human prostate cancer, we searched online databases for the publicly available TCGA (The Cancer Genome Atlas) dataset. We found that, compared to healthy tissues, inceptor was downregulated in pancreatic adenocarcinoma, but upregulated in ovarian, uterine, breast and prostate carcinoma (Fig. S1b). In prostate cancer, gene expression levels of *IIR* correlated with *AR* and AR-associated genes such as *PSA* (prostate-specific antigen, also known as *KLK3*) and *PSMA* (also known as *FOLH1*) (Figs. S1c—e). Further, *IIR* correlated with *IGF1R* and *IR* (*INSR*) (Figs. S1f and g). As tumor progression often goes along with increasing mutation status, we evaluated the frequency of different types of mutations in progressively more dedifferentiated tumor stages. We found that in all stages, mutations of *IIR* frequently co-occurred with mutations of *EGFR, IR, IGF1R, IGF2R, PI3K* subunits C2a and C2b, *AR*, *PSA* and *PSMA* (Table S1). The mutation rate of *IIR*

was low in prostate adenocarcinoma; however, the frequency of gene amplifications was notably enriched in castration-resistant prostate cancer and neuroendocrine carcinoma (Fig. S2a). For comparison, *AR* was also frequently amplified or mutated in castration-resistant prostate cancer and neuroendocrine carcinoma (Fig. S2f), presumably to facilitate androgen-dependent proliferation despite low androgen levels. A similar pattern could be observed for *IGF1R, IR, EGFR* and *PI3K* (Figs. S2b–e). Of note, deletion of *IIR* was very rare in all prostate cancer stages (Fig. S2a). In addition, we analyzed 121 human prostate tissue samples consisting of 71 benign and 50 cancer samples (Table S2). The *IIR* mRNA expression showed a significant positive correlation with the tumor content of the respective specimen (Figure 2a). Further, we plotted the *IIR* expression against the expression of *AR* and the AR-associated genes *PSA* and *PSMA* (Figure 2b–d). All three genes showed a strong positive correlation ($p < 0.0001$) with *IIR*. Moreover, there was a positive correlation between *IIR* and *MDM2* (Fig. 2e). The expression of *IIR* also showed a positive correlation with *IRa/IRb* ratio and a negative correlation with *IRb/IGF1R* ratio (Figure 2f,g).

3.3. Inceptor and androgen signaling of prostate cancer cells

As previously reported, androgen deprivation leads to differentiation of LNCaP cells towards a more invasive, neuroendocrine cancer-like cell type [48]. To model prostate cancer progression *in vitro*, we cultured LNCaP cells in androgen-free medium. During deprivation, the expression levels of inceptor and PSMA increased gradually (Figure 3a,b). The increase in inceptor levels after androgen deprivation was also reflected in immunocytochemistry (Fig. 3c).

The expression of inceptor and AR, as well as the nuclear localization of AR, seemed to be heterogeneous among single cells (Fig. 3c). To investigate this heterogeneity, we measured the ratio of nuclear AR to total AR and inceptor fluorescence intensity in single cells (Fig. 3d). There was a correlation between inceptor intensity and AR nuclear localization after androgen depletion ($p = 0.038$). This suggests that inceptor might be associated with nuclear translocation and thus activation of AR. Therefore, we analyzed the levels of PSA, which is a direct AR target, in LNCaP cells overexpressing the fusion protein inceptor-venus compared to venus overexpressing cells and wildtype (WT) cells as controls (Fig. 3e). In normal growth conditions, as well as after 5 days of androgen deprivation, there was more PSA expression in inceptor-venus overexpressing cells.

3.4. Inceptor trafficking

To investigate the trafficking of inceptor in prostate cancer cells, we performed co-stainings of inceptor with the Golgi markers GM130 and giantin and the lysosomal protein LAMP1 in LNCaP cells. All markers revealed a high degree of overlap with inceptor, with LAMP1 colocalization being slightly higher compared to GM130 and giantin (Figure 4a). Thus, we found the main fraction of inceptor in the endosomal-lysosomal compartment. This is consistent with bioinformatic predictions (Supplementary Table S3), particularly with the assumed mannose-6-phosphate receptor domain of inceptor (Fig. S3), as this domain is responsible for lysosomal trafficking. To track the internalization of inceptor, we used LNCaP cells overexpressing inceptor-venus. We have previously shown that inceptor-venus shows the same localization and trafficking dynamics as endogenous inceptor and is therefore a valid tool to study the function of inceptor [33]. This cell line was imaged after pulse-labeling with an AlexaFluor555-conjugated inceptor antibody (Fig. 4b). After 5 min, the antibody was visible on the plasma membrane, before it was gradually endocytosed and showed high colocalization with inceptor-venus after 30 min. These results show that inceptor is cycled between the plasma membrane, lysosomes and Golgi complex in LNCaP cells.

To test if inceptor is involved in the trafficking of receptor tyrosine kinases in prostate cancer cells, we performed an endocytosis assay with labeled insulin and EGF (Figure 4c,d). We observed an overlap between the inceptor antibody and insulin, indicating that both proteins are internalized via the same endocytosis pathway. In contrast, we did not see overlap between inceptor and EGF.

To further analyze the co-trafficking of inceptor with receptor tyrosine kinases, we performed co-stainings of IR, IGF1R and EGFR with the membrane marker E-cadherin (Figure 4e,f). We found that slightly but significantly more IGF1R was localized at the plasma membrane in inceptor overexpressing cells compared to WT. There was no significant change in EGFR or IR localization (quantification in Figure 4f, images not shown).

3.5. Inceptor and insulin/IGF1 signaling

Since receptor trafficking is crucial for the initiation and termination of signaling cascades, we investigated the connection of inceptor with IR and IGF1R activation in prostate cancer cells.

To confirm IGF1R and IR as interaction partners of inceptor, we performed co-IP in LNCaP cells (Figure 5a). We successfully pulled down inceptor using an IGF1R and an IR antibody.

Next, we analyzed the impact of inceptor on relevant signaling pathways in LNCaP cells overexpressing inceptor-venus or venus only as a control. The signaling pathways were analyzed by depletion of growth factors in the medium, followed by stimulation with insulin, IGF1 or EGF. In LNCaP cells overexpressing inceptor-venus, EGFR levels appeared to decrease slightly after androgen deprivation and after stimulation (Figure 5b,c). The phosphorylation of EGFR upon EGF induction was not changed. Upon stimulation with IGF1, the phosphorylation of IR/IGF1R was substantially increased. This was not the case for stimulation with insulin, at a concentration of 10 nM, where insulin almost exclusively activates IR [27].

3.6. Migration of LNCaP cells upon inceptor overexpression

Since inceptor seems to be upregulated in more advanced prostate tumors, we investigated the functional effect of inceptor overexpression in prostate cancer cells. The proliferation rate of the inceptor-venus overexpressing cell line was assessed by incubation with EdU in normal growth medium. There was no significant difference compared to WT and Venus control (Figure 6a,b).

To investigate the migration of inceptor-venus overexpressing cells, we performed a spheroid migration assay, adapted from previously published studies [49,50] (Fig. 6c). To quantify the effect, we measured the area of invading cells leaving the compact spheroid structure (marked in green color in Fig. 6c). The migration rate of the inceptor-venus overexpressing cells was significantly higher compared to WT and Venus control (Fig. 6d).

4. DISCUSSION

According to publicly available databases, inceptor is downregulated in pancreatic adenocarcinoma compared to healthy tissue, but upregulated in ovarian, uterine, breast, and prostate carcinoma, which is in line with previous reports [34–36].

Both databases and our evaluation of human samples revealed that inceptor is expressed in benign and malignant prostate epithelium, with the expression in malignancies being significantly higher. The *IIR* gene is more frequently amplified in the more aggressive forms of castration-resistant prostate cancer and neuroendocrine carcinoma, compared to

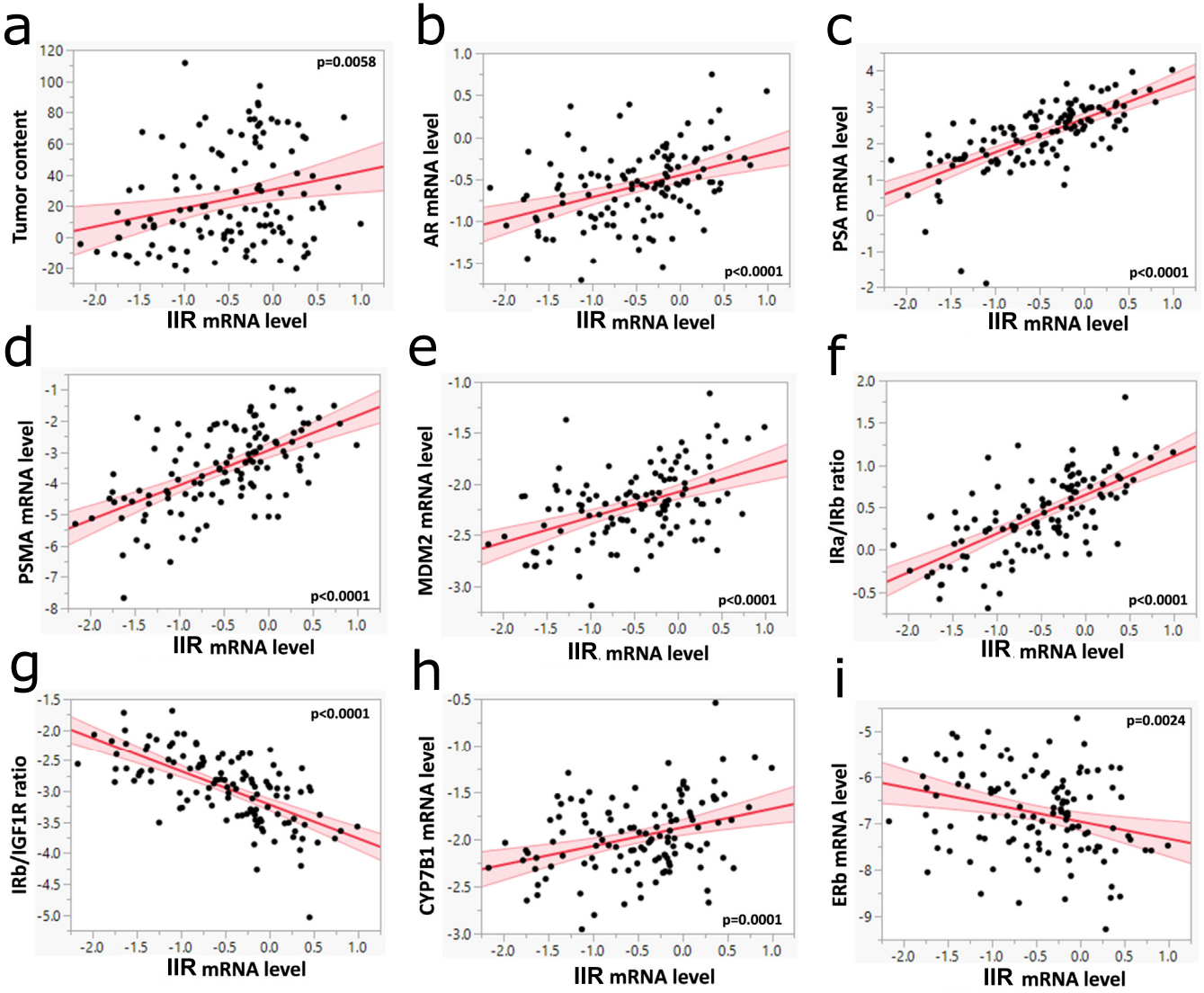

Figure 2: Inceptor expression correlates with carcinogenic markers in human prostate samples. a. The mRNA expression of *IIR* in human benign prostate tissues (n = 71) and prostate cancer samples (n = 50) were determined with real-time PCR and normalized to ubiquitin c. Multivariate linear regression models were adjusted to age and BMI. Log transformed mRNA level of inceptor was correlated with tumor content (in %). b,c,d,e,h,i. Correlation of log transformed mRNA levels of inceptor with the indicated genes. f,g. Ratios of log transformed mRNA levels of key players of the Ins/IGF1 system, plotted against inceptor expression.

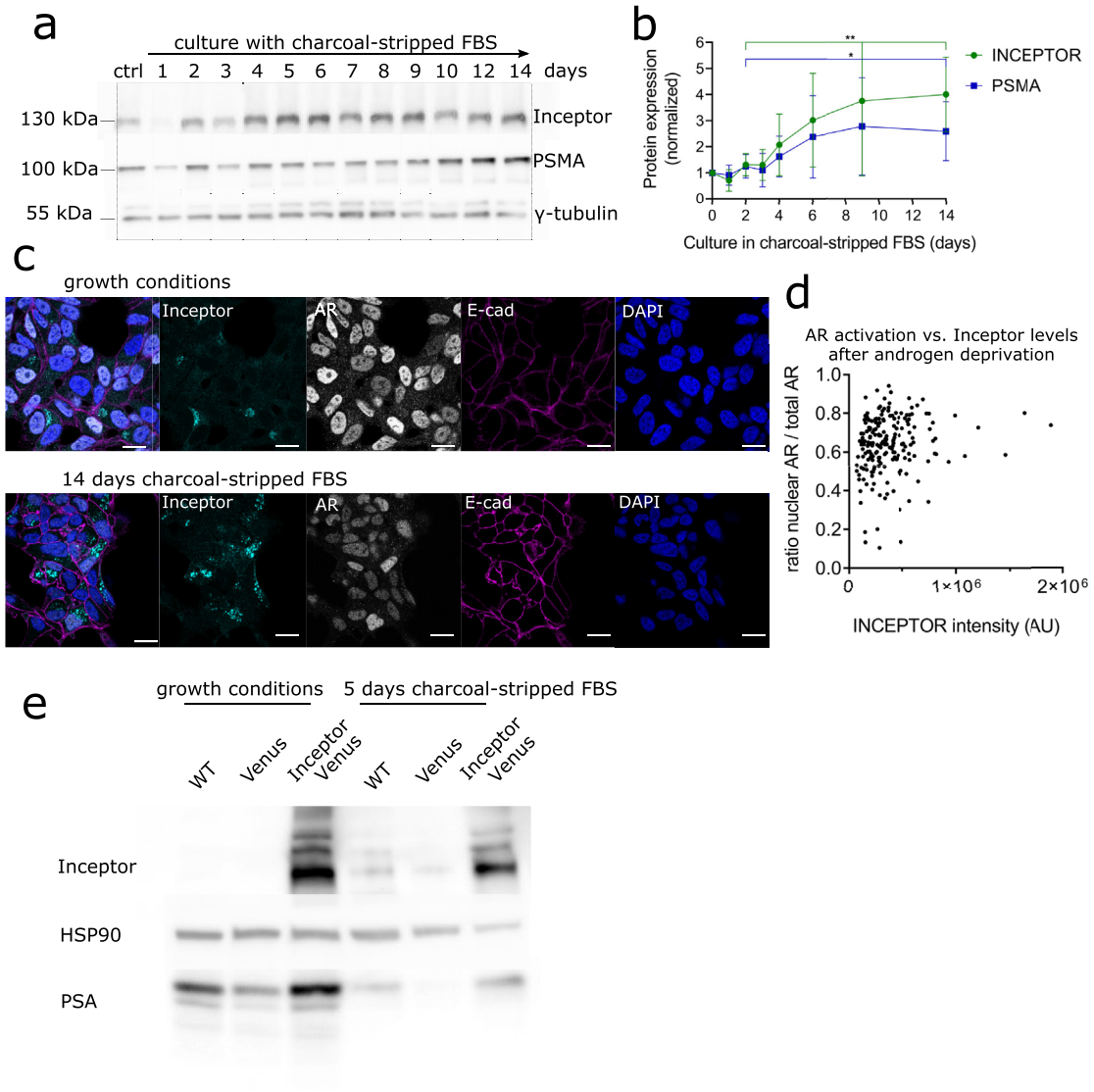

Figure 3: Inceptor expression is dependent on the hormone status of prostate cancer cells. a. Expression of inceptor, PSMA and AR after up to 14 days of culture in RPMI 1640 + 10% charcoal-stripped FBS (androgen deprivation conditions). The control was cultured in the same medium for 14 days, with the addition of 10 nM dihydrotestosterone. b. Densitometric quantification of a, normalized to γ-tubulin as loading control (selected time points from n = 5 independent experiments). Values show fold change compared to control. P = 0.0049 for inceptor and p = 0.0441 for PSMA, determined by unpaired student's t test. c. LNCaP cells in normal growth medium (RPMI 1640 + 10% FBS) or RPMI 1640 + 10% charcoal-stripped FBS were stained for inceptor, AR and E-cadherin. Laser and detector settings were kept constant between both images (scale bar: 20 μm). d. Quantification of fluorescence intensity of nuclear AR vs. total AR, shown in dependence of inceptor intensity (Figure 3 c, left). Single cells from two independent experiments were analyzed, after 14 days in charcoal-stripped FBS (>100 cells/n), p = 0.038 (linear regression). e. LNCaP WT, LNCaP venus or LNCaP inceptor-venus cells were cultured in normal growth medium (RPMI 1640 + 10% FBS) or RPMI 1640 + 10% charcoal-stripped FBS for 5 days.

adenocarcinoma. The prostate is a secretory organ, containing mainly luminal secretory cells, basal cells and neuroendocrine cells. Inceptor is expressed in luminal and intermediate cells. This is of particular interest since luminal cells are the main origin of prostate cancer [51].

In human prostate cancer samples, the gene expression levels of *IIR* in this study correlated with the expression of *AR, PSA* and *PSMA*, which are well established hallmarks of disease progression [52,53]. *MDM2*, which also correlated with *IIR* expression, is an E3 ubiquitin protein ligase responsible for degradation of the tumor suppressor p53. Thus, it is considered a progression marker in many cancer types, including prostate cancer [54,55]. Notably, MDM2 has been shown to promote migration of cancer cells by ubiquitinating E-cadherin and thus tagging it for lysosomal degradation [56]. Taken together, these results show that inceptor correlates with carcinogenic markers.

Our analyses of human prostate cancer samples further showed positive correlation of inceptor with the IRa/IRb ratio and negative correlation with the IRb/IGF1R ratio. It was previously demonstrated that the ratio of insulin receptor isoforms IRa to IRb is significantly higher in prostate cancer compared to benign tissue [57]. In contrast to IRb, which only binds insulin with high affinity and is mainly responsible for mediating metabolic functions, IRa can activate proliferation via insulin, IGF1 or IGF2 binding [27]. Thus, higher IRa to IRb ratio and lower IRb/IGF1R ratios in tumors with high inceptor expression indicate an activation of mitogenic pathways rather than metabolic pathways, mediated via the insulin/IGF1 cascade.

We pulled down inceptor with IGF1R and IR, showing that inceptor physically interacts with receptor tyrosine kinases in prostate cancer cells. This is consistent with our previous results in β-cells [33]. The

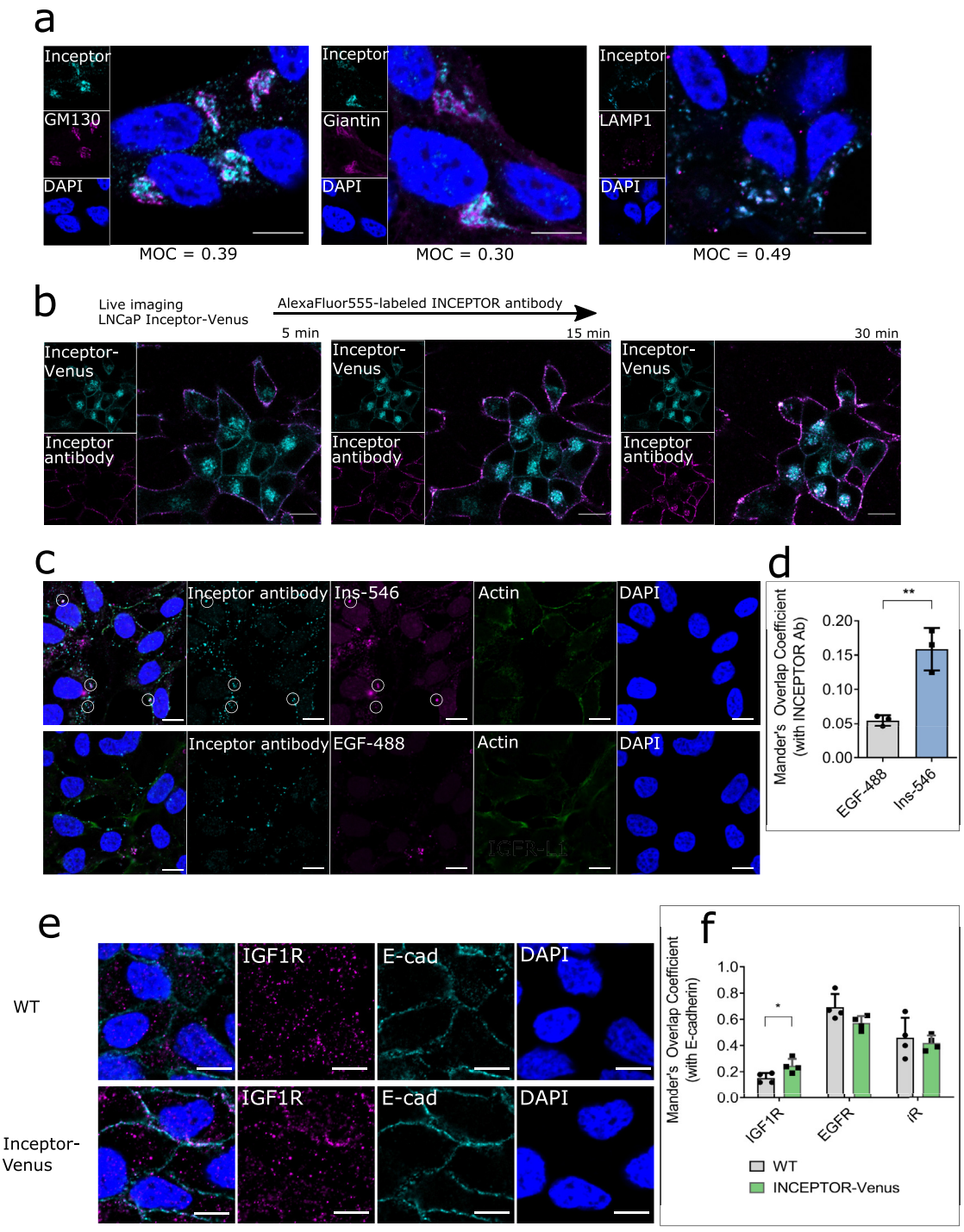

Figure 4: Inceptor is involved in the trafficking of IR/IGF1R. a. Staining of LNCaP cells for inceptor and GM130 (cis-Golgi), Giantin (medial Golgi) or LAMP1 (Lysosome) to determine the subcellular localization of inceptor. The Mander's overlap coefficient was calculated from >80 cells/n (n = 3). Scale bar: 10 μm. b. LNCaP cells expressing inceptor-venus were pulse-labeled with an AlexaFluor555-conjugated inceptor antibody. Internalization of the antibody was tracked in live imaging. Images are representative for two independent experiments (>60 cells/n). Scale bar: 10 μm. c. Endocytosis assay in LNCaP C4-2 cells incubated with 10 μg/ml inceptor antibody (rat) and 100 nM AlexaFluor546-labeled insulin or 1 μg/ml AlexaFluor488-labeled EGF for 60 min, before fixation and staining with an AlexaFluor488 or 555-labeled secondary anti-rat antibody. Scale bar: 10 μm. d. Quantification of c. The Mander's Overlap Coefficient was calculated from >50 cells/n, n = 3. P = 0.0049 (unpaired student's t test). e. Staining of WT and inceptor overexpressing LNCaP cells using an IGF1R or EGFR antibody, along with an E-cadherin antibody. Scale bar: 10 μm. f. Quantification of e (including IR and EGFR, not shown in d). The Mander's Overlap Coefficient was calculated from >40 cells/n, n = 4 (p = 0.0403, unpaired student's t test).

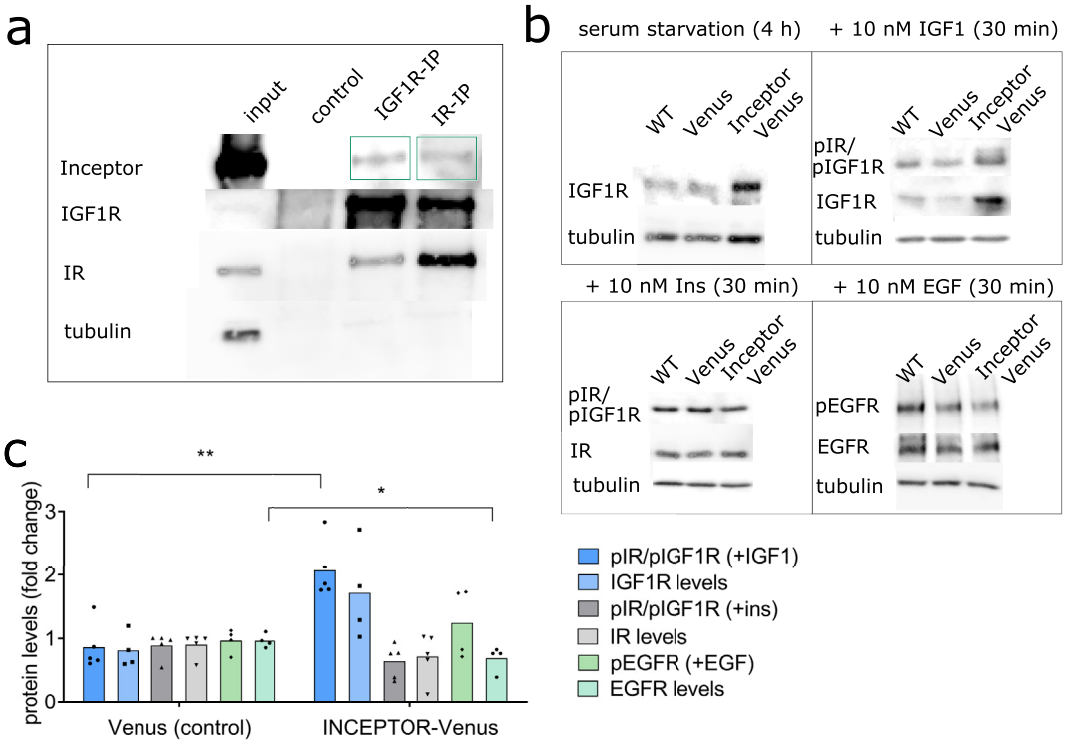

Figure 5: Inceptor modulates Insulin/IGF1 signaling in prostate cancer cells. a. Co-IP using an IGF1R antibody or IR antibody or beads only (control) in LNCaP cells overexpressing inceptor-venus. To show total levels of each protein, 20 μg lysate were loaded (input), while for each IP 400 μg lysate were used. Image is representative for 4 indepenent experiments. b. Signaling assay in LNCaP cells overexpressing inceptor-venus, compared to venus only and WT cells. The cells were growth factor starved in serum-free RPMI 1640 for 4 h, before induction with 10 nM insulin, 10 nM IGF1 or 10 nM EGF for 30 min, and subsequent lysis for Western blot. c. Densitometric quantification of b ($n = 4$). Values were normalized to tubulin as loading control, the graph shows fold change compared to WT LNCaP. pIR/pIGF1R (+IGF1): $p = 0.0017$; IGF1R levels: $p = 0.0636$; EGFR levels: $p = 0.0491$ (unpaired student's t test).

total levels of IGF1R were comparatively low, thus it seems that the pulldown of inceptor with IGF1R was efficient. In our endocytosis assay, insulin was internalized via the same routes as inceptor. It is important to note that insulin can be a ligand for IGF1R, especially at the high concentration used in the endocytosis experiment (100 nM) [27]. Thus, it is possible that the observed colocalization was due to co-trafficking with IGF1R rather than IR. Overexpression of inceptor led to increased IGF1R levels and more IGF1R on the membrane. Therefore, we hypothesize that inceptor has a role in the trafficking of IGF1R. Analysis of the subcellular localization has shown that inceptor resides mainly in the Golgi complex and in the lysosome. This localization pattern is expected since inceptor contains a mannose-6-phosphate receptor domain. The cation-independent mannose-6-phosphate receptor, also known as IGF2R, is responsible for sequestering excess IGF2 from the plasma membrane and routing it to the lysosome for degradation, and for delivering lysosomal enzymes from the Golgi complex [58]. The high colocalization of inceptor with lysosomes raises the question of a potential function of inceptor in lysosomal degradation. It has previously been speculated that inceptor might be involved in EGFR degradation in breast cancer [59], although further studies are required to test this hypothesis. Taken together, our results show a correlation of inceptor levels and IGF1R signaling, which may be associated with altered IGF1R trafficking and/or degradation.

Proliferation of LNCaP cells was not affected by inceptor overexpression. This is counterintuitive, since it is known that insulin/IGF1 signaling can propagate mitogenic effects in cancer [1]. However, our data showed that the migration of LNCaP cells was increased upon inceptor overexpression. Importantly, IGF1R levels but not IR levels were elevated upon inceptor overexpression. Accordingly, IGF1 stimulation induced higher signaling activation when inceptor was overexpressed, while this effect could not be observed upon stimulation with insulin. However, we have observed increased migration in a 3D spheroid model upon inceptor overexpression. The main advantage of spheroid assays compared to conventional trans-well migration or wound-healing assays is that spheroid invasion in a 3D collagen matrix closely mimics invasion *in vivo* [60]. Thus, this indicates a potential involvement of inceptor in cancer cell migration. It has been shown that migration of cancer cells can be induced via IGF1 [61–63]. The proliferation assay was carried out in normal growth medium, in presence of androgens. As androgen signaling is the main driver for proliferation in LNCaP cells and it is known that IGF1R and IR are essential factors of androgen-independent survival mechanisms [12], the growth-promoting effect of inceptor might be masked in these conditions.

In our previous study analyzing the role of inceptor in pancreatic β-cells, we have shown that inceptor counteracts insulin signaling [33]. Based on this finding, decreased aggressiveness of cancers with high inceptor levels would be expected, which is in contrast with the results obtained in the present study. We hypothesize that inceptor has diverse effects on signaling pathways, depending on the cellular context. This hypothesis would explain the seemingly contradictory literature studies

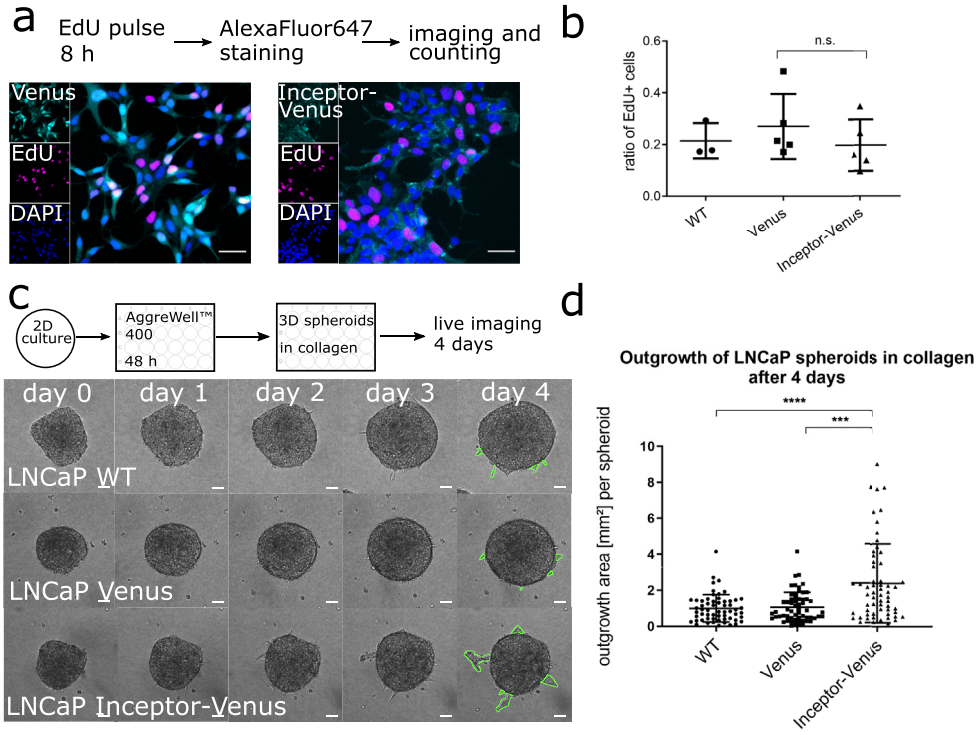

Figure 6: Inceptor overexpression induces migration in prostate cancer cells. a. Proliferation assay of stable LNCaP cell lines overexpressing inceptor-venus or Venus only. b. Quantification of a, by image segmentation of EdU vs. DAPI. >5000 cells/n were counted; n = 5 for Venus and inceptor-venus overexpressing cells, n = 3 for WT cells. P = 0.3381, determined by unpaired student's t test. c. Migration of LNCaP spheroids in a collagen matrix (experimental scheme shown above). Scale bar: 50 μm. d. Quantification of c by measuring the outgrowth area (as indicated in green color in c) of 60 spheroids for each cell line from three independent experiments. P < 0.0001 as determined by unpaired student's t test; two outliers were removed, based on Grubb's outlier test.

analyzing the effects of high inceptor levels in different cancers. These studies indicated favorable prognosis in pancreatic neuroendocrine tumors and gastric cancer [35,36] but poor prognosis in endometrial cancer and ovarian cancer [37,38].

We found that inceptor was upregulated upon androgen deprivation of LNCaP cells. Androgen deprivation *in vitro* induces differentiation towards a more aggressive cell type [48]. Cells that expressed high levels of inceptor showed more nuclear AR localization. The dynamic inceptor expression during androgen deprivation mirrored PSMA expression. Further, the *PSMA* gene was highly correlated to *IIR* in human prostate cancer. PSMA is an enzyme with peptidase and hydrolase activity whose function in prostate cancer is poorly understood. However, it is well established that PSMA is highly overexpressed in prostate cancer and increases with tumor grade [64]. It has been suggested that AR downregulates the PSMA enhancer PSME [65]. Accordingly, there are studies showing PSMA upregulation upon androgen deprivation therapy of prostate cancer patients [66,67]. Since inceptor showed similar expression dynamics as PSMA, it is possible that inceptor is downregulated by androgens in a comparable manner as PSMA. Alternatively, inceptor may be estrogen-regulated, as suggested in literature [34,38], considering that estrogen and androgen signaling are highly interconnected in prostate cancer [68]. Taken together, our results from human samples and cell culture experiments suggest that inceptor might be associated with the hormone status of prostate tumors.

In this study we demonstrate for the first time that inceptor is associated with prostate cancer, possibly connected to IGF1R signaling. Further studies are needed to evaluate the clinical significance of inceptor in prostate cancer.

DATA AVAILABILITY

Data will be made available on request.

ACKNOWLEDGEMENTS

Part of the results shown are based upon data generated by the TCGA Research Network: https://www.cancer.gov/tcga. We are grateful to Silvia Schirge (Helmholtz-Zentrum München) for animal breeding and support with mouse dissection, to Regina Feederle (Helmholtz-Zentrum München) for antibody generation, and to Oliver Plettenburg (Helmholtz-Zentrum München) for providing labeled insulin. Further, we want to thank Kerstin Diemer, Ines Kunze, Jessica Jaki and Lisa Appel (Helmholtz-Zentrum München) for lab organization and Alke Guirguis (University Hospital Tübingen) for technical assistance.

CONFLICT OF INTEREST

None declared.

APPENDIX A. SUPPLEMENTARY DATA

Supplementary data to this article can be found online at https://doi.org/10.1016/j.molmet.2023.101706.

REFERENCES

[1] Belfiore A, Malaguarnera R. Insulin receptor and cancer. Endocr Relat Cancer 2011;18(4):R125–47.

[2] Crawley D, Chamberlain F, Garmo H, Rudman S, Zethelius B, Holmberg L, et al. A systematic review of the literature exploring the interplay between prostate cancer and type two diabetes mellitus. Ecancermedicalscience 2018;12:802.

[3] Bensimon L, Yin H, Suissa S, Pollak MN, Azoulay L. Type 2 diabetes and the risk of mortality among patients with prostate cancer. Cancer Causes Control 2014;25(3):329–38.

[4] Cai H, Xu Z, Xu T, Yu B, Zou Q. Diabetes mellitus is associated with elevated risk of mortality amongst patients with prostate cancer: a meta-analysis of 11 cohort studies. Diabetes Metabol Res Rev 2015;31(4):336–43.

[5] Currie CJ, Poole CD, Jenkins-Jones S, Gale EAM, Johnson JA, Morgan CL. Mortality after incident cancer in people with and without type 2 diabetes: impact of metformin on survival. Diabetes Care 2012;35(2):299–304.

[6] Lutz SZ, Todenhöfer T, Wagner R, Hennenlotter J, Ferchl JM, Scharpf MO, et al. Higher prevalence of lymph node metastasis in prostate cancer in patients with diabetes. Endocr Relat Cancer 2018;25(3):L19–22.

[7] Franko A, Berti L, Hennenlotter J, Rausch S, Scharpf MO, Hrabe de Angelis M, et al. Transcript levels of aldo-keto reductase family 1 subfamily C (AKR1C) are increased in prostate tissue of patients with type 2 diabetes. J Personalized Med 2020;10(3):124.

[8] Bray F, Ferlay J, Soerjomataram I, Siegel RL, Torre LA, Jemal A. Global cancer statistics 2018: GLOBOCAN estimates of incidence and mortality worldwide for 36 cancers in 185 countries. CA A Cancer J Clin 2018;68(6):394–424.

[9] Elia I, Schmieder R, Christen S, Fendt S. Organ-specific cancer metabolism and its potential for therapy. In: Herzig S, editor. Metabolic control. Cham: Springer International Publishing; 2016. p. 321–53.

[10] Sharifi N, Gulley JL, Dahut WL. Androgen deprivation therapy for prostate cancer. JAMA 2005;294(2):238–44.

[11] Centenera MM, Selth LA, Ebrahimie E, Butler LM, Tilley WD. New opportunities for targeting the androgen receptor in prostate cancer. Cold Spring Harbor perspectives in medicine 2018;8(12):a030478.

[12] Feldman BJ, Feldman D. The development of androgen-independent prostate cancer. Nat Rev Cancer 2001;1(1):34–45.

[13] Visakorpi T, Hyytinen E, Koivisto P, Tanner M, Keinänen R, Palmberg C, et al. In vivo amplification of the androgen receptor gene and progression of human prostate cancer. Nat Genet 1995;9(4):401–6.

[14] Taplin M-E, Bubley GJ, Ko YJ, Small EJ, Upton M, Rajeshkumar B, et al. Selection for androgen receptor mutations in prostate cancers treated with androgen antagonist. Cancer Res 1999;59(11):2511–5.

[15] Gioeli D, Mandell JW, Petroni GR, Frierson HF, Weber MJ. Activation of mitogen-activated protein kinase associated with prostate cancer progression. Cancer Res 1999;59(2):279–84.

[16] Culig Z, Hobisch A, Cronauer MV, Radmayr C, Trapman A, Hittmair A, et al. Androgen receptor activation in prostatic tumor cell lines by insulin-like growth factor-I, keratinocyte growth factor, and epidermal growth factor. Cancer Res 1994;54(20):5474–8.

[17] Nickerson T, Chang F, Lrimer D, Smeekens SP, Sawyers CL, Pollak M. In vivo progression of LAPC-9 and LNCaP prostate cancer models to androgen independence is associated with increased expression of insulin-like growth factor I (IGF-I) and IGF-I receptor (IGF-IR). Cancer Res 2001;61(16):6276–80.

[18] Krueckl SL, Sikes RA, Edlund NM, Bell RH, Hurtado-Coll A, Fazli L, et al. Increased insulin-like growth factor I receptor expression and signaling are components of androgen-independent progression in a lineage-derived prostate cancer progression model. Cancer Res 2004;64(23):8620–9.

[19] Fan W, Yanase T, Morinaga H, Okabe T, Nomura M, Daitoku H, et al. Insulin-like growth factor 1/insulin signaling activates androgen signaling through direct interactions of Foxo1 with androgen receptor. J Biol Chem 2007;282(10):7329–38.

[20] Hopkins BD, Goncalves MD, Cantley LC. Insulin–PI3K signalling: an evolutionarily insulated metabolic driver of cancer. Nat Rev Endocrinol 2020;16(5):276–83.

[21] Zhao L, Vogt PK. Class I PI3K in oncogenic cellular transformation. Oncogene 2008;27(41):5486–96.

[22] Carver BS, Chapinski C, Wongvipat J, Hieronymus H, Chen Y, Chandarlapaty S, et al. Reciprocal feedback regulation of PI3K and androgen receptor signaling in PTEN-deficient prostate cancer. Cancer Cell 2011;19(5):575–86.

[23] Carracedo A, Ma L, Teruya-Feldstein J, Rojo F, Salmena L, Alimonti A, et al. Inhibition of mTORC1 leads to MAPK pathway activation through a PI3K-dependent feedback loop in human cancer. J Clin Investig 2008;118(9):3065–74.

[24] O'Reilly KE, Rojo F, She Q-B, Solit D, Mills GB, Smith D, et al. mTOR inhibition induces upstream receptor tyrosine kinase signaling and activates Akt. Cancer Res 2006;66(3):1500–8.

[25] Chen HX, Sharon E. IGF-1R as an anti-cancer target–trials and tribulations. Chin J Cancer 2013;32(5):242–52.

[26] Niu X-B, Fu G-B, Wang L, Ge X, Liu W-T, Wen Y-Y, et al. Insulin-like growth factor-I induces chemoresistence to docetaxel by inhibiting miR-143 in human prostate cancer. Oncotarget 2017;8(63):107157–66.

[27] Belfiore A, Frasca F, Pandini G, Sciacca L, Vigneri R. Insulin receptor isoforms and insulin receptor/insulin-like growth factor receptor hybrids in physiology and disease. Endocr Rev 2009;30(6):586–623.

[28] Weinstein D, Sarfstein R, Laron Z, Werner H. Insulin receptor compensates for IGF1R inhibition and directly induces mitogenic activity in prostate cancer cells. Nature 2014;3(1):24.

[29] Hopkins BD, Pauli C, Du X, Wang DG, Li X, Wu D, et al. Suppression of insulin feedback enhances the efficacy of PI3K inhibitors. Nature 2018;560(7719):499–503.

[30] Lutz SZ, Hennenlotter J, Scharpf MO, Sailer C, Fritsche L, Schmid V, et al. Androgen receptor overexpression in prostate cancer in type 2 diabetes. Mol Metabol 2018;8:158–66.

[31] Vikram A, Jena G. Diet-induced hyperinsulinemia accelerates growth of androgen-independent PC-3 cells in vitro. Nutr Cancer 2012;64(1):121–7.

[32] Venkateswaran V, Haddad AQ, Fleshner NE, Fan R, Sugar LM, Nam R, et al. Association of diet-induced hyperinsulinemia with accelerated growth of prostate cancer (LNCaP) xenografts. J Natl Cancer Inst 2007;99(23):1793–800.

[33] Ansarullah Jain C, Fathi Far F, Homberg S, Wißmiller K, Gräfin von Hahn F, et al. Inceptor counteracts insulin signalling in β-cells to control glycaemia. Nature 2021;590(7845):326–31.

[34] Deng L, Broaddus RR, McCampbell A, Shipley GL, Loose DS, Stancel GM, et al. Identification of a novel estrogen-regulated gene, EIG121, induced by hormone replacement therapy and differentially expressed in type I and type II endometrial cancer. Clin Cancer Res 2005;11(23):8258–64.

[35] Kang JM, Park S, Kim SJ, Kim H, Lee B, Kim J, et al. KIAA1324 suppresses gastric cancer progression by inhibiting the oncoprotein GRP78. Cancer Res 2015;75(15):3087–97.

[36] Estrella JS, Ma LT, Milton DR, Yao JC, Wang H, Rashid A, et al. Expression of estrogen-induced genes and estrogen receptor beta in pancreatic neuroendocrine tumors: implications for targeted therapy. Pancreas 2014;43(7):996–1002.

[37] Ran X, Zhou P, Zhang K. Autophagy plays an important role in stemness mediation and the novel dual function of EIG121 in both autophagy and stemness regulation of endometrial carcinoma JEC cells. Int J Oncol 2017;51(2):644–56.

[38] Schlumbrecht MP, Xie S-S, Shipley GL, Urbauer DL, Broaddus RR. Molecular clustering based on ERα and EIG121 predicts survival in high-grade serous carcinoma of the ovary/peritoneum. Mod Pathol 2011;24(3):453–62.

[39] Uhlen M, Zhang C, Lee S, Sjöstedt E, Fagerberg L, Bidkhori G. A pathology atlas of the human cancer transcriptome. Science 2017;357(6352):eaan2507.

[40] Franko A, Berti L, Guirguis A, Hennenlotter J, Wagner R, Scharpf MO, et al. Characterization of hormone-dependent pathways in six human prostate cancer cell lines: a gene expression study. Genes 2020;11(10):1174.

[41] Franko A, Shao Y, Heni M, Hennenlotter J, Hoene M, Hu C. Human prostate cancer is characterized by an increase in urea cycle metabolites. Cancers 2020;12(7):1814.
[42] Cunningham F, Achuthan P, Akanni W, Allen J, Amode MR, Armean IM, et al. Ensembl 2019. Nucleic Acids Res 2019;47(D1):D745–51.
[43] Tang Z, Li C, Kang B, Gao G, Li C, Zhang Z. GEPIA: a web server for cancer and normal gene expression profiling and interactive analyses. Nucleic Acids Res 2017;45(W1):W98–102.
[44] Beltran H, Prandi D, Mosquera JM, Benelli M, Puca L, Carta J, et al. Divergent clonal evolution of castration-resistant neuroendocrine prostate cancer. Nat Med 2016;22(3):298–305.
[45] Cerami E, Gao J, Dogrusoz U, Gross BE, Sumer SO, Aksoy BA, et al. The cBio cancer genomics portal: an open platform for exploring multidimensional cancer genomics data. Cancer Discov 2012;2(5):401–4.
[46] Wegner KA, Cadena MT, Trevena R, Turco AE, Gottschalk A, Halberg RB, et al. An immunohistochemical identification key for cell types in adult mouse prostatic and urethral tissue sections. PLoS One 2017;12(11):e0188413.
[47] Anthony Di Sant'Agnese P. Neuroendocrine differentiation in human prostatic carcinoma. Hum Pathol 1992;23(3):287–96.
[48] Yuan T-C, Veeramani S, Lin F-F, Kondrikou D, Zelivianski S, Igawa T, et al. Androgen deprivation induces human prostate epithelial neuroendocrine differentiation of androgen-sensitive LNCaP cells. Endocrine-Related Cancer Endocr Relat Cancer 2006;13(1):151–67.
[49] Crosas-Molist E, Bertran E, Rodriguez-Hernandez I, Herraiz C, Cantelli G, Fabra A, et al. The NADPH oxidase NOX4 represses epithelial to amoeboid transition and efficient tumour dissemination. Oncogene 2017;36(21):3002–14.
[50] Valcarcel-Jimenez L, Macchia A, Crosas-Molist E, Schaub-Clerigue A, Camacho L, Martin-Martin N, et al. PGC1α suppresses prostate cancer cell invasion through ERRα transcriptional control. Cancer Res 2019;79(24):6153–65.
[51] Wang ZA, Toivanen R, Bergren SK, Chambon P, Shen MM. Luminal cells are favored as the cell of origin for prostate cancer. Cell Rep 2014;8(5):1339–46.
[52] Edwards J, Krishna NS, Grigor KM, Bartlett JMS. Androgen receptor gene amplification and protein expression in hormone refractory prostate cancer. Br J Cancer 2003;89(3):552–6.
[53] Perner S, Hofer MD, Kim R, Shah RB, Li H, Möller P, et al. Prostate-specific membrane antigen expression as a predictor of prostate cancer progression. Hum Pathol 2007;38(5):696–701.
[54] Leite KRM, Franco MF, Srougi M, Nesrallah LG, Bevilacqua RG, Darini E, et al. Abnormal expression of MDM2 in prostate carcinoma. Mod Pathol 2001;14(5):428–36.
[55] Wade M, Li Y-C, Wahl GM. MDM2, MDMX and p53 in oncogenesis and cancer therapy. Nat Rev Cancer 2013;13(2):83–96.
[56] Yang J-Y, Zong CS, Xia W, Wei Y, Ali-Seyed M, Li Z, et al. MDM2 promotes cell motility and invasiveness by regulating E-cadherin degradation. Mol Cell Biol 2006;26(19):7269.
[57] Heni M, Hennenlotter J, Scharpf M, Lutz SZ, Schwentner C, Todenhöfer T, et al. Insulin receptor isoforms A and B as well as insulin receptor substrates-1 and -2 are differentially expressed in prostate cancer. PLoS One 2012;7(12):e50953.
[58] Ghosh P, Dahms NM, Kornfeld S. Mannose 6-phosphate receptors: new twists in the tale. Nat Rev Mol Cell Biol 2003;4(3):202–13.
[59] Meseure D, Alsibai KD, Vacher S, Hatem R, Nicolas A, Callens C, et al. Altered expression of three EGFR posttranslational regulators MDGI, MIG6, and EIG121 in invasive breast carcinomas. Anal Cell Pathol 2020;2020:9268236.
[60] Kramer N, Walzl A, Unger C, Rosner M, Krupitza G, Hengstschläger M, et al. In vitro cell migration and invasion assays. Mutat Res, Rev Mutat Res 2013;752(1):10–24.
[61] Hellawell GO, Turner GDH, Davies DR, Poulsom R, Brewster SF, Macaulay VM. Expression of the type 1 insulin-like growth factor receptor is up-regulated in primary prostate cancer and commonly persists in metastatic disease. Cancer Res 2002;62(10):2942–50.
[62] Pandini G, Mineo R, Frasca F, Roberts CT, Marcelli M, Vigneri R, et al. Androgens up-regulate the insulin-like growth factor-I receptor in prostate cancer cells. Cancer Res 2005;65(5):1849–57.
[63] Burfeind P, Chernicky CL, Rininsland F, Ilan J, Ilan J. Antisense RNA to the type I insulin-like growth factor receptor suppresses tumor growth and prevents invasion by rat prostate cancer cells in vivo. Proc Natl Acad Sci USA 1996;93(14):7263–8.
[64] Eder M, Eisenhut M, Babich J, Haberkorn U. PSMA as a target for radiolabelled small molecules. Eur J Nucl Med Mol Imag 2013;40(6):819–23.
[65] Ghosh A, Heston WDW. Tumor target prostate specific membrane antigen (PSMA) and its regulation in prostate cancer. J Cell Biochem 2004;91(3):528–39.
[66] Meller B, Bremmer F, Sahlmann CO, Hijazi S, Bouter C, Trojan L. Alterations in androgen deprivation enhanced prostate-specific membrane antigen (PSMA) expression in prostate cancer cells as a target for diagnostics and therapy. EJNMMI Res 2015;5(1):66.
[67] Murga JD, Moorji SM, Han AQ, Magargal WW, DiPippo VA, Olson WC. Synergistic co-targeting of prostate-specific membrane antigen and androgen receptor in prostate cancer. Prostate 2015;75(3):242–54.
[68] Carruba G. Estrogen and prostate cancer: an eclipsed truth in an androgen-dominated scenario. J Cell Biochem 2007;102(4):899–911.

Supplementary Figure S1

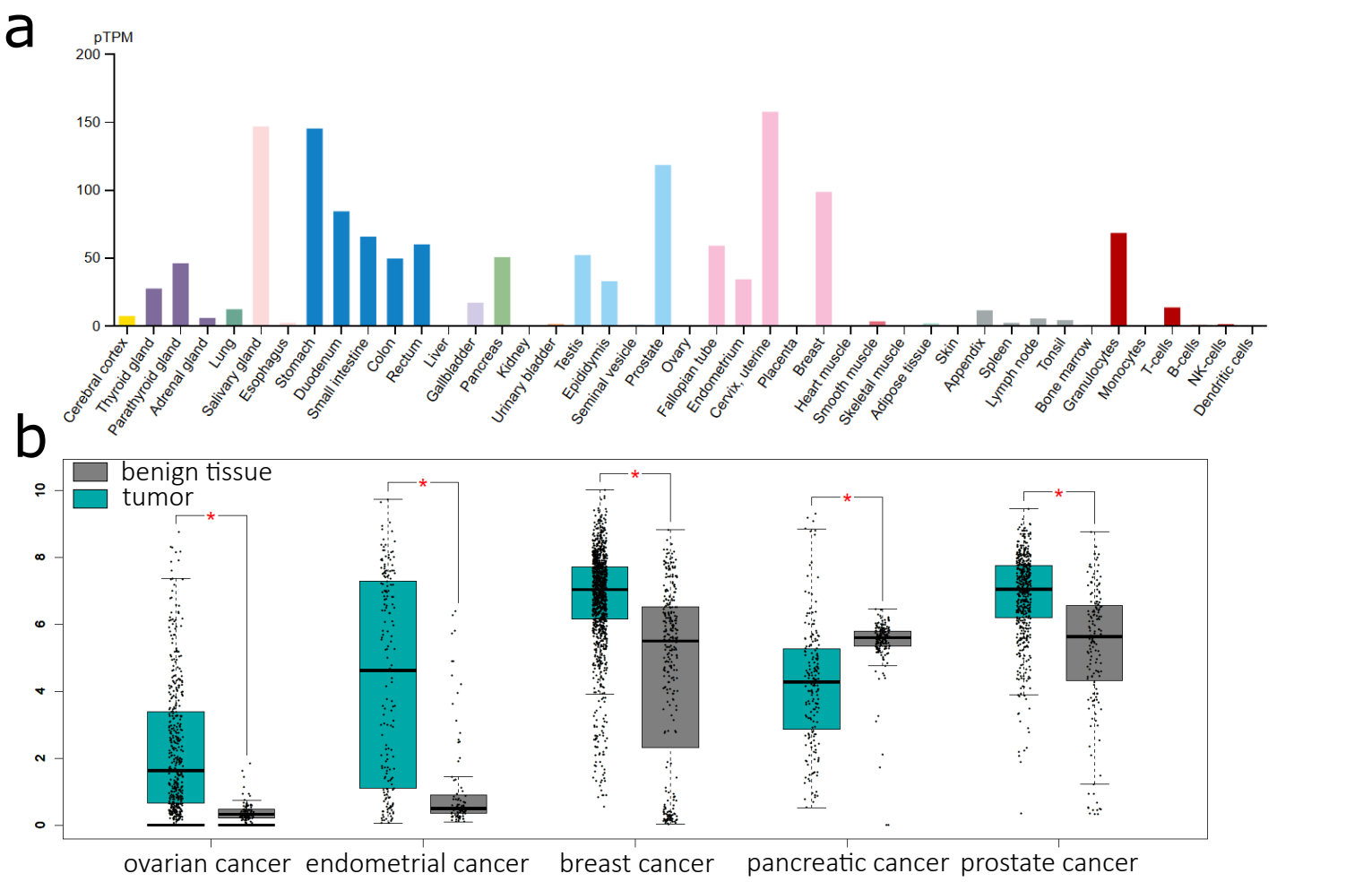

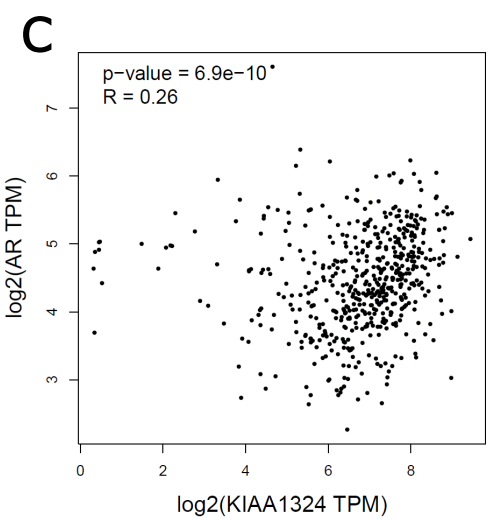

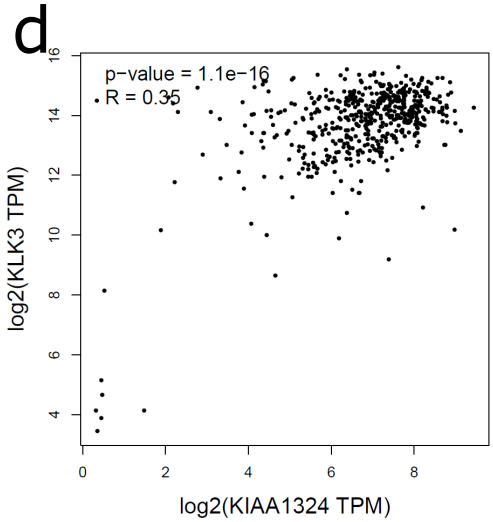

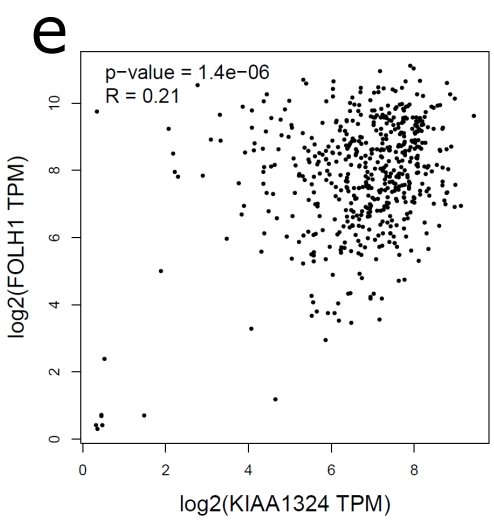

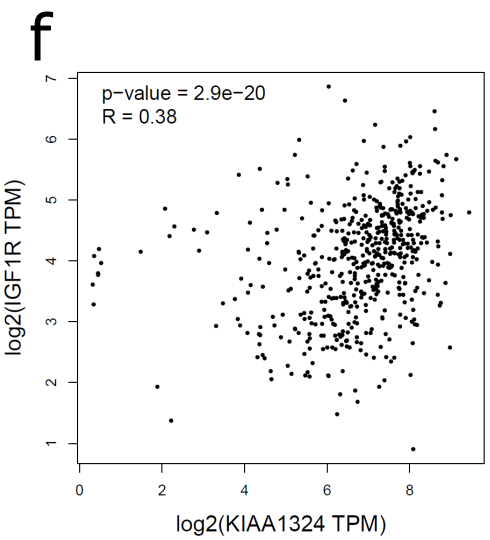

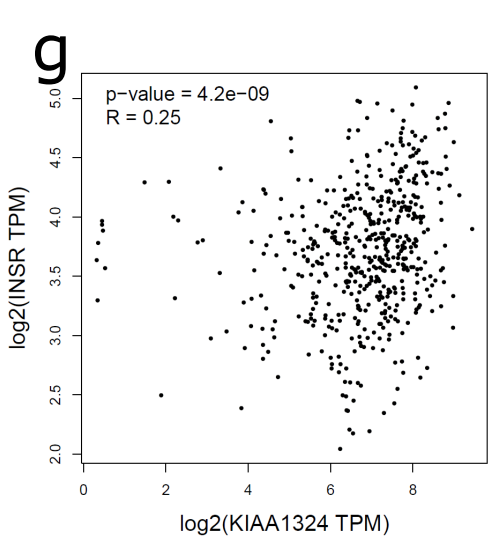

a. RNA expression levels of inceptor in pTPM (protein-coding transcripts per million), according to the Human Protein Atlas.

b. Expression of inceptor in tumor (cyan) vs. healthy tissue (gray) for Ovarian serous cystadenocarcinoma (OV), Uterine Corpus Endometrial Carcinoma (UCEC), Breast invasive carcinoma (BRCA), Pancreatic adenocarcinoma (PAAD) and Prostate adenocarcinoma (PRAD).

c-g. Correlation of log transformed mRNA levels of inceptor with AR, KLK3 (PSA), FOLH1 (PSMA), IGF1R and IR (INSR). Data was retrieved via the GEPIA web server.

Supplementary Figure S2

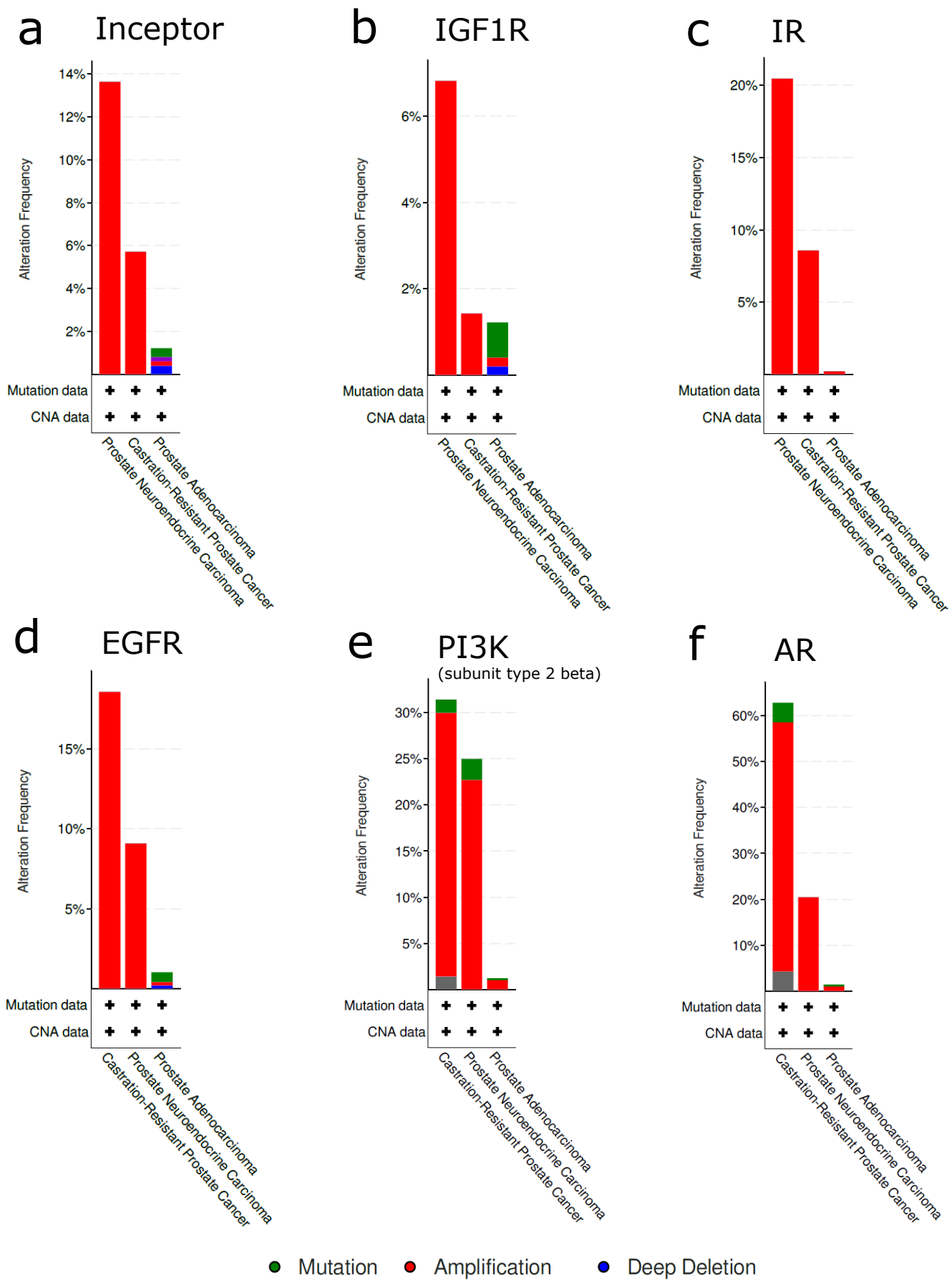

Frequency of amplification (red), mutation (green) or deep deletion (blue) of indicated genes in prostate adenocarcinoma, castration-resistant prostate cancer and prostate neuroendocrine carcinoma based on the TCGA and Neuroendocrine Prostate Cancer (NatMed) datasets. Data was analyzed via CBioPortal.

Supplementary Figure S3

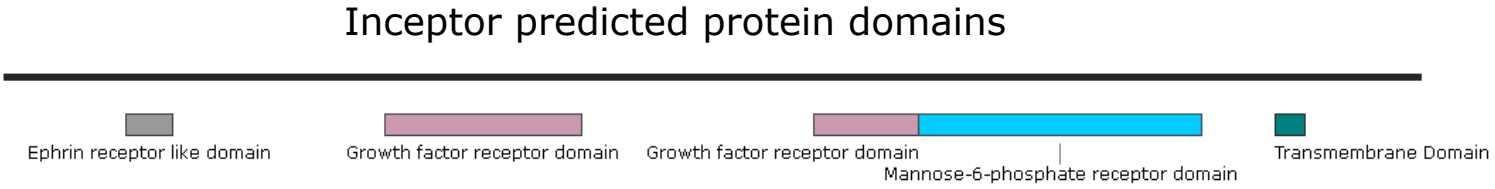

The protein sequence was analyzed using the ENSEMBL database, extracting the recognized protein domains with highest similarities.

Supplementary Figure S4

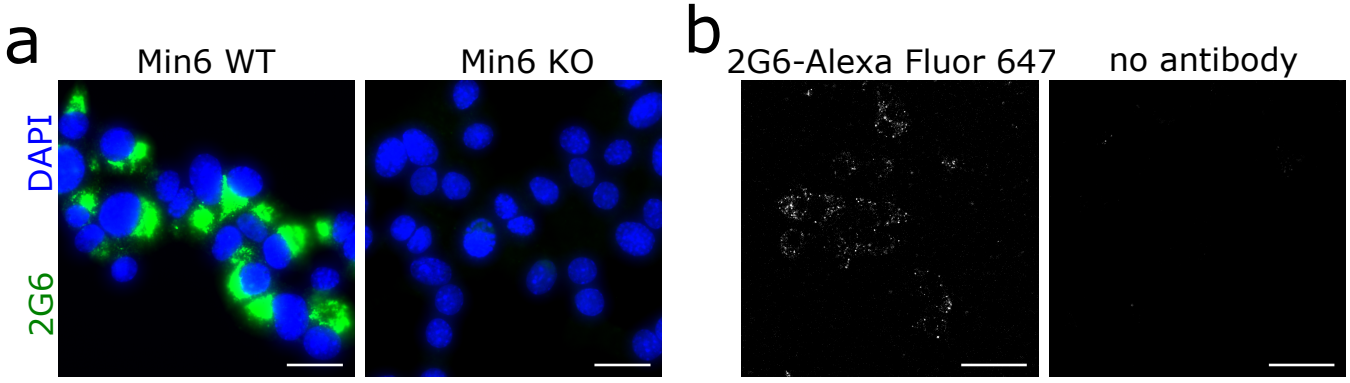

a. The inceptor antibody #2G6 was initially tested via immunocytochemistry in the mouse insulinoma cell line Min6. The specificity was validated by applying the antibody to inceptor knockout Min6 in the same conditions.

b. The labeled antibody #2G6-Alexa Fluor 647 was tested on live Min6 cells at an initial concentration of 100 µg/ml in DMEM.